



**BUCKY-1 – A 1-D Radiation Hydrodynamics
Code for Simulating Inertial Confinement
Fusion High Energy Density Plasmas**

J.J. MacFarlane, G.A. Moses, R.R. Peterson

August 1995

UWFDM-984

***FUSION TECHNOLOGY INSTITUTE
UNIVERSITY OF WISCONSIN
MADISON WISCONSIN***

DISCLAIMER

This report was prepared as an account of work sponsored by an agency of the United States Government. Neither the United States Government, nor any agency thereof, nor any of their employees, makes any warranty, express or implied, or assumes any legal liability or responsibility for the accuracy, completeness, or usefulness of any information, apparatus, product, or process disclosed, or represents that its use would not infringe privately owned rights. Reference herein to any specific commercial product, process, or service by trade name, trademark, manufacturer, or otherwise, does not necessarily constitute or imply its endorsement, recommendation, or favoring by the United States Government or any agency thereof. The views and opinions of authors expressed herein do not necessarily state or reflect those of the United States Government or any agency thereof.

**BUCKY-1 – A 1-D Radiation Hydrodynamics Code
for Simulating Inertial Confinement Fusion
High Energy Density Plasmas***

J. J. MacFarlane, G. A. Moses, and R. R. Peterson

Fusion Technology Institute
University of Wisconsin-Madison
1500 Johnson Drive
Madison, WI 53706

August 1995

UWFDM-984

*This work has been supported in part by the U.S. Department of Energy through Contract No. DE-AS08-88DP10754.

Contents

1. Overview	1-1
2. BUCKY-1 Units and Notation	2-1
2.1. Units	2-1
2.2. Notation	2-1
2.2.1. Notation in the Documentation	2-1
2.2.2. Notation in the Code	2-2
2.3. Lagrangian Coordinates	2-2
3. Conservation Equations	3-1
3.1. Mass Conservation	3-1
3.2. Momentum Conservation	3-2
3.2.1. Quiet Start	3-4
3.3. Energy Conservation	3-4
3.4. Coefficients and Source Terms in the Energy Equations	3-9
3.4.1. Thermal Conductivity	3-9
3.4.2. Electron-Ion Coupling Coefficient	3-11
3.4.3. Coupling to the Radiation Field	3-11
3.4.4. Coupling to the Thermonuclear Burn Reaction Products	3-13
3.4.5. Ion Beam and Laser Energy Deposition Source Terms	3-13
4. Radiation Transport Models	4-1
4.1. Multigroup Diffusion	4-1
4.2. Method of Short Characteristics	4-4
4.3. Variable Eddington Model	4-4
4.4. Non-LTE CRE Line Transport	4-11
4.4.1. Introduction	4-11
4.4.2. Statistical Equilibrium Model	4-12
4.4.3. Radiative Transfer Model	4-15
4.4.4. Atomic Physics Models	4-22
4.4.5. Interface Between CRE and Radiation-Hydrodynamics Models	4-23
4.5. Mechanics of CRE/Radiation-Hydrodynamics Interface	4-24

5. Equations of State and Opacity Tables	5-1
5.1. EOSOPA EOS and Opacity Tables	5-2
5.2. SESAME EOS Tables	5-3
6. Fast Ion Energy Deposition	6-1
7. Laser Deposition Model	7-1
8. Fusion Burn Energy Deposition	8-1
8.1. Fusion Reactions	8-1
8.2. Fusion Charged Particle Reaction Product Transport	8-4
8.2.1. Time-Dependent Particle Tracking Method	8-4
8.2.2. Implementation of TDPT	8-10
8.3. Nuclear Energy Deposition Model	8-20
9. Rapid X-ray Deposition in Cold Media	9-1
10. Vaporization and Condensation Modeling	10-1
11. Energy Conservation Check	11-1
12. Time Step Control	12-1
13. Code Structure	13-1
13.1. Subroutines	13-1
13.2. The Common Blocks	13-18
14. Input and Output Files	14-1
15. NAMELIST Input Variables	15-1
16. Compiling and Running	16-1

17. Sample Calculations	17-1
17.1. Example 1: Isentropic Compression of a DT Shell	17-1
17.2. Example 2: Al Witness Plate Shock Breakout	17-3
17.3. Example 3: LIBRA Implosion Simulation	17-3
17.4. LIBRA Fusion Burn and Target Breakup	17-8
17.5. Example 5: Target Chamber Non-LTE Buffer Gas Simulation	17-11

1. Overview

BUCKY-1 is a one-dimensional (1-D) radiation-hydrodynamics code developed at the University of Wisconsin Fusion Technology Institute to study Inertial Confinement Fusion (ICF) high energy density plasmas. This code has been constructed in large part by integrating pieces from several other simulation codes which were developed at the University of Wisconsin to study target physics and target chamber design issues for ICF reactors. Its history is rooted primarily in the following codes:

- **PHD-IV** [1] — A 1-D radiation-hydrodynamics code written to simulate ICF target implosions, fusion burn, and energy partitioning during target breakup.
- **MF-FIRE** [2] — A 1-D radiation-hydrodynamics code for simulating the response of a target chamber buffer gas to a high-gain ICF microexplosion.
- **CONRAD** [3] — A descendant of MF-FIRE which includes the capability of simulating the vaporization of solid or liquid surfaces exposed to the x-rays and fast debris ions from high-gain targets.
- **NLTERT** [4] — A non-LTE collisional-radiative equilibrium (CRE) code with detailed radiation transport packages used to study the radiative, atomic, and spectral properties of ICF-related laboratory plasmas.

The code utilizes high-quality equation of state (EOS) and multigroup opacity tables generated by EOSOPA [5], which provides data for both low-Z and high-Z plasmas over densities ranging from the dilute ideal gas region to highly compressed matter. In addition to integrating parts of previously written codes, a number of new packages and options have been added. These include: a new multiangle, multifrequency radiation transfer model based on the method of short characteristics; an escape probability model for energy deposition of neutrons created during the DT burn phase; a simple laser energy deposition model; the

ability to simulate the response of thin foil targets to an external radiation source; and more flexibility in setting up and running multilayer, multimaterial problems, including the ability to select different EOS packages (EOSOPA or SESAME) for each layer. Also it is worth noting that the output from this code has been set up to interface readily with our non-LTE spectral analysis code. This allows for an efficient means of turning temperature and density distributions predicted by BUCKY-1 into detailed emission or absorption spectra, which can then be directly compared with spectra obtained in laboratory plasma experiments.

This code and its predecessors have been used to simulate a variety of plasmas. Examples include:

- Simulation of the breakup and energy partitioning of high-gain ICF targets [6]–[8];
- Simulating the response of materials (Au foils, Al witness plates) to hohlraum radiation drives [9]–[11];
- Investigating the response of non-LTE buffer gas plasmas to ICF high-gain microexplosions [12, 13] and to laser-produced blast waves generated by fast ions [14];
- Studying the vaporization and condensation of solid and liquid surfaces exposed to ICF target x-rays and debris ions [15, 16];
- Simulation of “plastic sandwich” targets heated by intense Li beams [17, 18];
- Investigating the x-ray emission from shocks generated in the winds of high-luminosity stars [19].

At various stages of development, many of the models in the code have been tested and benchmarked. The reader should note, however, that the code is continually being modified and upgraded, and that we must continue our efforts to test the code and benchmark against experimental data whenever possible.

The major features of BUCKY-1 are as follows. It is a 1-D Lagrangian hydrodynamics code which can simulate plasmas in planar, cylindrical, or spherical geometries. It solves a single fluid equation of motion (electrons and ions are assumed to move together) with pressure contributions from electrons, ions, radiation, and fast charged particles. Shocks are handled using a von Neumann artificial viscosity. Energy transfer in the plasma can be treated using either a one-temperature ($T_i = T_e$) or two-temperature ($T_i \neq T_e$) model. Both the electrons and ions are assumed to have Maxwellian distributions defined by T_i and T_e . Thermal conduction for each species is treated using Spitzer conductivities, with the electron conduction being flux-limited. The two temperature equations are coupled by an electron-ion energy exchange term and each equation has a PdV work term.

Radiation emission and absorption terms are coupled to the electron temperature equation. Multifrequency radiation intensities are computed using a choice of several radiation transport packages: (1) a flux-limited radiation diffusion model; (2) a multiangle radiative transfer model based on the method of short characteristics (presently, planar geometry only); (3) a variable Eddington radiative transfer model (spherical geometries); and (4) a non-LTE line radiation transport package based on escape probability techniques. The sum of the contributions to emission and absorption from all frequency groups are then coupled to the electron energy equation as source terms. Multifrequency opacities are obtained from EOSOPA tables. When the CRE line transport model is invoked, non-LTE atomic level populations are computed self-consistently with the line radiation field. In this case, collisional and radiative atomic data are obtained from ATBASE [20] tables.

In addition to radiation, a number of other physical processes are included in the electron and ion energy equations as source terms: fast ion (beam or target debris) energy deposition; heating due to the deposition of fast charged particles and neutrons during the fusion burn phase; laser energy deposition; and x-ray heating of a cold buffer gas. Fusion burn equations from DT, DD, and DHe³ reactions are solved and the charged particle reaction

products are transported and slowed using a time-dependent particle tracking algorithm. Neutrons are deposited in the target using an escape probability model. Fast ions from an ion beam or target microexplosion debris are tracked using a time-, energy-, and species-dependent stopping power model. Stopping powers are computed using a Lindhard model at low projectile energies and a Bethe model at high energies [21]. Laser energy is deposited using an inverse Bremsstrahlung attenuation model, with a dump of the remaining laser energy at the critical surface.

The source code for BUCKY-1 (without common blocks inserted) is about 27,000 lines. The code is typically run on UNIX workstations (HP 700 series, SUN, IBM RS6000, Silicon Graphics) which have 32 – 80 MB of RAM. The memory required depends on the size of the arrays, which are easily adjusted by the user. A preprocessor is used to allow for ease in adjusting array sizes and machine portability. The main functions of the preprocessor are to: insert common blocks in the source code; define array sizes through PARAMETER statements; and insert machine-dependent source code. The CPU time required for typical calculations on HP 715 and 735 workstations ranges from several minutes to several hours, depending on the complexity of the problem. Results are plotted using separate software which reads a binary output file created during the simulation.

2. BUCKY-1 Units and Notation

2.1. Units

The units in BUCKY-1 are primarily those listed in Table 2.1. However, two sections of the code which were extracted from PHD-IV (the fusion burn package) and NLTE (the non-LTE line radiation package) remain in the units of their original code. Thus, some unit conversion is done at the beginning and end of calls to these packages. The units for these are listed in the last two columns in Table 2.1.

Table 2.1. BUCKY-1 Units

Quantity	General Units	Fusion Burn Units	Non-LTE Line Transport Units
Mass	grams	grams	grams
Length	cm	cm	cm
Time	s	shakes = 10^{-8} s	s
Temperature	eV	keV	eV
Energy	J	jerks = 10^{16} ergs	ergs
Pressure	J/cm ³	jerks/cm ³	—

2.2. Notation

2.2.1. Notation in the Documentation

The notation in the documentation for the time and space indices used in solving the partial differential equations is quite standard. The time index appears as a superscript and the space index appears as a subscript (e.g., $T_{e_{j-1/2}}^{n+1/2}$). The zone boundaries are denoted by whole integer subscripts and the zone centers are denoted by half integer subscripts. The inner zone boundary has the subscript $j = 0$ and the outer boundary has the index $j = \text{JMAX}$. The equation of motion is “advanced” from time level $t^{n-1/2}$ to time level $t^{n+1/2}$ and the temperature and radiation equations are advanced from level t^n to level t^{n+1} .

2.2.2. Notation in the Code

The notation in BUCKY-1 is summarized in Table 2.2. The last two characters of the variable name distinguish whether it is a zone centered or a zone boundary quantity, and the time level in the finite difference equations at which the quantity is evaluated. The first four or less characters represent the name of the quantity. This will describe either a physical quantity (e.g., TE2A is the zone center and electron temperature at time level $n + 1$) or the name will correspond to the notation used in the documentation (e.g., OMC2B is the electron-ion coupling coefficient, ω_c , at time level $n + 1/2$). The letter “E” generally means electron, “N” means ion, and “R” means radiation.

Table 2.2. Variable Notation

1 – zone boundary	A – t^{n+1}
2 – zone center	B – $t^{n+1/2}$
	C – t^n
	D – $t^{n-1/2}$

2.3. Lagrangian Coordinates

The hydrodynamic description of a fluid can be expressed in two equivalent forms. In the Eulerian approach, attention is centered at positions \mathbf{r} in a fixed reference frame and the change in the fluid properties is observed at this position. In other words, the coordinate system is stationary and the fluid flows through it. In the Lagrangian approach, the coordinate system is tied to the fluid at time $t = 0$ and moves with the fluid velocity, $\mathbf{u}(\mathbf{r}, t)$. We observe a “cell” of fluid at time $t = 0$ and follow its evolution for $t > 0$. In the Lagrangian form, a new independent variable is defined to replace the spatial vector, \mathbf{r} . In one dimension this is given by

$$dm_o = \rho(r)r^{\delta-1}dr \quad (2.1)$$

where the units of the Lagrangian mass, m_o , are given in Table 2.3.

Table 2.3. Lagrangian Units

Geometry	δ	Mass (m_0)	Energy
Planar	1	grams/cm ²	J/cm ²
Cylindrical	2	grams/cm·radian	J/cm·radian
Spherical	3	grams/steradian	J/steradian

In Lagrangian coordinates, the mass within each zone remains constant throughout the calculation, while the zone boundary radii, r_j , are functions of time. The continuity equation is automatically satisfied and new densities are computed by new zone boundary positions and the ratio of mass to volume. (The constant zone mass is not strictly true when thermonuclear burn calculations are done and particles are transported across zone boundaries.)

3. Conservation Equations

3.1. Mass Conservation

The conservation of mass equation is given in Lagrangian coordinates as

$$\frac{\partial V}{\partial t} = V \frac{\partial u}{\partial r} = \frac{\partial}{\partial m_o} (r^{\delta-1} u) \quad (3.1)$$

where $V = 1/\rho$ is the specific volume, u is the fluid velocity, and m_o is the Lagrangian mass variable. This equation is actually not solved by BUCKY-1 because the mass in each zone is automatically conserved. The density or specific volume is computed after the time-dependent radii are computed from the updated velocities. Once the velocities of the boundaries at $t^{n+1/2}$ are known, one can calculate new boundary positions at t^{n+1} :

$$r_j^{n+1} = r_j^n + \Delta t^{n+1/2} u_j^{n+1/2} \quad \text{and} \quad \Delta r_{j-1/2}^{n+1} = r_j^{n+1} - r_{j-1}^{n+1}. \quad (3.2)$$

With the new boundary positions, new densities or specific volumes are calculated as:

Planar ($\delta = 1$):

$$V_{j-1/2}^{n+1} = \frac{\Delta r_{j-1/2}^{n+1}}{\Delta m_{o_{j-1/2}}};$$

Cylindrical ($\delta = 2$):

$$V_{j-1/2}^{n+1} = \frac{1}{2} \left(\frac{\Delta r_{j-1/2}^{n+1}}{\Delta m_{o_{j-1/2}}} \right) (r_j^{n+1} + r_{j-1}^{n+1});$$

Spherical ($\delta = 3$):

$$V_{j-1/2}^{n+1} = \left(\frac{\Delta r_{j-1/2}^{n+1}}{\Delta m_{o_{j-1/2}}} \right) \left[r_j^{n+1} r_{j-1}^{n+1} + \frac{1}{3} (\Delta r_{j-1/2}^{n+1})^2 \right].$$

The rate of change in specific volume is:

$$\dot{V}_{j-1/2}^{n+1/2} = \left(\frac{V_{j-1/2}^{n+1} - V_{j-1/2}^n}{\Delta t^{n+1/2}} \right). \quad (3.3)$$

All of these computations are done in subroutine HYDROD.

Although the mass density is normally used by the hydrodynamic equations, it is also necessary to compute the number density of the ions and electrons. If a thermonuclear burn

calculation is done then the ionic species in each zone can change and the ion number density (n_i), average charge (Z), and average atomic weight (A) are given by:

$$n_i = n_D + n_T + n_{He^4} + n_{He^3} + n_P + n_o, \quad (3.4)$$

$$Z = \frac{[(n_D + n_T + n_P) * 1 + (n_{He^4} + n_{He^3}) * 2 + n_o * Z_o]}{n_i}, \quad (3.5)$$

$$A = \frac{[n_P + n_D * 2 + (n_T + n_{He^3}) * 3 + (n_{He^4}) * 4 + n_o * A_o]}{n_i}, \quad (3.6)$$

where n_D and n_T are the deuterium and tritium particle densities, n_{He^3} and n_{He^4} are the He isotope particle densities, and n_o and Z_o refer to the density and mean charge of non-burn ($Z > 2$) species.

3.2. Momentum Conservation

The momentum conservation equation is solved in the one fluid approximation, where the plasma electrons and ions are assumed to flow together as one fluid with no charge separation effects (i.e., electric fields) included. In the one-dimensional approximation there are also no self-generated magnetic fields, and the conservation of momentum equation, in Lagrangian form, becomes simply:

$$\frac{\partial u}{\partial t} = -\frac{1}{\rho} \frac{\partial}{\partial r} (P + q) = -r^{\delta-1} \frac{\partial}{\partial m_o} (P + q) + \dot{u}_{TN}, \quad (3.7)$$

where $P = P_e + P_i + P_r$ is the total fluid pressure, q is the von Neumann artificial viscosity, and \dot{u}_{TN} is the velocity change due to momentum exchange from the slowing down of fast (non-thermal) particles. The explicit difference equation used to solve this P.D.E. is given by:

$$\frac{u_j^{n+1/2} - u_j^{n-1/2}}{\Delta t^n} = -(r^{\delta-1})_j^n \frac{[\Delta P_j^n + \Delta q_j^{n-1/2}]}{\Delta m_{o_j}} + \dot{u}_{TNj}; \quad (3.8)$$

hence

$$u_j^{n+1/2} = u_j^{n-1/2} - (r^{\delta-1})_j^n [\Delta P_j^n + \Delta q_j^{n-1/2}] \left(\frac{\Delta t^n}{\Delta m_{o_j}} \right) + \Delta t^n \dot{u}_{TNj} \quad (3.9)$$

where

$$\begin{aligned}
P_{j-1/2}^n &= P_{e_{j-1/2}}^n + P_{i_{j-1/2}}^n + P_{r_{j-1/2}}^n & \Delta P_j^n &= P_{j+1/2}^n - P_{j-1/2}^n \\
\Delta m_{o_j} &= (\Delta m_{o_{j+1/2}} + \Delta m_{o_{j-1/2}})/2 & \Delta q_j^{n-1/2} &= q_{j+1/2}^{n-1/2} - q_{j-1/2}^{n-1/2} \\
\Delta t^n &= (\Delta t^{n+1/2} + \Delta t^{n-1/2})/2
\end{aligned} \tag{3.10}$$

and u_{TN} is defined in Section 8. Equation (3.9) is solved in subroutine HYDROD. The artificial viscosity is introduced into the inviscid equation of motion to handle shocks. Its function is to smooth shock fronts over about 3 zones by adding a small amount of dissipation into the equation. It is non-zero only when a zone is under compression. It is given by the following expressions which are computed in subroutine QUE:

$$\begin{aligned}
q_{j-1/2}^{n-1/2} &= 0 & \frac{\partial V_{j-1/2}^{n-1/2}}{\partial t} &> 0 & \text{(expansion)} \\
q_{j-1/2}^{n-1/2} &= 2 \frac{(u_j^{n-1/2} - u_{j-1/2}^{n-1/2})^2}{V_{j-1/2}^{n-1/2}} & \frac{\partial V_{j-1/2}^{n-1/2}}{\partial t} &< 0 & \text{(compression)}.
\end{aligned} \tag{3.11}$$

The difference equation advances the velocities at the zone boundaries from $t^{n-1/2}$ to $t^{n+1/2}$. It is an explicit difference equation in that the unknown, $u_j^{n+1/2}$, is explicitly expressible in terms of known quantities at earlier times. For constant Δt and Δx , this equation is accurate to order Δx^2 and Δt^2 . The numerical stability of this equation away from shocks is insured if

$$\frac{c_s \Delta t}{\Delta x} < 1, \tag{3.12}$$

where c_s is the maximum sound speed in the system. This is the Courant condition and is derived from purely mathematical arguments, but has physical interpretation as well. When this condition is maintained, a disturbance in the fluid cannot pass through more than one mesh interval in a time step, thus assuring that it will be resolved by the finite difference mesh. The time step in BUCKY-1 is adjusted on each time cycle to insure that the Courant condition is satisfied. The time step control algorithm is discussed in Section 12.

The pressure boundary condition for this equation can take several forms in BUCKY-1. It is computed in function PRESBC, and any boundary condition option can be easily added by the user by simply amending PRESBC.

3.2.1. Quiet Start

At the beginning of a target implosion calculation involving a DT gas filled glass microballoon, for instance, the pressure in the glass shell is essentially zero. However, the gas is pushing on the shell with a pressure of typically several atmospheres. This is a very difficult situation for plasma hydrodynamics codes to handle. We know that the shell does not expand; however, the code will predict motion due to the difference in pressures computed by the equation of state routines. This phenomenon will also occur in many other circumstances due to the differences in equations of state for different materials. The method that is used to solve this problem is called the “quiet start”. When the quiet start option is used, all spatial zones are initially flagged as quiet start zones. The equation of state routine always returns $P = 0$ for quiet start zones. A zone is returned to “normal” when its electron temperature exceeds an input parameter, CON(19). A typical value for this is 0.1 eV. Once this value of temperature is exceeded, then the pressure is computed from the EOS table. The quiet start option is set using the input variable ISW(13).

3.3. Energy Conservation

Conservation of energy is represented by temperature diffusion equations for the electrons and ions. In Lagrangian coordinates these two equations take the form:

$$C_{v_e} \frac{\partial T_e}{\partial t} = \frac{\partial}{\partial m_o} \left(r^{\delta-1} K_e \frac{\partial T_e}{\partial r} \right) - \omega_c (T_e - T_i) - [(E_e)_V + P_e] \frac{\partial V}{\partial t} T_e + A - J + S_e \quad (3.13)$$

$$C_{v_i} \frac{\partial T_i}{\partial t} = \frac{\partial}{\partial m_o} \left(r^{\delta-1} K_i \frac{\partial T_i}{\partial r} \right) + \omega_c (T_e - T_i) - [(E_i)_V + P_i] \frac{\partial V}{\partial t} T_i - q \frac{\partial V}{\partial t} + S_i \quad (3.14)$$

where:

C_{v_e} and C_{v_i} are the electron and ion specific heats,

K_e and K_i are the electron and ion thermal conductivities,

$\omega_c(T_e - T_i)$ is the electron-ion collisional coupling term,

$(E_e)_V \equiv \partial E_e / \partial V$,

$(E_i)_V \equiv \partial E_i / \partial V$,

A and J are the radiative heating and cooling terms, and

S_e and S_i are source inputs to the electrons and ions.

These equations can be posed in a convenient matrix form for the purposes of numerical solution:

$$\begin{aligned}
\alpha_{j-1/2}^* \frac{[\theta_{j-1/2}^{n+1} - \theta_{j-1/2}^n]}{\Delta t^{n+1/2}} &= \frac{a_j^*}{2} (r^{\delta-1})_j \frac{[\Delta \theta_j^{n+1} + \Delta \theta_j^n]}{\Delta m_{o_{j-1/2}} * \Delta r_j} \\
&- \frac{a_{j-1}^*}{2} (r^{\delta-1})_{j-1} \frac{[\Delta \theta_{j-1}^{n+1} + \Delta \theta_{j-1}^n]}{\Delta m_{o_{j-1/2}} * \Delta r_{j-1}} - \omega_{j-1/2}^* \frac{(\theta_{j-1/2}^{n+1} + \theta_{j-1/2}^n)}{2} \\
&- \gamma_{j-1/2}^* \frac{(\theta_{j-1/2}^{n+1} + \theta_{j-1/2}^n)}{2} + \beta_{j-1/2}^*
\end{aligned} \tag{3.15}$$

where

$$\begin{aligned}
\theta_{j-1/2}^n &= \begin{pmatrix} T_i \\ T_e \end{pmatrix}_{j-1/2}^n & \Delta \theta_j^n &= \theta_{j+1/2}^n - \theta_{j-1/2}^n \\
\beta_{j-1/2}^* &= \begin{pmatrix} S_i - q\dot{V} \\ S_e + A - J \end{pmatrix}_{j-1/2} \\
\alpha_{j-1/2}^* &= \begin{pmatrix} C_{v_i} & 0 \\ 0 & C_{v_e} \end{pmatrix}_{j-1/2} & a_j^* &= \begin{pmatrix} K_i & 0 \\ 0 & K_e \end{pmatrix}_j \\
\omega_{j-1/2}^* &= \begin{pmatrix} \omega_c & -\omega_c \\ -\omega_c & \omega_c \end{pmatrix}_{j-1/2} & \gamma_{j-1/2}^* &= \begin{pmatrix} [(E_i)_V + P_i] & 0 \\ 0 & [(E_e)_V + P_e] \end{pmatrix}_{j-1/2} \dot{V}_{j-1/2}.
\end{aligned}$$

Rearranging we find

$$\begin{aligned} \alpha_{j-1/2}(\theta_{j-1/2}^{n+1} - \theta_{j-1/2}^n) &= a_j(\Delta\theta_j^{n+1} + \Delta\theta_j^n) - a_{j-1}(\Delta\theta_{j-1}^{n+1} + \Delta\theta_{j-1}^n) \\ &\quad - \omega_{j-1/2}(\theta_{j-1/2}^{n+1} + \theta_{j-1/2}^n) - \gamma_{j-1/2}(\theta_{j-1/2}^{n+1} + \theta_{j-1/2}^n) + \beta_{j-1/2} \end{aligned} \quad (3.16)$$

where

$$\begin{aligned} \alpha_{j-1/2} &= \begin{pmatrix} C_{v_i} & 0 \\ 0 & C_{v_e} \end{pmatrix}_{j-1/2} \frac{\Delta m_{o_{j-1/2}}}{\Delta t^{n+1/2}} \\ \beta_{j-1/2} &= \begin{pmatrix} S_i - q\dot{V} \\ S_e + A - J \end{pmatrix}_{j-1/2} \Delta m_{o_{j-1/2}} \\ a_j &= \frac{1}{2} \begin{pmatrix} K_i & 0 \\ 0 & K_e \end{pmatrix}_j \frac{(r^{\delta-1})_j}{\Delta r_j} \\ \omega_{j-1/2} &= \frac{1}{2} \begin{pmatrix} \omega_c & -\omega_c \\ -\omega_c & \omega_c \end{pmatrix}_{j-1/2} \Delta m_{o_{j-1/2}} \\ \gamma_{j-1/2} &= \frac{1}{2} \begin{pmatrix} [(E_i)_V + P_i] & 0 \\ 0 & [(E_e)_V + P_e] \end{pmatrix}_{j-1/2} \dot{V}_{j-1/2} \Delta m_{o_{j-1/2}}. \end{aligned} \quad (3.17)$$

Combining terms in identical values of θ we finally obtain the familiar form:

$$-A_{j-1/2}\theta_{j+1/2}^{n+1} + B_{j-1/2}\theta_{j-1/2}^{n+1} - C_{j-1/2}\theta_{j-3/2}^{n+1} = D_{j-1/2} \quad (3.18)$$

where

$$\begin{aligned} A_{j-1/2} &= a_j \\ B_{j-1/2} &= \alpha_{j-1/2} + \omega_{j-1/2} + \gamma_{j-1/2} + a_j + a_{j-1} \\ C_{j-1/2} &= a_{j-1} \\ D_{j-1/2} &= a_j(\theta_{j+1/2}^n - \theta_{j-1/2}^n) - a_{j-1}(\theta_{j-1/2}^n - \theta_{j-3/2}^n) \\ &\quad - (\gamma_{j-1/2} + \omega_{j-1/2} - \alpha_{j-1/2})(\theta_{j-1/2}^n) + \beta_{j-1/2}. \end{aligned} \quad (3.19)$$

In the above difference equations, all coefficient matrices are evaluated at $t^{n+1/2}$, hence $\alpha_{j-1/2} = \alpha_{j-1/2}^{n+1/2}$, etc. The solution to Eq. (3.18) of the form [22]:

$$\theta_{j-1/2}^{n+1} = E_{j-1/2} \theta_{j+1/2}^{n+1} + F_{j-1/2} \quad (3.20)$$

where

$$\begin{aligned} E_{j-1/2} &= (B_{j-1/2} - C_{j-1/2} \cdot E_{j-3/2})^{-1} \cdot A_{j-1/2} \\ F_{j-1/2} &= (B_{j-1/2} - C_{j-1/2} \cdot E_{j-3/2})^{-1} \cdot (D_{j-1/2} + C_{j-1/2} \cdot F_{j-3/2}). \end{aligned} \quad (3.21)$$

The boundary conditions determine $E_{1/2}$, $F_{1/2}$, and $\theta_{\text{JMAX}+1/2}^{n+1}$. For plasma boundaries where there is no heat flux (such as the inner boundary in spherical geometry):

$$E_{1/2} = (B_{1/2})^{-1} \cdot A_{1/2} \quad F_{1/2} = (B_{1/2})^{-1} \cdot D_{1/2}. \quad (3.22)$$

At the outer boundary, the option of specifying a temperature boundary condition or a zero heat flux condition is reserved. For a temperature boundary condition

$$\theta_{\text{JMAX}+1/2}^{n+1} = \theta_{bc}^{n+1}. \quad (3.23)$$

For zero heat flux we demand

$$\theta_{\text{JMAX}+1/2}^{n+1} = \theta_{\text{JMAX}-1/2}^{n+1}. \quad (3.24)$$

Hence, there are two equations and two unknowns:

$$\begin{aligned} \theta_{\text{JMAX}-1/2}^{n+1} &= \theta_{\text{JMAX}+1/2}^{n+1} \\ \theta_{\text{JMAX}-1/2}^{n+1} &= E_{\text{JMAX}-1/2} \theta_{bc}^{n+1} + F_{\text{JMAX}-1/2}. \end{aligned} \quad (3.25)$$

This specification of θ_{bc}^{n+1} will insure no conductive heat flux across the outer plasma boundary which is an appropriate condition for a plasma expanding into a vacuum. Since the boundary is moving in the Lagrangian scheme, it will always be a plasma-vacuum interface and no heat flux can be conducted across it.

The BUCKY-1 subroutine structure, as in PHD-IV [1], closely follows this algorithm for solving the temperature equations. The matrices and vector, α , \mathbf{a} , ω , γ , and β , are evaluated in the subroutine MATRIX and the matrices and vectors, \mathbf{A} , \mathbf{B} , \mathbf{C} , \mathbf{D} , \mathbf{E} , \mathbf{F} , are evaluated in the subroutine ABCPL2. The final solution for the temperatures, Eq. (3.20), is executed in subroutine ENERGY. The boundary conditions are obtained from the subroutine TEMPBC. The segregation of this algorithm into these subroutines was done to isolate the numerical analysis from the physics of the code. Subroutine PLSCF2 takes physical quantities, ω_e , K_e , etc., and combines them into quantities that are used for the numerical solution. In this sense it is the interface routine between the physics and numerical parts of the code. To add new terms to the temperature equations, only PLSCF2 (and PLSCF1 for the 1-T option) needs to be changed, minimizing the chance of disturbing the numerics of ABCPL2.

The difference method used here is a backward substitution solution to the implicit Crank-Nicholson difference scheme. All values of θ are evaluated at both t^n and t^{n+1} , hence we cannot express θ^{n+1} in terms of only variables at t^n . This implicit numerical scheme requires the solution of a matrix equation. Because we are solving two coupled equations and the usual scalar coefficients are now matrices, the matrix to be inverted is block tridiagonal with 2×2 blocks. For linear equations the Crank-Nicholson scheme is unconditionally stable and accurate to order $(\Delta t)^2$ and $(\Delta x)^2$ and will generally allow much larger time steps for this diffusion equation than an explicit scheme. For this nonlinear problem, however, stability problems can arise unless the time step is restricted, as is done in subroutine TIMING and discussed in Section 12.

3.4. Coefficients and Source Terms in the Energy Equations

3.4.1. Thermal Conductivity

The conduction coefficients are the classical, Spitzer values of thermal conductivity and electron-ion coupling [23]. The electron thermal conductivity is given by:

$$K_e = 20 \left(\frac{2}{\pi} \right)^{3/2} \frac{(k_B T_e)^{5/2} k_B \varepsilon \delta_T}{m_e^{1/2} e^4 Z \ln \Lambda_{ei}} \quad (3.26)$$

where:

$$\varepsilon \delta_T = \frac{0.43 Z}{(3.44 + Z + 0.26 \ln Z)}$$

$$\ln \Lambda_{ei} = \max \left\{ 1, \ln \left(\frac{3}{2e^3} \right) \left(\frac{k_B^3 T_e^3}{\pi n_e} \right)^{1/2} \frac{1}{Z} \right\}$$

n_e = electron number density.

The ion thermal conductivity is given by:

$$K_i = 20 \left(\frac{2}{\pi} \right)^{3/2} \frac{(k_B T_i)^{5/2} k_B}{m_i^{1/2} e^4 Z^4 \ln \Lambda_{ii}} \quad (3.27)$$

where

$$\ln \Lambda_{ii} = \max \left\{ 1, \ln \left(\frac{3}{2e^3 Z^2} \right) \left(\frac{k_B^3 T_i^3}{\pi n_e} \right)^{1/2} \left(\frac{1}{Z^{1/2}} \right) \right\}.$$

In finite difference form the thermal conductivities must be evaluated on the zone boundaries, hence averaged quantities from the adjacent zone centers must be used. This average is taken using the harmonic mean:

$$r^{\delta-1} K_e \frac{\partial T_e}{\partial r} \simeq \frac{r^{\delta-1}}{\frac{\Delta r_j^+}{K_{e_j}^+} + \frac{\Delta r_j^-}{K_{e_j}^-}} \Delta T_e, \quad (3.28)$$

where

$$\Delta r_j^+ = r_{j+1} - r_j \quad (3.29)$$

$$\Delta r_j^- = r_j - r_{j-1} \quad (3.30)$$

$$\begin{aligned}
K_{e_j}^+ &= \frac{C_2 T_{e_j}^2 T_{e_{j+1/2}}^{1/2}}{(4 + Z_{j+1/2}) (\ln \Lambda_{ei})_{j+1/2}} \\
K_{e_j}^- &= \frac{C_2 T_{e_j}^2 T_{e_{j-1/2}}^{1/2}}{(4 + Z_{j-1/2}) (\ln \Lambda_{ei})_{j-1/2}}.
\end{aligned} \tag{3.31}$$

A similar expression is used for the ions, with

$$\begin{aligned}
K_i^+ &= \frac{C_1 T_{i_j}^2 T_{i_{j+1/2}}^{1/2}}{(\Lambda_{j+1/2})^{1/2} (Z_{j+1/2})^4 (\ln \Lambda_{ii})_{j+1/2}} \\
K_i^- &= \frac{C_1 T_{i_j}^2 T_{i_{j-1/2}}^{1/2}}{(\Lambda_{j-1/2})^{1/2} (Z_{j-1/2})^4 (\ln \Lambda_{ii})_{j-1/2}}.
\end{aligned} \tag{3.32}$$

These expressions will most heavily weight the lowest conductivity in the zones centered at $j + 1/2$ or $j - 1/2$.

In the presence of strong thermal gradients, that is large fluxes, the diffusion approximation can break down and predict unphysically large thermal fluxes. To adjust for this, the electron thermal conduction is augmented with a flux limiter. This maximum permissible flux is defined in the classical manner:

$$q_{\max} = \frac{3\sqrt{3}}{8} (n_e k_B T_e) \left(\frac{k_B T_e}{m_e} \right)^{1/2}. \tag{3.33}$$

In finite difference form, this is expressed as

$$q_{\max_j}^{n+1/2} = C_3 (n_{e_{j-1/2}}^{n+1/2} + n_{e_{j+1/2}}^{n+1/2}) T_{e_j}^{n+1/2} [(T_{e_{j-1/2}}^{n+1/2})^{1/2} + (T_{e_{j+1/2}}^{n+1/2})^{1/2}]. \tag{3.34}$$

Note that this quantity is evaluated on a zone boundary. The electron and ion thermal conductivities and the electron thermal flux limit are computed in the subroutine PCOND2.

The flux limit is implemented by redefining the electron element of the \mathbf{a} matrix as

$$a_{22_j} = \frac{(r_j^{n+1/2})^{\delta-1}}{\frac{\Delta r_{j+1/2}}{K_{e_j}^+} + \frac{\Delta r_{j-1/2}}{K_{e_j}^-} + \frac{|T_{e_{j+1/2}}^{n+1/2} - T_{e_{j-1/2}}^{n+1/2}|}{q_{\max_j}}}. \tag{3.35}$$

This quantity is computed in subroutine PLSCF2.

3.4.2. Electron-Ion Coupling Coefficient

The electron and ion temperatures are coupled by the expression

$$\frac{\partial T_e}{\partial t} = \frac{T_i - T_e}{t_{ei}}. \quad (3.36)$$

In terms of the electron and ion diffusion equations this expression becomes

$$C_{v_e} \frac{\partial T_e}{\partial t} = \dots + \frac{C_{v_e}}{t_{ei}} (T_i - T_e) + \dots$$

hence, the definition of the coupling coefficient is

$$\omega_c = \frac{C_{v_e}}{t_{ei}} = C_{v_e} \nu_{ei} \quad (3.37)$$

where:

$$\nu_{ei} = \frac{8(2\pi)^{1/2}}{3} m_e^{1/2} e^4 N_A^2 \left(\frac{Z}{A}\right)^2 \frac{\ln \Lambda_{ei}}{(k_B T_e)^{3/2}} \rho \quad (3.38)$$

N_A = Avogadro's number

A = ion atomic weight

Z = ion charge

C_{v_e} = electron specific heat.

In finite difference form this is

$$\omega_{c_{j-1/2}} = C_{28} C_{v_{e,j-1/2}} \left(\frac{Z_{j-1/2}}{A_{j-1/2}}\right)^2 \frac{(\ln \Lambda_{ei})_{j-1/2}}{V_{j-1/2} (T_{e_{j-1/2}})^{3/2}}, \quad (3.39)$$

where all quantities are evaluated at time level $n + 1/2$. This coefficient is computed in subroutine OMEGAC.

3.4.3. Coupling to the Radiation Field

The electron temperature equation is explicitly coupled to the radiation field through emission and absorption terms. The radiative transfer models used to determine these terms are described in Section 4.

The emission term is simply computed as

$$J = 4\sigma_{SB} V \sigma_P^E T_e^4 \quad (3.40)$$

where

σ_{SB} = Stefan-Boltzmann constant

V = specific volume

σ_P^E = Planck emission opacity

T_e = electron temperature.

For multigroup calculations this term has a corresponding multigroup value, J^g , such that

$$J = \sum_{g=1}^G J^g, \quad (3.41)$$

where

$$J_g = \frac{8\pi(kT_e)^4}{c^2 h^3} \sigma_{P,g}^E \int_{x_g}^{x_{g+1}} dx \frac{x^3}{e^x - 1},$$

$$x_g \equiv \frac{h\nu_g}{kT_e}.$$

The absorption term is given by

$$A = c\sigma_P^A E_R \quad (3.42)$$

where

c = speed of light

σ_P^A = Planck absorption opacity

E_R = radiation energy density.

In multifrequency group calculations this is given by

$$A = c \sum_{g=1}^G \sigma_P^g E_R^g. \quad (3.43)$$

These terms are SRE2B (emission) and SER2B (absorption) in the code and they are computed in RADTRn (n = 1, 2, or 3, depending on the transport model). They contribute to the electron source term, BET22B, which is computed in PLSCF2.

3.4.4. Coupling to the Thermonuclear Burn Reaction Products

The charged particle reaction products from the fusion reactions are transported through the plasma and slowed down as described in Section 9. This calculation is done independent of the plasma hydrodynamics and is coupled to the hydrodynamics explicitly through source terms in the electron and ion temperature equations. The energy source in each zone due to charged particle energy redeposition to electrons and ions is accumulated in the variables SETN2B and SNTN2B by the routine TNBURN. These quantities then contribute to the BET12B and BET22B source terms in the temperature equations. These are computed in PLSCF2.

Neutrons produced during the fusion burn can redeposit their energy back in the target. The neutron energy deposition rate is computed in TNBURN and stored in the array SNEU2B. It then contributes to the ion source term BET12B in PLSCF2.

3.4.5. Ion Beam and Laser Energy Deposition Source Terms

The deposited energy from the incident ion beam or target debris is computed in IONDEP. The energy is put into the vector SION2B for the source to electrons. This source rate contributes to the BET22B term in the energy equations. It is computed in PLSCF2. The laser energy deposited is put into the vector SLAS2B, and is handled similar to SION2B. It is computed in subroutine LASDEP.

4. Radiation Transport Models

4.1. Multigroup Diffusion

In the multigroup diffusion option, the radiation transport equation can be written as:

$$V \frac{\partial E_R^g}{\partial t} = \frac{\partial}{\partial m_o} \left(r^{\delta-1} \kappa_R^g \frac{\partial E_R^g}{\partial r} \right) - \frac{4}{3} E_R^g \dot{V} - c \sigma_{P,A}^g E_R^g + J^g, \quad g = 1, \dots, G \quad (4.1)$$

where

E_R is the radiation energy density,

κ_R^g is the radiation conductivity for frequency group g ,

J^g is the rate of radiation emitted by the plasma into group g ,

$\sigma_{P,A}^g$ is the Planck absorption opacity for group g ,

$\sigma_{P,E}^g$ is the Planck emission opacity for group g ,

σ_R^g is the Rosseland opacity for group g .

Mathematically,

$$E_R^g = \int_{h\nu_g}^{h\nu_{g+1}} d h\nu E_R(r, h\nu, t) \quad (4.2)$$

$$A^g = c \sigma_{P,A}^g E_R^g \quad (4.3)$$

$$J^g = \frac{8\pi k T_e^4}{c^2 h^3} \sigma_{P,E}^g \int_{x_g}^{x_{g+1}} dx \frac{x^3}{e^x - 1}; \quad x = \frac{h\nu}{kT_e} \quad (4.4)$$

$$\kappa_R^g = \frac{cV}{3\sigma_R^g} \quad (4.5)$$

$$A = \sum_{g=1}^G A^g \quad (4.6)$$

$$J = \sum_{g=1}^G J^g. \quad (4.7)$$

This set of $G+1$ equations is solved individually and the terms A and J are computed. These terms are then explicitly included in the electron temperature equation which is solved next.

The multigroup equations are written in finite difference form as:

$$\begin{aligned}
\frac{E_R^{g,n+1} - E_R^{g,n}}{\Delta t^{n+1/2}} &= \frac{1}{\Delta m_{o_{j-1/2}}} \left[\frac{r_j^{\delta-1}}{\left(\frac{\Delta r}{K_R^g}\right)_j + \left(\frac{\Delta E_R^g}{F_R^g}\right)_j} (E_{R_{j+1/2}}^{g,n+1} - E_{R_{j-1/2}}^{g,n+1}) \right. \\
&\quad \left. - \frac{r_{j-1}^{\delta-1}}{\left(\frac{\Delta r}{K_R^g}\right)_{j-1} + \left(\frac{\Delta E_R^g}{F_R^g}\right)_{j-1}} (E_{R_{j-1/2}}^{g,n+1} - E_{R_{j-3/2}}^{g,n+1}) \right] \\
&\quad - E_{R_{j-1/2}}^{g,n+1} \frac{4}{3} \dot{V}_{n-1/2} - c\sigma_{P,A_{j-1/2}}^g E_R^{g,n+1} + J_R^{g,n+1}
\end{aligned} \tag{4.8}$$

for group g . The quantity F_R is the flux limiter. This is reduced using the notation

$$\begin{aligned}
\alpha_{j-1/2} (E_{R_{j-1/2}}^{g,n+1} - E_{R_{j-1/2}}^{g,n}) &= a_j (E_{R_{j+1/2}}^{g,n+1} - E_{R_{j-1/2}}^{g,n+1}) - a_{j-1} (E_{R_{j-1/2}}^{g,n+1} - E_{R_{j-3/2}}^{g,n+1}) \\
&\quad - \gamma_{j-1/2} E_{R_{j-1/2}}^{g,n+1} - \omega_{j-1/2} E_{R_{j-1/2}}^{g,n+1} + \beta_{j-1/2}
\end{aligned} \tag{4.9}$$

where:

$$\begin{aligned}
\alpha_{j-1/2} &= V_{j-1/2} \Delta m_{o_{j-1/2}} / \Delta t^{n-1/2} \\
a_j &= r_j^{\delta-1} / \left(\left(\frac{\Delta r}{K_R^g}\right)_j + \frac{\Delta E_{R_j}^g}{F_{R_j}^g} \right) \\
\gamma_{j-1/2} &= (4 \dot{V}_{j-1/2} / 3) \Delta m_{o_{j-1/2}} \\
\omega_{j-1/2} &= c\sigma_{P,A_{j-1/2}}^g \Delta m_{o_{j-1/2}} \\
\beta_{j-1/2} &= J_{j-1/2}^g \Delta m_{o_{j-1/2}}
\end{aligned}$$

The coefficients α , a , γ , ω , and β should in principle be evaluated at $t^{n+1/2}$. However, values at that time are not yet known so they are evaluated at t^n . These terms are regrouped in the familiar form

$$-A_{j-1/2} E_{R_{j+1/2}}^{g,n+1} + B_{j-1/2} E_{R_{j-1/2}}^{g,n+1} - C_{j-1/2} E_{R_{j-3/2}}^{g,n+1} = D_{j-1/2}, \tag{4.10}$$

where

$$A_{j-1/2} = a_j$$

$$B_{j-1/2} = \alpha_{j-1/2} + a_j + a_{j-1} + \gamma_{j-1/2} + \omega_{j-1/2}$$

$$C_{j-1/2} = a_{j-1}$$

$$D_{j-1/2} = \alpha_{j-1/2} E_{R_{j-1/2}}^{g,n} + \beta_{j-1/2}.$$

We then express the solution as

$$E_{R_{j-1/2}}^{g,n+1} = EE_{j-1/2} * E_{R_{j+1/2}}^{g,n+1} + FF_{j-1/2} \quad 1 \leq j \leq \text{JMAX} \quad (4.11)$$

$$E_{R_{\text{JMAX}+1/2}}^{n+1} = E_{R_{BC}} \quad \text{Boundary Condition.}$$

Then we can compute

$$EE_{j-1/2} = A_{j-1/2} / (B_{j-1/2} - C_{j-1/2} * EE_{j-3/2}) \quad (4.12)$$

$$FF_{j-1/2} = (D_{j-1/2} + C_{j-1/2} * FF_{j-3/2}) / (B_{j-1/2} - C_{j-1/2} * EE_{j-3/2}) \quad (4.13)$$

for $2 < j \leq \text{JMAX}$ and

$$EE_{1/2} = A_{1/2} / B_{1/2} \quad (4.14)$$

$$FF_{1/2} = D_{1/2} / B_{1/2} \quad (4.15)$$

for $j = 1$. The above radiative boundary conditions, which apply to spherical plasmas, are the default. The radiative boundary conditions can be adjusted with the parameter ISW(9).

Once the radiation specific energies have been computed, then the absorption is computed as:

$$A_{j-1/2}^g = c\sigma_{P,A_{j-1/2}}^g E_{R_{j-1/2}}^{g,n+1} \quad (4.16)$$

$$A_{j-1/2} = \sum_{g=1}^G A_{j-1/2}^g. \quad (4.17)$$

4.2. Method of Short Characteristics

(To be supplied)

4.3. Variable Eddington Model

The multigroup variable Eddington method in BUCKY-1 is based on the model in PHD-IV. This is a moment expansion of the photon transport equation in the angular variable where only the first two moment equations are kept. These moment equations are given by:

$$\mu^0 : \frac{\partial E_\nu}{\partial t} + \frac{1}{r^{\alpha-1}} \frac{\partial}{\partial r} (r^{\alpha-1} F_\nu) + c\sigma_{a,\nu} E_\nu = J^\nu \quad (4.18)$$

$$\mu^1 : \frac{1}{c} \frac{\partial F_\nu}{\partial t} + c \left[\frac{\partial P_\nu}{\partial r} + \frac{\alpha-1}{2r} (3P_\nu - E_\nu) \right] + (\sigma_{a,\nu} + \sigma_{s,\nu}) F_\nu = 0. \quad (4.19)$$

The specific intensity $I_\nu(r, \mu, t)$ is related to the radiation energy density $E_\nu(r, t)$, the radiation flux $F_\nu(r, t)$, and radiation pressure $P_\nu(r, t)$, by:

$$E_\nu(r, t) = \frac{2\pi}{c} \int_{-1}^1 d\mu I_\nu(r, \mu, t)$$

$$F_\nu(r, t) = \frac{2\pi}{c} \int_{-1}^1 d\mu \mu I_\nu(r, \mu, t)$$

$$P_\nu(r, t) = \frac{2\pi}{c} \int_{-1}^1 d\mu \mu^2 I_\nu(r, \mu, t) \quad .$$

Other definitions are:

$\alpha = 3$ spherical, $\alpha = 1$ planar geometry

$\sigma_{a,\nu}$ = absorption cross section

$\sigma_{s,\nu}$ = scattering cross section

J_ν = emission source function.

This truncated set of equations is closed by a semi-empirical expression for the pressure tensor

$$P_\nu = f_\nu E_\nu, \quad (4.20)$$

where f_ν is called the Eddington factor. A major requirement of f_ν is that it reduce to a value of 1/3 in optically thick regions and to a value of 1 in optically thin regions. This gives the correct result for both diffusion and free-streaming radiation.

The frequency dependence of the radiation equations is treated using a multifrequency group formalism. The spectrum is divided into G groups and the equations are written as:

$$\frac{\partial E^g}{\partial t} + \frac{\partial \tilde{F}^g}{\partial r^\alpha} + c\sigma_{P,A}^g E^g = J^g \quad g = 1, \dots, G \quad (4.21)$$

$$\frac{1}{c} \frac{\partial \tilde{F}^g}{\partial t} + \alpha c \left(\frac{3f^g - 1}{2f^g} \right) \frac{\partial}{\partial r} (r^{\alpha-1} f^g E^g) + \alpha c \left(\frac{1 - f^g}{2f^g} \right) r^{\alpha-1} \frac{\partial}{\partial r} (f^g E^g) + \sigma_R^g \tilde{F}^g = 0 \quad (4.22)$$

where

$$E^g = \int_g^{g+1} E^\nu d\nu \quad (4.23)$$

$$F^g = \int_g^{g+1} F^\nu d\nu \quad (4.24)$$

$$f^g = \frac{1}{3} \left[1 + \frac{2}{c} \frac{F^g}{E^g} \mu_i(g) \right] \quad (4.25)$$

$$\sigma_P^g = \int_g^{g+1} B^\nu(T) \sigma_a^\nu d\nu / \int_g^{g+1} B^\nu(T) d\nu \quad (4.26)$$

$$(\sigma_R^g)^{-1} = \int_g^{g+1} (\sigma_a^\nu + \sigma_s^\nu)^{-1} \frac{\partial B^\nu(T)}{\partial T} d\nu / \int_g^{g+1} \frac{\partial B^\nu}{\partial t} d\nu \quad (4.27)$$

and

$$\tilde{F}^g = \alpha r^{\alpha-1} F^g. \quad (4.28)$$

This set of G one-group equations can now be solved using an implicit numerical method. When the number of frequency groups is specified to be one, then a one temperature variable Eddington treatment is used. The variable Eddington equations require no flux limiting in their solution.

In the case of the diffusion limit we have

$$f^g \rightarrow 1/3 \quad (4.29)$$

and

$$\frac{1}{c} \frac{\partial \tilde{F}^g}{\partial t} \ll \sigma_R^{g_{Fg}} \quad (4.30)$$

hence, we get

$$\alpha c r^{\alpha-1} \frac{\partial}{\partial r} \frac{E^g}{3} + \sigma_R^{g_{Fg}} = 0 \quad (4.31)$$

or

$$\tilde{F}^g = -\frac{\alpha c}{3\sigma_R^g} r^{\alpha-1} \frac{\partial}{\partial r} E^g \quad (4.32)$$

or

$$F^g = -\frac{c}{3\sigma_R^g} \frac{\partial E^g}{\partial r} \quad (\text{Fick's Law}). \quad (4.33)$$

In the limit of free streaming:

$$f^g \rightarrow 1 \quad (4.34)$$

$$\sigma_R^g \rightarrow 0 \quad (4.35)$$

hence we get

$$\frac{1}{c} \frac{\partial \tilde{F}^g}{\partial t} + \alpha c \frac{\partial}{\partial r} (r^{\alpha-1} E^g) = 0. \quad (4.36)$$

Plugging this into the “energy equation” gives us a wave-like solution.

Next we write these two equations in finite difference form using a fully implicit differencing scheme as follows:

$$\frac{E_{j-1/2}^{n+1} - E_{j-1/2}^n}{\Delta t^{n+1/2}} + \frac{\tilde{F}_j^{n+1} - \tilde{F}_{j-1}^{n+1}}{r_j^\alpha - r_{j-1}^\alpha} + c \sigma_{j-1/2}^P E_{j-1/2}^{n+1} = J_{j-1/2}^{n+1/2} \quad (4.37)$$

$$\begin{aligned} & \frac{\tilde{F}_j^{n+1} - \tilde{F}_j^n}{\Delta t^{n+1/2}} + \alpha c \left(\frac{3f-1}{2f} \right)_j^n \frac{(r^{\alpha-1} f E)_{j+1/2}^{n+1} - (r^{\alpha-1} f E)_{j-1/2}^{n+1}}{\frac{1}{2}(r_{j+1} - r_{j-1})} \\ & + \alpha c \left(\frac{1-f}{2f} \right)_j^n r_j^{\alpha-1} \frac{(f E)_{j+1/2}^{n+1} - (f E)_{j-1/2}^{n+1}}{\frac{1}{2}(r_{j+1} - r_{j-1})} + \sigma_j^R \tilde{F}_j^{n+1} = 0 \end{aligned} \quad (4.38)$$

where we have dropped the group index g for convenience. The flux equation is written again for

$$\frac{\tilde{F}_{j-1}^{n+1} - \tilde{F}_{j-1}^n}{\Delta t^{n+1/2}} = \text{r.h.s.}, \quad (4.39)$$

and these two equations are solved for

$$\tilde{F}_j^{n+1} - \tilde{F}_{j-1}^{n+1}.$$

This expression is substituted into the energy equation and terms multiplying $E_{j+1/2}^{n+1}$, $E_{j-1/2}^{n+1}$, and $E_{j-3/2}^{n+1}$ are collected as

$$-A_{j-1/2} E_{j+1/2}^{n+1} + B_{j-1/2} E_{j-1/2}^{n+1} - C_{j-1/2} E_{j-3/2}^{n+1} = D_{j-1/2} \quad (4.40)$$

where

$$A_{j-1/2} = \left\{ \frac{1}{r_j^\alpha - r_{j-1}^\alpha} \frac{\alpha c^2 \Delta t^2}{1 + c \Delta t \sigma_j^R} \frac{f_{j+1/2}}{\Delta r_j} \left[\left(\frac{3f-1}{2f} \right)_j^n r_{j+1/2}^{\alpha-1} + \left(\frac{1-f}{2f} \right)_j^n r_j^{\alpha-1} \right] \right\} \quad (4.41)$$

$$\begin{aligned} B_{j-1/2} = & \frac{\alpha c^2 \Delta t^2}{r_j^\alpha - r_{j-1}^\alpha} f_{j-1/2} \left\{ \frac{1}{1 + c \Delta t \sigma_j^R} \frac{1}{\Delta r_j} \left[\left(\frac{3f-1}{2f} \right)_j^n r_{j-1/2}^{\alpha-1} + \left(\frac{1-f}{2f} \right)_j^n r_j^{\alpha-1} \right] \right. \\ & \left. + \frac{1}{1 + c \Delta t \sigma_{j-1}^R} \frac{1}{\Delta r_{j-1}} \left[\left(\frac{3f-1}{2f} \right)_{j-1}^n r_{j-1/2}^{\alpha-1} + \left(\frac{1-f}{2f} \right)_{j-1}^n r_{j-1}^{\alpha-1} \right] \right\} + 1 + c \Delta t \sigma_{j-1/2}^P \end{aligned} \quad (4.42)$$

$$C_{j-1/2} = \frac{1}{r_j^\alpha - r_{j-1}^\alpha} \frac{1}{1 + c \Delta t \sigma_{j-1}^R} \frac{f_{j-3/2}}{\Delta r_{j-1}} \left[\left(\frac{3f-1}{2f} \right)_{j-1}^n r_{j-3/2}^{\alpha-1} + \left(\frac{1-f}{2f} \right)_{j-1}^n r_{j-1}^{\alpha-1} \right] \quad (4.43)$$

$$D_{j-1/2} = \Delta t J_{j-1/2}^{n+1/2} + E_{j-1/2}^n + \frac{\Delta t}{r_j^\alpha - r_{j-1}^\alpha} \left[\frac{\tilde{F}_{j-1}^n}{1 + c \Delta t \sigma_{j-1}^R} - \frac{\tilde{F}_j^n}{1 + c \Delta t \sigma_j^R} \right]. \quad (4.44)$$

In terms of some code variables, these expressions reduce to:

$$\begin{aligned} RAD_{j-1/2} &= r_j^\alpha - r_{j-1}^\alpha & RD_j &= \frac{r_{j+1} - r_{j-1}}{2} & RS2B_{j-1/2} &= r_{j-1/2}^{\alpha-1} \\ ED3_j &= \left(\frac{3f-1}{2f} \right)_j^n & ED1_j &= \left(\frac{1-f}{2f} \right)_j^n \\ A1_j &= \frac{1}{1 + c \Delta t \sigma_j^R} & T1 &= \alpha c^2 \Delta t^2 \end{aligned} \quad (4.45)$$

where all values in these coefficients are taken at t^{n+1} . Substituting, we get:

$$A_{j-1/2} = \frac{T1}{RAD_{j-1/2}} A1_j \frac{f_{j+1/2}}{RD_j} [ED3_j RS2B_{j+1/2} + ED1_j RS1B_j] \quad (4.46)$$

$$B_{j-1/2} = \frac{T1}{RAD_{j-1/2}} f_{j-1/2} \left[\frac{A1_j}{RD_j} (ED3_j RS2B_{j-1/2} + ED1_j RS1B_j) \right. \\ \left. + \frac{A1_{j-1}}{RD_{j-1}} (ED3_{j-1} RS2B_{j-1/2} + ED1_{j-1} RS1B_{j-1}) \right] + 1 + c\Delta t \sigma_{j-1/2}^P \quad (4.47)$$

$$C_{j-1/2} = \frac{T1}{RAD_{j-1/2}} A1_{j-1} \frac{f_{j-3/2}}{RD_{j-1}} [ED3_{j-1} RS2B_{j-3/2} + ED1_{j-1} RS1B_{j-1}] \quad (4.48)$$

$$D_{j-1/2} = E_{j-1/2}^n + \Delta t J_{j-1/2}^{n+1/2} + \frac{\Delta t}{RAD_{j-1/2}} [\tilde{F}_{j-1}^n A1_{j-1} - \tilde{F}_j^n A1_j]. \quad (4.49)$$

This tridiagonal set of equations is now solved in the standard way using a forward sweep of the mesh and then a backward substitution, just as we do with the electron and ion temperature equations. That is,

$$E_{j-1/2} = EE_{j-1/2} E_{j+1/2} + FF_{j-1/2} \quad (4.50)$$

where

$$EE_{j-1/2} = \frac{A_{j-1/2}}{B_{j-1/2} - C_{j-1/2} EE_{j-3/2}} \quad (4.51)$$

$$FF_{j-1/2} = \frac{D_{j-1/2} + C_{j-1/2} FF_{j-3/2}}{B_{j-1/2} - C_{j-1/2} EE_{j-3/2}}. \quad (4.52)$$

Once the energy densities are computed, the flux is computed as

$$\tilde{F}_j^{n+1} = \frac{\tilde{F}_j^n}{1 + c\Delta t \sigma_j^R} - \frac{\alpha c^2 \Delta t}{1 + c\Delta t \sigma_j^R} \frac{1}{\Delta r_j} \left\{ \left(\frac{3f-1}{2f} \right)_j^n [(r^{\alpha-1} fE)_{j+1/2}^{n+1} \right. \\ \left. - (r^{\alpha-1} fE)_{j-1/2}^{n+1}] + \left(\frac{1-f}{2f} \right)_j^n r_j^{\alpha-1} [(fE)_{j+1/2}^{n+1} - (fE)_{j-1/2}^{n+1}] \right\}. \quad (4.53)$$

The boundary conditions for these equations must be carefully applied. There are two different cases of interest depending on whether the boundary zone is optically thick or thin. At the boundary, the radiation field can be specified by an incoming component I_- and an outgoing component I_+ . For streaming radiation

$$\begin{aligned}
I(\mu) &= I_+ \delta(\mu - 1) & \mu &\geq 0 \\
I(\mu) &= 0 & \mu &< 0 \\
I(\mu) &= 0 & \mu &\geq 0 \\
I(\mu) &= I_- \delta(\mu + 1) & \mu &< 0
\end{aligned} \tag{4.54}$$

which gives for the total boundary flux

$$F = cE - 2F_- . \tag{4.55}$$

For optically thin boundary zones we use the form

$$F_{\text{JMAX}} = cE_{\text{JMAX}-1/2} - 2F_- , \tag{4.56}$$

where the energy density is evaluated at the zone center. This is admissible because in the thin case the energy density is nearly uniform over the boundary zone.

For piecewise isotropic radiation

$$\begin{aligned}
I(\mu) &= I_+ & \mu &\geq 0 \\
I(\mu) &= I_- & \mu &< 0 ,
\end{aligned} \tag{4.57}$$

which gives for the total boundary flux

$$F = \frac{c}{2} E - 2F_- , \tag{4.58}$$

where F_- is the incoming flux. For the case of thick boundary zones E_{JMAX} is extrapolated from $E_{\text{JMAX}-1/2}$ using the expression

$$E_{\text{JMAX}} = -c \left(\frac{f_{\text{JMAX}-1/2} E_{\text{JMAX}} - f_{\text{JMAX}-1/2} E_{\text{JMAX}-1/2}}{\frac{1}{2} \sigma_{R_{\text{JMAX}-1/2}} \Delta r_{\text{JMAX}-1/2}} \right) . \tag{4.59}$$

The boundary flux for the thick case then becomes

$$F_{\text{JMAX}} = \frac{c}{2} \left(\frac{f_{\text{JMAX}-1/2}}{\text{DENOM}} \right) E_{\text{JMAX}-1/2} - 2 \left(\frac{f_{\text{JMAX}-1/2}}{\text{DENOM}} \right) F_- \tag{4.60}$$

where $\text{DENOM} = f_{\text{JMAX}-1/2} + \frac{1}{4}\sigma_{R_{\text{JMAX}-1/2}}\Delta r_{\text{JMAX}-1/2}$. These forms of the boundary conditions require that the A, B, C , and D coefficients be reformulated for the boundary zone. For the thin boundary condition

$$\begin{aligned}
A_{\text{JMAX}} &= 0 \\
B_{\text{JMAX}} &= 1 + c\Delta t\sigma_{j-1/2}^P + \frac{\alpha c\Delta t r_j^{\alpha-1}}{r_j^\alpha - r_{j-1}^\alpha} + \frac{\alpha c^2\Delta t^2}{1 + c\Delta t\sigma_{j-1}^R} \frac{f_{j-1/2}}{r_j^\alpha - r_{j-1}^\alpha} \frac{1}{\Delta r_{j-1}} \\
&\quad \left[\left(\frac{3f-1}{2f} \right)_j^n r_j^{\alpha-1} + \left(\frac{1-f}{2f} \right)_{j-1}^n r_{j-1}^{\alpha-1} \right] \\
C_{\text{JMAX}} &= \frac{\alpha c^2\Delta t^2}{1 + c\Delta t\sigma_{j-1}^R} \frac{f_{j-3/2}}{r_j^\alpha - r_{j-1}^\alpha} \frac{1}{\Delta r_{j-1}} \left[\left(\frac{3f-1}{2f} \right)_{j-1}^n r_{j-3/2}^{\alpha-1} + \left(\frac{1-f}{2f} \right)_{j-1}^n r_{j-1}^{\alpha-1} \right] \\
D_{\text{JMAX}} &= E_{j-1/2}^n + \Delta t J_{j-1/2}^{n+1/2} + \frac{\Delta t}{r_j^\alpha - r_{j-1}^\alpha} \left[2\tilde{F}_-^{n+1} + \frac{\tilde{F}_{j-1}^n}{1 + c\Delta t\sigma_{j-1}^R} \right] \tag{4.61}
\end{aligned}$$

where $j = \text{JMAX}$. For the thick case

$$\begin{aligned}
A_{\text{JMAX}} &= 0 \\
B_{\text{JMAX}} &= 1 + c\Delta t\sigma_{j-1/2}^R + \left(\frac{2\alpha c\Delta t r_j^{\alpha-1}}{r_j^\alpha - r_{j-1}^\alpha} \right) \left(\frac{\frac{1}{2}f_{j-1/2}}{f_{j-1/2} + \frac{1}{4}\sigma_{j-1/2}^R\Delta r_{j-1/2}} \right) \\
&\quad + \frac{\alpha c^2\Delta t^2}{1 + c\Delta t\sigma_{j-1}^R} \frac{f_{j-1/2}}{(r_j^\alpha - r_{j-1}^\alpha)} \frac{1}{\Delta r_{j-1}} \left[\left(\frac{3f-1}{2f} \right)_{j-1}^n r_j^{\alpha-1} + \left(\frac{1-f}{2f} \right)_{j-1}^n r_{j-1}^{\alpha-1} \right] \\
C_{\text{JMAX}} &= \frac{\alpha c^2\Delta t^2}{1 + c\Delta t\sigma_{j-1}^R} \frac{f_{j-3/2}}{(r_j^\alpha - r_{j-1}^\alpha)} \frac{1}{\Delta r_{j-1}} \left[\left(\frac{3f-1}{2f} \right)_{j-1}^n r_{j-3/2}^{\alpha-1} + \left(\frac{1-f}{2f} \right)_j^n r_{j-1}^{\alpha-1} \right] \\
D_{\text{JMAX}} &= E_{j-1/2}^n + \Delta t J_{j-1/2}^{n+1/2} \\
&\quad + \frac{\Delta t}{r_j^\alpha - r_{j-1}^\alpha} \left[\frac{2\tilde{F}_-^{n+1} + f_{j-1/2}}{f_{j-1/2} + \frac{1}{4}\sigma_{j-1/2}^R\Delta r_{j-1/2}} + \frac{\tilde{F}_{j-1}^n}{1 + c\Delta t\sigma_{j-1}^R} \right]. \tag{4.62}
\end{aligned}$$

The energy densities and fluxes are computed in RADTR1. The A , B , C , and D coefficients are obtained from ABCRD1.

A very important quantity in this transport technique is the Eddington factor. It is this factor that closes the set of moment equations and also determines the accuracy of the method. The Eddington factor is computed from a model of two concentric radiating spheres. The factor is given as

$$f^g = \frac{1}{3} \left[1 + \frac{2F^g}{cE^g} \mu_i^g \right] \quad (4.63)$$

where μ_i^g is the cosine of the angle between the point of interest and the surface of a sphere that is $2/3$ of a mean free path inward from the point of interest. Hence, f^g is determined by σ_P^g , F^g , and E^g . The values of F^g and E^g from the previous evaluation of multifrequency energy densities and fluxes are used to compute f^g . These computations are done in subroutine EDFACT. [For slab geometry the diffusion limit is always used (i.e., $f^g = 1/3$). This is not correct and should be fixed at some time.]

4.4. Non-LTE CRE Line Transport

4.4.1. Introduction

As has been noted in previous work [12, 13], multigroup radiation diffusion models, which are commonly used in radiation-hydrodynamics codes, can sometimes be very inaccurate for simulating the radiative properties of laboratory plasmas. This is especially true for plasmas which are optically thick to line radiation but optically thin to the continuum. This occurs for several reasons. First, resonant self-absorption — that is, the trapping of line radiation in their optically thick cores — can significantly inhibit the flow of radiation through the plasma. This cannot be accurately treated in “multigroup” models unless the photon energy grid is chosen such that individual lines are resolved. Second, high temperature laboratory plasmas are often not in local thermodynamic equilibrium (LTE). In many cases, the atomic level populations — and therefore the opacities — are a function

of not only the local temperature and density, but also the radiation field. Because of this, models utilizing table look-up opacities which depend only on the temperature and densities can be inaccurate. Third, radiation diffusion models are based on the assumption that the photon mean free paths are small compared to the plasma dimensions. This assumption is also not valid for many types of laboratory plasmas.

In this section, we describe the features of a radiation transport algorithm we have developed to investigate the radiative properties of high energy density plasmas. This is a non-LTE radiative transfer model, or collisional-radiative equilibrium (CRE) model, which can be used to calculate emission and absorption spectra, as well as radiative energy transport. Given a temperature and density distribution for a plasma, the CRE model computes atomic level populations and the radiative flux through the plasma. The models are 1-D, and can be applied to plasmas in planar, cylindrical, and spherical geometries. Opacity effects are considered in computing both the atomic level populations (via photoexcitation and photoionization) and the radiation flux.

4.4.2. Statistical Equilibrium Model

Atomic level populations are calculated by solving multilevel, steady-state atomic rate equations self-consistently with the radiation field. For multilevel systems, the rate equation for atomic level i can be written as:

$$\frac{dn_i}{dt} = -n_i \sum_{j \neq i}^{N_L} W_{ij} + \sum_{j \neq i}^{N_L} n_j W_{ji} = 0, \quad (4.64)$$

where W_{ij} and W_{ji} represent the depopulating and populating rates between levels i and j , n_i is the number density of level i , and N_L is the total number of levels in the system. For upward transitions ($i < j$),

$$W_{ij} = B_{ij} \bar{J}_{ij} + n_e C_{ij} + \beta_{ij} + n_e \gamma_{ij}, \quad (4.65)$$

while for downward transitions,

$$W_{ji} = A_{ji} + B_{ji} \bar{J}_{ji} + n_e D_{ji} + n_e (\alpha_{ji}^{RR} + \alpha_{ji}^{DR}) + n_e^2 \delta_{ji}, \quad (4.66)$$

where n_e is the electron density and $\bar{J}_{ij} (\equiv \int \phi_{ij}(\nu) J_\nu d\nu)$ is the frequency-averaged mean intensity of the radiation field for a bound-bound transition. The rate coefficients in the above equations are:

$$\begin{aligned} A_{ij} &= \text{spontaneous emission} \\ B_{ij} &= \text{stimulated absorption } (i < j) \text{ or emission } (i > j) \\ C_{ij} &= \text{collisional excitation} \\ D_{ij} &= \text{collisional deexcitation} \\ \alpha_{ij}^{RR} &= \text{radiative recombination} \\ \alpha_{ij}^{DR} &= \text{dielectronic recombination} \\ \beta_{ij} &= \text{photoionization plus stimulated recombination} \\ \gamma_{ij} &= \text{collisional ionization} \\ \delta_{ij} &= \text{collisional recombination.} \end{aligned}$$

Atomic cross sections for the above terms are described briefly in Section 4.4.4. In this detailed configuration accounting model each atomic level of a given gas species can in principle be coupled to any other level in that gas. The degree of coupling between levels depends on how the atomic data files are generated by ATBASE [20].

The statistical equilibrium equations depend on the atomic level populations in a nonlinear fashion (through the radiation intensity and electron density). Because of this, an iterative procedure is used to obtain atomic level populations which are self-consistent with the radiation field. At present, the coupled set of steady-state rate equations is solved using the LAPACK linear algebra package [24]. Besides inverting the statistical equilibrium

equation matrix to obtain the level populations, LAPACK also contains algorithms for improving the condition of the matrix via scaling, as well as iterative refinement. The overall procedure for computing the level populations is as follows:

1. Make an initial guess for population distributions (e.g., LTE, optically thin, or populations from previous hydrodynamics time step)
2. Compute radiative rate coefficients
3. Compute coefficients for statistical equilibrium matrix ($N_L \times N_L$)
4. Solve matrix for level populations
5. If new populations are consistent with previous iteration, calculation is complete; otherwise go back to step 2.

Steps 2 through 4 are performed one spatial zone at a time. This is possible because we employ an accelerated lambda iteration procedure (ALI) which utilizes the diagonal of the Λ -operator [25].

To improve the rate of convergence for this iterative procedure we utilize an acceleration technique based on the work of Ng [26, 27]. The Ng acceleration method is applied every several (typically 2 to 6) iterations to obtain updated solutions to the solution vector \mathbf{x} . In our case, the solution vector is the level population of a spatial zone. The “accelerated” solution is calculated from solutions obtained during the previous several iterations — that is, the evolution, or history, of the convergence becomes important. The accelerated solution vector after the n ’th iteration can be written as:

$$\mathbf{x}^n = \left(1 - \sum_{m=1}^M \alpha_m\right) \mathbf{x}^{n-1} + \sum_{m=1}^M \alpha_m \mathbf{x}^{n-m-1}, \quad (4.67)$$

where \mathbf{x}^{m-n} is the solution vector of the $(n-m)$ ’th iteration. The acceleration coefficients, α , are determined from the solution of

$$\mathbf{A}\alpha = \mathbf{b}, \quad (4.68)$$

where the elements of \mathbf{A} and \mathbf{b} are given by:

$$\begin{aligned} A_{ij} &= \sum_{d=1}^D (\Delta x_d^n - \Delta x_d^{n-i})(\Delta x_d^n - \Delta x_d^{n-j}), \\ b_i &= \sum_{d=1}^D \Delta x_d^n (\Delta x_d^n - \Delta x_d^{n-i}), \end{aligned} \quad (4.69)$$

and

$$\Delta x_d^k \equiv x_d^k - x_d^{k-i}.$$

The quantity x_d^k refers to the d 'th element of \mathbf{x} on iteration cycle k . The order of the acceleration method, M , represents the number of previous cycles used to compute the accelerated solution for \mathbf{x} .

In our radiative transfer code M can be chosen to have a value from 2 to 4. It is found that using $M = 2$ provides very good acceleration to the converged solution. This method has proven to be particularly valuable in improving the computational efficiency of our radiative transfer simulations.

4.4.3. Radiative Transfer Model

The CRE algorithms utilize an angle- and frequency-averaged escape probability model. The advantage of the escape probability model is that it is fast; i.e., it is a computationally efficient method for computing resonant self-absorption effects on both the non-LTE atomic level populations and the radiation flux. In this model, the stimulated absorption and emission rates can be written in terms of zone-to-zone coupling coefficients:

$$n_j^a B_{ji} \bar{J}_{ij} - n_i^a B_{ij} \bar{J}_{ij} = \begin{cases} -A_{ji} \sum_{e=1}^{N_D} n_j^e Q_{ji}^{ea} & (i < j) \\ A_{ij} \sum_{e=1}^{N_D} n_i^e Q_{ij}^{ea} & (i > j) \end{cases}$$

where Q^{ea} is defined as the probability a photon emitted in zone e is absorbed in zone a , n_i is the population density of level i , the superscripts e and a denote the emitting and absorbing zones, respectively, and N_D is the number of spatial zones. Our model utilizes a computationally efficient method for computing angle- and frequency-averaged

escape probability coupling coefficients in planar, cylindrical, and spherical geometries for Doppler, Lorentz, and Voigt line profiles. (This method is based largely on the work of J. Apruzese et al. [28]–[30]).

Consider first the 1-D planar geometry shown in Fig. 4.1. The distance traversed as a photon travels from point 1 to point 2 is z_{12}/μ , where $\mu \equiv \cos\theta$ and θ is the angle between the direction of propagation and the normal to the slab surface. In this geometry, the angle- and frequency-averaged escape probability, \bar{P}_e , can be computed directly:

$$\bar{P}_e(\tau_c) = \int_0^1 P_e(\tau_c/\mu) d\mu, \quad (4.70)$$

where P_e is the frequency-averaged escape probability (described below). The probability a photon emitted in zone e traverses a depth τ_B between zones e and a , and is then absorbed in zone a is

$$Q^{ea} = \frac{1}{2\tau_e} \int_0^{\tau_e} [\bar{P}_e(\tau_B + \tau) - \bar{P}_e(\tau_B + \tau_a + \tau)] d\tau. \quad (4.71)$$

Note that τ_e, τ_B , and τ_a are the optical depths in the direction normal to the slab surface. The first term within the integral represents the probability a photon will get to the nearer surface of zone a without being absorbed, while the second term represents the probability the photon is absorbed before exiting the surface farther from zone e . The coupling coefficients are efficiently computed using analytic expressions.

Evaluation of the coupling coefficients in cylindrical and spherical geometries is more difficult because Eq. (4.70) is not valid and angle-averaged escape probabilities cannot be computed directly. For these geometries, it was found [29] that introducing a “mean diffusivity angle,” $\bar{\theta} \equiv \cos^{-1} \bar{\mu}$, for which

$$P_e\left(\frac{\tau}{\bar{\mu}}\right) \cong \int_0^1 P_e\left(\frac{\tau}{\mu}\right) d\mu, \quad (4.72)$$

leads to solutions that compare reasonably well with exact solutions. The meaning of the mean diffusivity angle is clarified in Fig. 4.2. The quantities τ_e, τ_a , and τ_B again represent the line center optical depths of the emitting and absorbing zones and the depth between

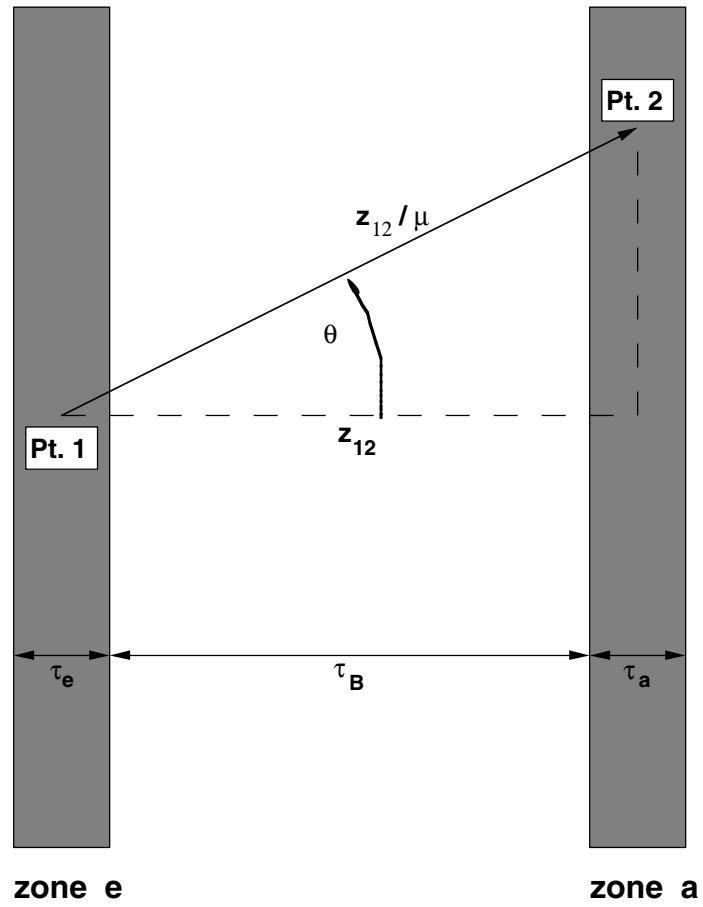


Figure 4.1. Schematic illustration of photon transport in planar geometry.

them, respectively. In this case, however, the optical depths are computed along the ray defined by $\bar{\theta}$ and the midpoint of the emitting zone.

It can also be seen from Fig. 4.2 that additional geometrical complications arise when the absorbing zone is inside the emitting zone. To overcome this, while at the same time maintaining computational efficiency, we take advantage of the reciprocity relation:

$$N^i Q^{ij} = N^j Q^{ji}, \quad (4.73)$$

where N^i and N^j are the total number of absorbing atoms in zones i and j , respectively. (A proof of this relation is given in Ref. [29]). Thus, in cylindrical and spherical geometries the coupling coefficients are given by:

$$Q^{ea} = \frac{1}{\tau_e} \int_0^{\tau_e} [P_e(\tau_B + \tau) - P_e(\tau_B + \tau_a + \tau)] d\tau, \quad (4.74)$$

where P_e is the non-angle-averaged escape probability. The Q^{ea} are calculated using Eq. (4.71) only for the cases when the absorbing zone is at a larger radius than the emitting zone. Otherwise, the reciprocity relation is used. It has been shown [29] that using $\bar{\mu} = 0.51$ leads to solutions for 2-level atoms that are accurate to within 25% for a wide range of total optical depths.

The frequency-averaged probability a photon will traverse a distance equivalent to a line center optical depth τ_c is:

$$P_e(\tau_c) = \int_0^\infty \phi(\nu) e^{-\tau_\nu} d\nu, \quad (4.75)$$

where $\phi(\nu)$ is the normalized line profile ($\int \phi(\nu) d\nu = 1$), and

$$\tau_\nu = \tau_c \phi(\nu) / \phi(\nu_0).$$

The quantity ν_0 represents the frequency at line center.

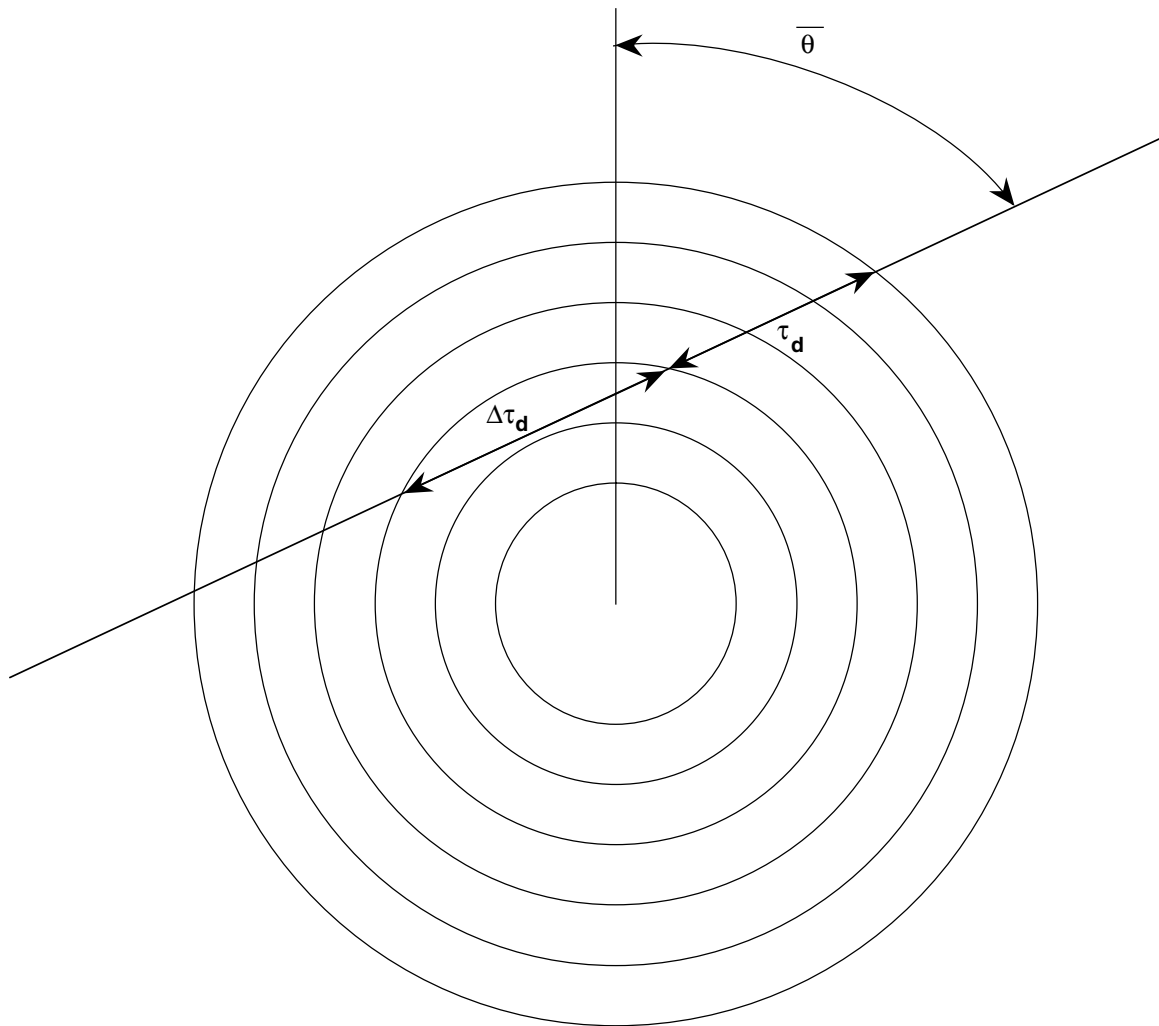


Figure 4.2. Schematic illustration of photon transport in cylindrical and spherical geometries.

The profiles considered for bound-bound transitions are:

$$\begin{aligned}
\text{Doppler : } \phi(\nu) &= (\pi^{1/2} \Delta\nu_D)^{-1} e^{-x_D^2}, & x_D &= \frac{\nu - \nu_0}{\Delta\nu_D} \\
\text{Lorentz : } \phi(\nu) &= \frac{4}{\Gamma} \frac{1}{1+x_L^2}, & x_L &= \frac{4\pi}{\Gamma} (\nu - \nu_0) \\
\text{Voigt : } \phi(\nu) &= (\pi^{1/2} \Delta\nu_D)^{-1} H(a, x_D), & a &= \frac{\Gamma}{4\pi \Delta\nu_D}.
\end{aligned} \tag{4.76}$$

The parameter Γ can be interpreted as the reciprocal of the mean lifetimes of the upper and lower states, $\Delta\nu_D$ is the Doppler width of the line, and

$$H(a, x_D) = \frac{a}{\pi} \int_{-\infty}^{\infty} \frac{e^{-y^2}}{(x_D - y)^2 + a^2} dy \tag{4.77}$$

is the Voigt function [31].

In evaluating the escape probability integrals we use an approach similar to that of Apruzese et al. [28]–[30]. Simple analytic fits to accurate numerical solutions to the frequency-averaged escape probabilities were obtained for each profile. For bound-bound transitions, complete frequency redistribution is assumed; i.e., the emission and absorption profiles are identical.

For Doppler profiles we use:

$$P_e(\tau_c) = \begin{cases} 2.329 [\tan^{-1}(0.675\tau_c + 0.757) - \tan^{-1}(0.757)], & \tau_c \leq 5.18 \\ 0.209 + 1.094 [\ln \tau_c]^{1/2}, & \tau_c > 5.18, \end{cases} \tag{4.78}$$

while for Lorentz profiles we use:

$$P_e(\tau_c) = \begin{cases} 1.707 \ln(1 + 0.586 \tau_c), & \tau_c \leq 5.18 \\ -0.187 + 1.128 \tau_c^{1/2}, & \tau_c > 5.18. \end{cases} \tag{4.79}$$

For Voigt profiles, the escape probability integrals were fitted to two different regimes of the Voigt broadening parameter a . For $a < 0.49$,

$$P_e(\tau) = \begin{cases} (1 + 1.5\tau)^{-1} & (\tau \leq 1), \\ 0.4\tau^{-1} & (1 < \tau \leq \tau_c), \\ 0.4(\tau_c\tau)^{-1/2} & (\tau > \tau_c), \end{cases} \tag{4.80}$$

where

$$\tau_c \equiv \frac{0.83}{a(1 + a^{1/2})}.$$

For $a \geq 0.49$,

$$P_e(\tau) = \begin{cases} (1 + \tau)^{-1} & (\tau \leq 1), \\ 0.5 \tau^{-1/2} & (\tau > 1). \end{cases} \quad (4.81)$$

The fits for Voigt profiles are typically accurate to about 20%, although errors of up to 40% can occur. Note, however, that in our model the frequency-averaged escape probability integrals are used only to compute the level populations self-consistently with the radiation field. The frequency-dependent spectral calculations do not directly use frequency-averaged escape probabilities.

We now discuss the transport of bound-free radiation in the context of the escape probability model. The frequency-averaged escape probability is obtained by averaging the attenuation factor, $e^{-\tau\nu}$, over the emission profile ϕ_E :

$$P_e(\tau_0, \alpha_0) = \int_{\nu_1}^{\infty} \phi_E(\nu, \alpha_0) \exp(-\tau\nu) d\nu, \quad (4.82)$$

where

$$\phi_E(\nu, \alpha_0) = \frac{\exp(-h\nu/kT_e)}{\nu E_1(\alpha_0)}$$

and

$$\alpha_0 \equiv h\nu_1/kT_e.$$

The optical depth and frequency at the photoionization edge are τ_0 and ν_1 , respectively, τ_ν is the optical depth at frequency ν , T_e is the electron temperature, and $E_1(x)$ represents the exponential integral of order 1. The quantities h and k as usual refer to the Planck constant and Boltzmann constant, respectively.

As in the case of line transport, frequency-averaged escape probabilities have been fitted to simple analytic functions to allow for computationally efficient solutions. The curve

fits are given by:

$$P_e(\tau_0, \alpha_0) = \begin{cases} e^{-\gamma_1 t} & , t \leq 1.0 \\ t^{-1/3} \exp[-\gamma_1 - \gamma_2(t^{1/3} - 1)] & , t > 1.0 \end{cases} \quad (4.83)$$

where

$$\begin{aligned} \gamma_1(\alpha_0) &= 2.01\alpha_0 - 1.23\alpha_0^{3/2} + 0.210\alpha_0^2, \\ \gamma_2(\alpha_0) &= 1.01\alpha_0 + 0.0691\alpha_0^{3/2} - 0.0462\alpha_0^2, \end{aligned}$$

and $t \equiv \tau_0/3$. The fits are accurate to about 15% over a wide range of parameter space: $0.3 < \alpha_0 < 10$ and values of τ_0 such that $P_e(\tau_0, \alpha_0) \geq 10^{-5}$.

The photoionization rate in zone a is obtained by summing the recombinations over all emitting zones e . Thus, the photoionization rate (corrected for stimulated recombinations) from lower level ℓ to upper level u can be written as:

$$\begin{aligned} \beta_{\ell u} &= 4\pi \int_{\nu_o}^{\infty} \frac{\alpha_{\nu}^{bf}}{h\nu} J_{\nu}^a \left(1 - \left(\frac{n_u^a}{n_{\ell}^a} \right) \left(\frac{n_{\ell}^a}{n_u^a} \right)^* e^{-h\nu/kT_e} \right) d\nu \\ &= \sum_{e=1}^{N_D} N_u^e n_e^e \alpha_{rr}^e Q^{ea}, \end{aligned} \quad (4.84)$$

where α_{ν}^{bf} is the photoionization cross section, J_{ν} is the radiation mean intensity, $(n_{\ell}/n_u)^*$ refers to the LTE population ratio [31], α_{rr}^e is the radiative recombination rate coefficient for zone e , n_e^e is the electron density in zone e , and N_D is the total number of spatial zones in the plasma.

4.4.4. Atomic Physics Models

Atomic structure calculations for energy levels are performed using a configuration interaction (CI) model using Hartree-Fock wavefunctions [20]. An L-S coupling scheme is used to define the angular momentum coupling of electrons. Rate coefficients for collisional and radiative transitions are calculated as follows. Collisional excitation and ionization rates

are computed using a combination of semiclassical impact parameter, Born-Oppenheimer, and distorted wave models [32]–[34]. The corresponding inverse processes were specified from detailed balance arguments. Rate coefficients for dielectronic recombination are computed using a Burgess-Mertz model [35] in conjunction with Hartree-Fock energies and oscillator strengths. Photoionization cross sections and radiative recombination rates are obtained from Hartree-Fock calculations. Details of the atomic physics calculations are given elsewhere [20].

4.4.5. Interface Between CRE and Radiation-Hydrodynamics Models

Overview of CRE/Radiation-Hydrodynamics Coupling

At present, the CRE model is coupled to BUCKY-1 as follows. Line radiation and continuum radiation are transported separately. The continuum radiation, which includes bound-free and free-free processes, is transported using the previously existing multigroup radiation diffusion model in BUCKY-1. This approach should provide a reasonable approximation because continuum opacities vary relatively smoothly with frequency (i.e., compared to bound-bound transitions). Continuum opacities for each photon energy group in this case are a function of the local density and temperature, but independent of the radiation field.

Line radiation is transported using the CRE escape probability model. Here, the rate at which energy is gained (absorbed) and lost (emitted) in each spatial zone is computed for each bound-bound transition. This transfer of energy is then included in the radiation-hydrodynamics plasma energy equation as a source term.

On each hydrodynamic time step, once $T(r)$, $n_e(r)$, and the atomic level populations are known, the radiation emission and absorption rates are easily computed from the zone-to-zone coupling coefficients, Q^{ea} . The emission rate in zone d due to all bound-bound

transitions can be written as:

$$J^d = \sum_{u>\ell} \Delta E_{u\ell} A_{u\ell} n_u^d \quad (4.85)$$

where $A_{u\ell}$ is the spontaneous emission rate for the transition $u \rightarrow \ell$, $\Delta E_{u\ell}$ is the transition energy, and n_u^d is the number density of atoms in the upper state of the transition in zone d . To determine the absorption rate for zone d , we add the contribution of photons emitted in each zone:

$$A^d = (\Delta V^d)^{-1} \sum_{u>\ell} \Delta E_{u\ell} A_{u\ell} \sum_e n_u^e \Delta V^e Q^{ed} \quad (4.86)$$

where ΔV^d is the volume of zone d .

The radiant energy flux escaping at the plasma boundary at each time step is computed by subtracting the absorption rate for all zones from the emission rate summed over zones:

$$F_{surface} = (Area)^{-1} \sum_{u>\ell} \Delta E_{u\ell} A_{u\ell} \sum_e n_u^e \Delta V^e (1 - \sum_a Q^{ea}). \quad (4.87)$$

4.5. Mechanics of CRE/Radiation-Hydrodynamics Interface

The interfacing between the CRE and radiation-hydrodynamics (R-H) models occurs at the following points:

- initialization and input,
- R-H plasma energy algorithm, and
- R-H radiation-dependent algorithms.

A single variable (NLTERT in BUCKY-1) must be read in during input to the R-H simulation to invoke the CRE line transport calculation. If the CRE model is not invoked, the above interface points are bypassed, in which case all CRE input and output files are not utilized.

Four CRE routines are utilized during the R-H initialization procedure:

- BDATAAC – a block data routine
- CLEARC – initializes variables to zero
- INNLTE – reads input for CRE model
- INITC1 – performs some CRE initializations.

The last three subroutines are called from the R-H initialization/input subroutine.

Four CRE subroutines are called from one of the R-H plasma energy subroutines for each hydrodynamic time step:

- LODCB1 – loads R-H variables into CRE common blocks
- NLPOPS – computes atomic level populations
- LINRAD – computes line radiation emission and absorption rates for each spatial zone
- LODCB2 – stores CRE results in R-H common blocks.

The CRE line transport algorithms are invoked during each time cycle of the R-H simulation prior to the solution of the plasma energy equation. The results are stored in the CRE common block /CREOUT/ (see also Section 13.2). The results are then read into R-H common block for use in the following algorithms:

- computation of plasma energy source term
- computation of flux across outer plasma boundary
- monitoring of energy conservation
- output.

The variable names used in the above algorithms are given in subroutine LODCB2.

5. Equations of State and Opacity Tables

The equations of state and opacities must be supplied for each material by the user in tabular form. The exception to this is when an ideal gas EOS is selected (using ISW(12)). Currently, BUCKY-1 has the capability of using EOSOPA [5] and IONMIX [36] EOS/opacity tables and SESAME [37] EOS tables. The selection of table type is made using the variables IZEOS, IDEOS, and IDOPAC. IZEOS is used to specify the EOS/opacity file name (our present convention is to use the atomic number; e.g., for Al IZEOS = 13, and the EOS file would be named either ‘eos.dat.uw.13’ (EOSOPA) or ‘eos.dat.sm.13’ (SESAME)). IDEOS and IDOPAC are used to specify the format type of the table:

$$\text{IDEOS}(\text{kmat}) = \begin{cases} 0 & \text{EOSOPA (old)} \\ 1 & \text{IONMIX} \\ 2 & \text{SESAME} \\ 3 & \text{EOSOPA (new)} \end{cases}$$

and

$$\text{IDOPAC}(\text{kmat}) = \begin{cases} 0 & \text{EOSOPA (old)} \\ 1 & \text{IONMIX} \\ 2 & \text{not used} \\ 3 & \text{EOSOPA (new)} \end{cases}$$

where ‘kmat’ is the material index.

Note that each material has its own identifier. This allows for considerable flexibility in selecting EOS and opacity data. For example, EOSOPA EOS and opacity data could be selected for material 1, while material 2 could use SESAME EOS tables and EOSOPA opacity tables. The option to use SESAME opacity data is currently not available because the multifrequency opacity data available to the open community is limited.

The option to use IONMIX EOS/opacity tables has been continued in BUCKY-1. IONMIX generates data using relatively simple (hydrogenic ion) atomic models, which were used in CONRAD ICF target chamber calculations. However, the data for EOSOPA tables is generated using considerably more sophisticated atomic models and should be used in

place of IONMIX whenever possible. We choose to continue the option for IONMIX tables to allow for ease in comparing with previous calculations.

EOS/opacity quantities are evaluated at the hydro temperature and densities by interpolating on the $T - \rho$ grid. Presently, a bilinear interpolation is used (based on a $\log T$, $\log \rho$ mesh). It is anticipated that higher order interpolation schemes will be added in the future.

5.1. EOSOPA EOS and Opacity Tables

EOSOPA generates EOS and multifrequency opacity data on a two-dimensional grid of temperatures and densities. The EOS and opacity tables can utilize different $T - \rho$ grids. Generally, EOSOPA computes multifrequency data for a large number of frequency groups (typically, ~ 500). Tables can then be generated with a smaller number of frequency groups using our REGROUP post-processor. This allows a convenient method for generating tables with a different frequency structure without having to needlessly recalculate large amounts of EOS and atomic data.

The data generated by EOSOPA includes the following:

Z	Mean charge state (esu)
E_P	Specific plasma (ions plus electrons) internal energy (J/g)
$(\partial E_P/\partial T)$	E_P temperature-derivative (J/g/eV)
$(\partial E_P/\partial n)$	E_P density-derivative (J/cm ³ /g)
E_i	Specific ion internal energy (J/g)
E_e	Specific electron internal energy (J/g)
$(\partial E_i/\partial T)$	E_i temperature-derivative (J/g/eV)
$(\partial E_e/\partial T)$	E_e temperature-derivative (J/g/eV)
P_i	Ion pressure (erg/cm ³)
P_e	Electron (erg/cm ³)

$(\partial P_i/\partial T)$	P_i temperature-derivative (erg/cm ³ /eV)
$(\partial P_e/\partial T)$	P_e temperature-derivative (erg/cm ³ /eV)
σ_R	Rosseland mean group opacity (cm ² /g)
σ_P^E	Planck mean emission group opacity (cm ² /g)
σ_P^A	Planck mean absorption group opacity (cm ² /g)

Separate emission and absorption Planck opacities are computed to allow for non-LTE conditions, in which case Kirchoff's relation ($\eta_\nu = \kappa_\nu B_\nu$) is not valid.

Example results from an EOSOPA calculation are shown in Figure 5.1, which shows energy and pressure isotherms for Al. In the low density regime, the nonlinear behavior due to ionization/excitation is clearly seen. The cohesive, degeneracy, and pressure ionization effects are also apparent in the high-density regime. EOSOPA also computes high quality opacities for both low-Z and high-Z materials.

5.2. SESAME EOS Tables

BUCKY-1 can also use SESAME-formatted EOS tables. This is presently done by copying tabular data for the material of interest into a file called 'eos.dat.sm.NN', where NN is specified by the input variable IZEOS. An example of a SESAME data file for Al is shown in Figure 5.2, where selected parts are shown indicating the various types of tables (e.g., 201, 301, \dots , 401). Note that BUCKY-1 reads SESAME data from a single ASCII file for each material, as opposed to one large SESAME library.

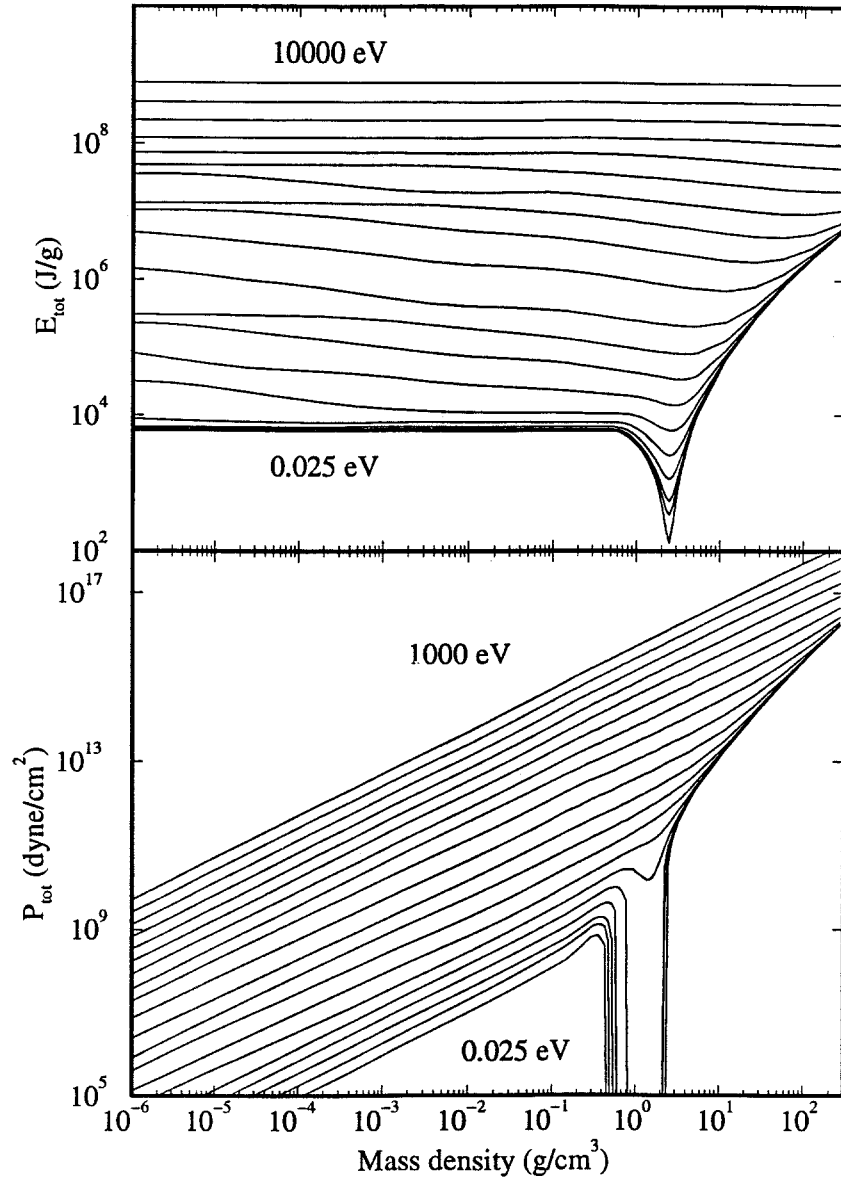


Figure 5.1. Isotherms of energy and pressure for Al generated using EOSOPA hybrid model.

```

0 3717 101 120 11889 11889 1 0
material. aluminum (z=13.0, a=26.9815) /source. j. barnes, s. lyon /date. aug 88
/refs. none /comp. al /codes. grizzly /
1 3717 102 552 11889 11889 1 1
tfd as calculated by candide in grizzly was used for the electronic contribution
. chartjd nuclear model with jd gamma (igrun=7). gamref = 2.136, dgamma = -1.6,
-2.2, gameps = 0.5, 1.0, debkel = 390.0, tmelt = 933.2. cold curve from shock da
ta and sound velocity. used us-up curve composed of a single straight line with
c0 = 5.35 and s1 = 1.34. also used ecohkc = 69.0, faclj = 0.235, cmat = 1.588 an
d xalpha = 0.2. both temperature and density grids enhanced with additional point
s. 301 table has van der waals loops. fits p(rho) hugoniot data well.
1 3717 201 5 11889 11889 1 1
1.30000000E+01 2.69815000E+01 2.70000000E+00 0.00000000E+00 0.00000000E+0011112
1 3717 301 12585 11889 11889 1 1
8.30000000E+01 5.00000000E+01 0.00000000E+00 2.70000000E-06 5.40000000E-0611211
1.35000000E-05 2.70000000E-05 5.40000000E-05 1.35000000E-04 2.70000000E-0411111
5.40000000E-04 1.35000000E-03 2.70000000E-03 4.05000000E-03 6.75000000E-0311111
.
.
-5.72089716E+07-5.62935185E+07-5.48490287E+07-5.28132564E+07-5.13688668E+0711111
-5.02485321E+07-4.82129596E+07-4.56486186E+07-4.32890457E+07-4.12540104E+0711111
-3.86903382E+07-3.52117842E+07-3.06117783E+07-2.71270411E+07-2.36303935E+0711111
1 3717 303 12283 11889 11889 1 1
8.10000000E+01 5.00000000E+01 2.70000000E-06 5.40000000E-06 1.35000000E-0511111
2.70000000E-05 5.40000000E-05 1.35000000E-04 2.70000000E-04 5.40000000E-0411111
1.35000000E-03 2.70000000E-03 4.05000000E-03 6.75000000E-03 1.08000000E-0211111
.
.
-9.69777432E+06-9.54306481E+06-9.43279210E+06-9.34690867E+06-9.18989758E+0611111
-8.98981704E+06-8.80266390E+06-8.63797900E+06-8.42463539E+06-8.11990274E+0611111
-7.67268167E+06-7.27747045E+06-6.79987347E+06 01110
1 3717 304 7543 11889 11889 1 1
6.70000000E+01 3.70000000E+01 2.70000000E-06 5.40000000E-06 1.35000000E-0511111
2.70000000E-05 5.40000000E-05 1.35000000E-04 2.70000000E-04 5.40000000E-0411111
1.35000000E-03 2.70000000E-03 4.05000000E-03 6.75000000E-03 1.08000000E-0211111
.
.
-4.51512544E+07-4.32701916E+07-4.19360747E+07-4.09016235E+07-3.90230621E+0711111
-3.66588016E+07-3.44863818E+07-3.26160314E+07-3.02657028E+07-2.70918814E+0711111
-2.29390967E+07-1.98495706E+07-1.68305201E+07 01110
1 3717 305 12283 11889 11889 1 1
8.10000000E+01 5.00000000E+01 2.70000000E-06 5.40000000E-06 1.35000000E-0511111
2.70000000E-05 5.40000000E-05 1.35000000E-04 2.70000000E-04 5.40000000E-0411111
1.35000000E-03 2.70000000E-03 4.05000000E-03 6.75000000E-03 1.08000000E-0211111
.
.
-9.69997291E+06-9.54653137E+06-9.43751152E+06-9.35286023E+06-9.19883950E+0611111
-9.00440868E+06-8.82511874E+06-8.67013067E+06-8.47443440E+06-8.20808192E+0611111
-7.85446609E+06-7.58573941E+06-7.31587947E+06 01110
1 3717 306 327 11889 11889 1 1
8.10000000E+01 1.00000000E+00 2.70000000E-06 5.40000000E-06 1.35000000E-0511111
2.70000000E-05 5.40000000E-05 1.35000000E-04 2.70000000E-04 5.40000000E-0411111
1.35000000E-03 2.70000000E-03 4.05000000E-03 6.75000000E-03 1.08000000E-0211111
.
.
3.46655838E+03 4.71942146E+03 5.95156296E+03 8.94191856E+03 1.45916465E+0411111
2.24548423E+04 3.21516695E+04 4.97990090E+04 8.81791815E+04 1.81784419E+0511111
3.08268965E+05 5.16005995E+05 01100
1 3717 401 161 11889 11889 1 1
2.00000000E+01 0.00000000E+00 1.26272829E-46 2.67385217E-25 4.10813158E-1512111
2.33032634E-09 1.00659699E-06 3.22649411E-06 9.70326824E-06 2.76790993E-0511111
7.54380556E-05 1.98830824E-04 5.16385229E-04 1.28603631E-03 3.06537205E-0311111
.
.
-1.73558751E+00-3.77632871E+00-4.22668260E+00-4.72780948E+00-5.28404899E+0011111
-5.90082838E+00-6.58398155E+00-7.33905595E+00-8.17483403E+00-9.09998760E+0011111
-1.01253598E+01-1.12642705E+01-1.25380591E+01-1.39812442E+01-1.56113366E+0111111
-1.73823007E+01 01000

```

Figure 5.2. Example SESAME data file for Al.

6. Fast Ion Energy Deposition

Fast ions, either due to an ion beam or target debris, transfer energy and momentum to a plasma by collisions. The rate at which ions transfer their momentum and energy to the background (target) is calculated by the stopping power expression:

$$S = \frac{1}{N_{bg}} \left[\left(\frac{dE}{dx} \right)_{fe} + \left(\frac{dE}{dx} \right)_{be} + \left(\frac{dE}{dx} \right)_{nucl} \right] \quad (6.1)$$

where $\frac{dE}{dx}$ is the kinetic energy lost by a projectile ion as it traverses a distance dx through a background medium of density N_{bg} . The 3 terms on the right hand side of Eq. (6.1) represent (from left to right) the contributions from collisions with free electrons, bound electrons, and nuclei of the target plasma.

The free electron contribution to the stopping power is given by [21]:

$$\left(\frac{dE}{dx} \right)_{fe} = \left(\frac{\omega_p q_1 e}{v_1} \right)^2 G(y^2) \ln \Lambda_{fe} \quad (6.2)$$

where

$$G(y^2) = \text{erf}(y) - \frac{2}{\sqrt{\pi}} e^{-y^2}$$

and

$$\omega_p = \left(\frac{4\pi e^2 n_e}{m_e} \right)^{1/2}$$

is the plasma frequency. The quantity y is the ratio of the projectile ion velocity v_1 to the mean electron velocity $\langle v_e \rangle$, $\text{erf}(y)$ is the error function, q_1 is the projectile ion charge state, e is the electron charge, n_e is the electron density, and m_e is the electron mass. The Coulomb logarithm is given by

$$\Lambda_{fe} = (0.764 v_1) / (\omega_p b_{\min})$$

where

$$b_{\min} = a_o \max \left[q_1 \left(\frac{v_1}{v_o} \right)^2, \frac{v_1}{2v_o} \right],$$

a_o is the Bohr radius, and v_o is the Bohr velocity ($= 2.2 \times 10^8$ cm/s). At high temperatures, the target plasma is highly ionized and the stopping power is dominated by the free electron term. Under these conditions, the stopping power is proportional to q_1^2 .

Inelastic scattering with bound electrons and elastic nuclear scattering are important at low temperatures. The nuclear contribution can be written as:

$$\left(\frac{dE}{dx}\right)_{nucl} = C_1 \varepsilon^{1/2} \exp\{-45.2(C_2 \varepsilon)^{0.277}\} \quad (6.3)$$

where

$$\varepsilon = E/A_1 \text{ (MeV/amu)}$$

$$C_1 = (4.14 \times 10^6 \text{ MeV cm}^2 \text{g}^{-1}) \frac{\rho_2}{A_2^2} \left(\frac{A_1 A_2}{A_1 + A_2}\right)^{3/2} \left(\frac{(Z_1 Z_2)^{1/2}}{Z_1^{2/3} + Z_2^{2/3}}\right)^{3/4}$$

and

$$C_2 = \left(\frac{A_1 A_2}{A_1 + A_2}\right) (Z_1 Z_2)^{-1} (Z_1^{2/3} + Z_2^{2/3})^{-1/2}.$$

The subscripts 1 and 2 refer to the projectile ion and target plasma, respectively. A , Z , and ρ represent the atomic weight, atomic number, and mass density, respectively.

The bound electron contribution is calculated using one of two theories, depending on the projectile ion velocity. Lindhard-Scharff theory [38] is valid when the projectile velocity is small compared to the orbital velocity of the bound electrons. In this case, the bound electrons are treated as a ‘‘cloud’’, as opposed to point charges. The expression for the Lindhard-Scharff stopping power is:

$$\left(\frac{dE}{dx}\right)_{LS} = (3.84 \times 10^{18} \text{ keV cm}^{-1}) N_2 \frac{Z_1^{7/6} Z_2^*}{[Z_1^{2/3} + (Z_2^*)^{2/3}]^{3/2}} \left(\frac{E_1}{A_1}\right)^{1/2} \quad (6.4)$$

where E_1 is the debris ion kinetic energy in keV, and Z_2^* is the average number of bound electrons per nucleus. At low velocities, the rate at which the debris ions lose their energy is proportional to their velocity. When the projectile ion velocities are large compared to the electron orbital velocities, the bound electrons can be treated as point charges, and Bethe

theory is used to determine the energy loss rate. The expression for the Bethe stopping power is [21]:

$$\left(\frac{dE}{dx}\right)_{Bethe} = \left(\frac{\omega_p q_1 e}{v_1}\right)^2 \left[\ln \left[\frac{2m_e v_1^2}{\langle \Phi_2 \rangle (1 - v_1^2/c^2)} \right] - \left(\frac{v_1}{c}\right)^2 \right] \quad (6.5)$$

where $\langle \Phi_2 \rangle$ is the average ionization potential of the background plasma. To ensure a smooth transition between the 2 models, we interpolate to get the total bound electron stopping power:

$$\left(\frac{dE}{dx}\right)_{be} = \begin{cases} \left(\frac{dE}{dx}\right)_{LS} & v_1 < v_L \\ (1-f)\left(\frac{dE}{dx}\right)_{LS} + f\left(\frac{dE}{dx}\right)_{Bethe} & v_L \leq v_1 \leq v_B \\ \left(\frac{dE}{dx}\right)_{Bethe} & v_1 > v_B \end{cases} \quad (6.6)$$

where $v_L = Z_1^{2/3} v_o$ and $v_B = 3 Z_1^{2/3} v_o$, and $f = (v_1 - v_L)/(v_B - v_L)$.

In some cases, the *time-dependence* of the projectile ions' charge states must be computed to accurately determine the energy deposition. In BUCKY-1, we consider the following reactions in calculating the rate of change in the mean ionization: collisional ionization and recombination, radiative recombination, and recombination due to charge exchange with the background plasma. The debris ion ionization populations are computed by solving the coupled set of rate equations:

$$\begin{aligned} \frac{dN_q}{dt} &= N_{q-1} n_e C_{q-1} + N_{q+1} (n_e^2 \alpha_{q+1}^{coll} + n_e \alpha_{q+1}^{rad} + N_{bg} v_1 \sigma_{cx,q+1}) \\ &- N_q (n_e C_q + n_e^2 \alpha_q^{coll} + n_e \alpha_q^{rad} + N_{bg} v_1 \sigma_{cx,q}) \end{aligned} \quad (6.7)$$

where N_q is the number of ions in the q^{th} ionization state, N_{bg} is the target plasma number density, and $\sigma_{cx,q}$ is the charge exchange cross section. C_q , α_q^{coll} , and α_q^{rad} represent the collisional ionization, collisional recombination, and radiative recombination rate coefficients, respectively. Expressions for these quantities are based on a hydrogenic ion model [36]. Eq. (6.7) neglects charge exchange reactions in which the projectile ions increase with charge. To properly include these reactions, BUCKY-1 would have to also track the time-dependence

of the background plasma ionization populations, something it is not currently set up to do. This can cause the projectile ion charge states to fall to anomalously low values. This will be discussed in more detail below.

To calculate the charge exchange reaction rates, we use the classical cross sections given by Knudson et al. [39]:

$$\frac{\alpha_q}{\pi a_o^2 q_1} = \begin{cases} \frac{1}{2} Z_2^{2/3} \left[\left(\frac{\alpha v_a}{v_o} \right)^{-2} - (\beta Z_2)^{-2} \right], & v_1 < \alpha v_a \\ \frac{8}{3} \xi^{-7} \left[\left(\frac{Z_2^{2/3}}{8} \xi^7 \right)^{3/5} - \left(\frac{\alpha v_a}{v_o} \right)^3 \right] \\ \quad + \frac{1}{2} Z_2^{2/3} \left[\left(\frac{Z_2^{2/3}}{8} \xi^7 \right)^{-2/5} - (\beta Z_2)^{-2} \right], & \alpha v_a < v_1 < \beta Z_2 v_o \\ \frac{8}{3} \xi^{-7} \left[(\beta Z_2)^3 - \left(\frac{\alpha v_a}{v_o} \right)^3 \right], & v_1 > \beta Z_2 v_o \end{cases} \quad (6.8)$$

where $\xi = q_1^{-2/7} (v_1/v_o)$, $v_a = v_o (\langle \Phi_2 \rangle / 13.6 \text{ eV})^{1/2}$, $\beta Z_2 = Z_2^{2/3} + \alpha v_a / v_o$, and α is an adjustable parameter.

Values for α were found by fitting Eq. (6.8) to experimental data for ion-neutral charge exchange reactions [39]. The selected values for α are: 0.25 for H, 0.40 for He, 0.46 for Ar, and 0.54 for Xe. Values for other atoms are obtained by simple interpolation. The agreement between the calculated and experimental cross sections is reasonably good, suggesting the scaling laws used by Knudson et al. are reliable for a wide range of projectile ions.

When the background plasma is ionized, the charge exchange cross sections decrease dramatically when the projectile ion kinetic energy is not large enough to overcome the Coulomb repulsion energy. To model this effect, we use a low velocity cutoff for the cross sections of ion-ion charge exchange reactions that is given by [40]:

$$v_{crit} = (6 \times 10^5 \text{ cm/s}) q^{2/7} (\Phi_2 / 13.6 \text{ eV}). \quad (6.9)$$

When the target plasma is ionized and the projectile ion velocity is less than the cutoff velocity, the charge exchange cross section is zero in BUCKY-1; otherwise, the Knudson values are used.

7. Laser Deposition Model

A simple laser energy deposition model has been recently added to BUCKY-1. Laser light is absorbed using an inverse Bremsstrahlung model at electron densities below the critical density:

$$n_{e,crit} = \frac{\varepsilon_o m_e w_L^2}{e^2}, \quad (7.1)$$

where ε_o is the permittivity in free space ($= 1/4\pi$ in cgs units), and $w_L = 2\pi c/\lambda_L$ is the angular frequency of the laser light. In terms of the laser wavelength,

$$n_{e,crit} = (1.11 \times 10^{21} \text{ cm}^{-3}) \lambda_{\mu m}^{-2}. \quad (7.2)$$

For a laser power incident on the outer boundary, $P_L(R_{\max})$, the energy absorbed in a time interval Δt within a zone bounded by r_1 and r_2 is:

$$\begin{aligned} \Delta E_d &= \Delta t \int_{r_1}^{r_2} dr P_L(r, t) \cdot \kappa \\ &= \Delta t P_L(R_{\max}, t) \int_{r_1}^{r_2} dr \kappa e^{-\kappa(R_{\max}-r)} \\ &= \Delta t P_L(R_{\max}, t) \int_{\tau_1}^{\tau_2} d\tau e^{-\tau}, \end{aligned} \quad (7.3)$$

where κ is the absorption coefficient, and $d\tau = -\kappa dr$ is the optical depth (which is measured with respect to the outer boundary).

The absorption coefficient can be written as [41]:

$$\begin{aligned} \kappa &= (2\pi)^{1/2} \left(\frac{16\pi}{3} \right) \frac{e^6}{c(m_e k T_e)^{3/2}} Z n_e^2 \frac{\ln \Lambda}{\omega_L^2 (1 - (\omega_P/\omega_L)^2)^{1/2}} \\ &= (1.08 \times 10^5 \text{ cm}^{-1}) T_{\text{eV}}^{-3/2} \lambda_{\mu m}^{-2} Z \frac{\beta^2}{(1 - \beta)^{1/2}} \ln \Lambda \end{aligned} \quad (7.4)$$

where ω_P is the plasma frequency, $\beta = n_e/n_{e,crit}$, and $\ln \Lambda$ is the Coulomb logarithm.

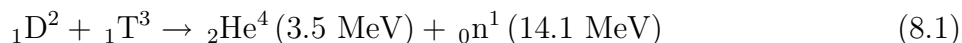
At present, there are no corrections for stimulated Brillouin scattering (SBS) or other anomalous processes. This geometry is currently limited to laser light which propagates radially inward, striking the outer boundary of the target plasma first. It is expected the laser deposition model in BUCKY-1 will be upgraded in the future.

8. Fusion Burn Energy Deposition

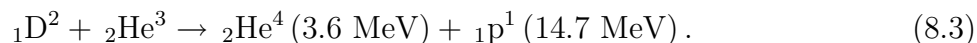
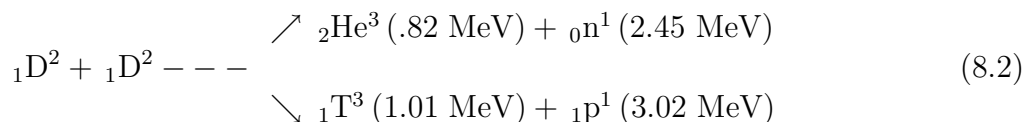
The fusion burn reaction and energy deposition package was extracted essentially intact from PHD-IV. The only modification is the addition of a neutron energy deposition model which currently utilizes a simple escape probability algorithm (described in Section 8.3).

8.1. Fusion Reactions

The thermonuclear reactions of greatest interest at this time are the deuterium-tritium reaction



and the deuterium-deuterium and deuterium-helium 3 reactions



The thermal reaction rates for these reactions are plotted in Fig. 8.1. BUCKY-1 includes the reaction rates for these three reactions and solves the rate equations describing the depletion of the individual species:

$$\begin{aligned} \frac{dn_{\text{T}}}{dt} &= -n_{\text{T}}n_{\text{D}}\langle\sigma v\rangle_{\text{DT}} \\ \frac{dn_{\text{D}}}{dt} &= -n_{\text{T}}n_{\text{D}}\langle\sigma v\rangle_{\text{DT}} - n_{\text{D}}^2\langle\sigma v\rangle_{\text{DD}} - n_{\text{He}^3}n_{\text{D}}\langle\sigma v\rangle_{\text{DHe}^3} \\ \frac{dn_{\text{He}^3}}{dt} &= -n_{\text{D}}n_{\text{He}^3}\langle\sigma v\rangle_{\text{DHe}^3} . \end{aligned} \quad (8.4)$$

These are solved using simple Euler difference equations. Several subroutines are involved in the solution of these equations. Subroutine TNREAC computes the number of reactions on a given time cycle and subroutine TNBURN computes the reduction in the number of

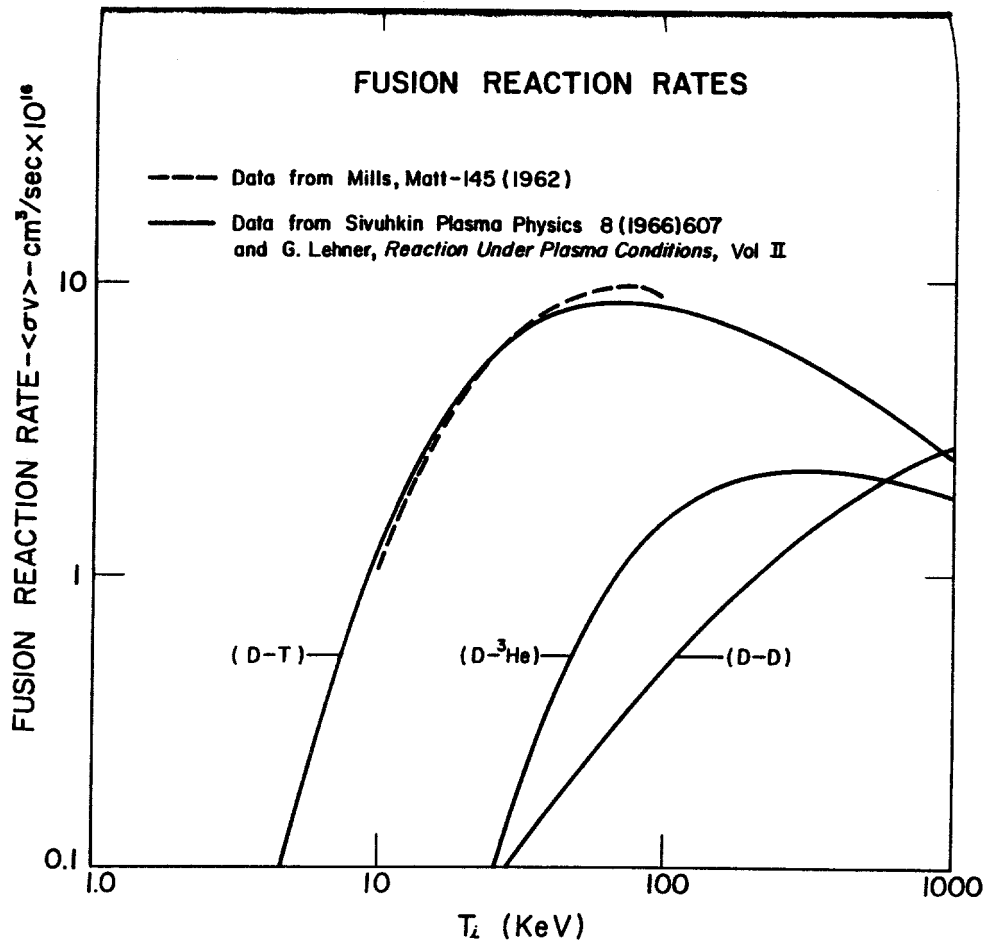


Figure 8.1. Temperature dependence of D-T, D-D, and D-³He reaction rates.

Table 8.1. Fitting Parameters for Reaction Rates

	DT	DD	DHe ³
A_1	-21.38	-15.51	-27.76
A_2	-25.20	-35.32	-31.02
A_3	-7.101×10^{-2}	-1.290×10^{-2}	2.789×10^{-2}
A_4	1.938×10^{-4}	2.680×10^{-4}	-5.532×10^{-4}
A_5	4.925×10^{-6}	-2.920×10^{-6}	3.029×10^{-6}
A_6	-3.984×10^{-8}	1.275×10^{-8}	-2.523×10^{-9}
r	.2935	.3735	.3597

deuterons, tritons, and He³ in each zone due to the reactions on a given cycle. Subroutine DEPLET computes new number densities of all of the ionic species as a result of depletion and transport of the ions. All of the reaction products from these three reactions may be transported and this will be discussed in the next section. The reaction rates are computed in subroutine SIGMAV using either a table look-up procedure or analytical formulas. The formulas are more accurate, particularly at the low temperatures characteristic of today's experiments. The table look-up is cheaper, however, and is well suited for thermonuclear burn studies of high gain pellets where the ion temperatures are between 10 and 100 keV. The tables of reaction rates cut off at 1 keV and are linearly interpolated. The analytical formula used to compute the reaction rates is:

$$\langle \sigma v \rangle = \exp[A_1/T^r + A_2 + A_3T + A_4T^2 + A_5T^3 + A_6T^4]$$

where A_{1-6} and r are tabulated for DT, DD, and DHe³ in Table 8.1.

8.2. Fusion Charged Particle Reaction Product Transport

8.2.1. Time-Dependent Particle Tracking Method

To accurately describe the fusion burn process, the transport and thermalization of reaction products must be treated along with the thermonuclear reaction rate equations. In BUCKY-1 the charged particle transport and slowing down is treated using the time-dependent particle tracking (TDPT) algorithm. This technique is not a finite difference method and is similar to Monte Carlo.

On each time step the reaction products created in each zone are equally divided into a number of directions and the “bunch” of particles in each direction is tracked along a ray, as shown in Fig. 8.2. The bunch is assumed to always move along this straight ray and slow down as it is transported. In crossing a zone the bunch of charged particles will lose some amount of energy which is tallied for each zone on each time step. This energy is then used as a source term in the electron and ion temperature equations.

If a bunch of particles loses all of its energy in crossing a zone then the ions in this bunch have thermalized and they are added back into the thermal background plasma in this zone. Particle bunches are tracked in this way until they lose all of their energy or until the current time step is completed. If they have not thermalized in a time Δt_{TN} , their number (N), position (R), direction (μ), and velocity (V) are saved in a data structure and their transport is continued in the next time step.

The basic equation solved by the TDPT algorithm is the range-energy relationship for a fast ion in a thermal plasma

$$-\frac{dv}{ds} = A + B/v^3 = K(v) \quad (8.5)$$

$$\begin{aligned} A &= A_o(Z^2/m) \ln \Lambda_e n_e / T_e^{3/2} & A_o &= \text{CONTN}_3 \\ B &= B_o(Z^2/m) \ln \Lambda_i \sum_i Z_i^2 n_i / \rho & B_o &= \text{CONTN}_4 \end{aligned} \quad (8.6)$$

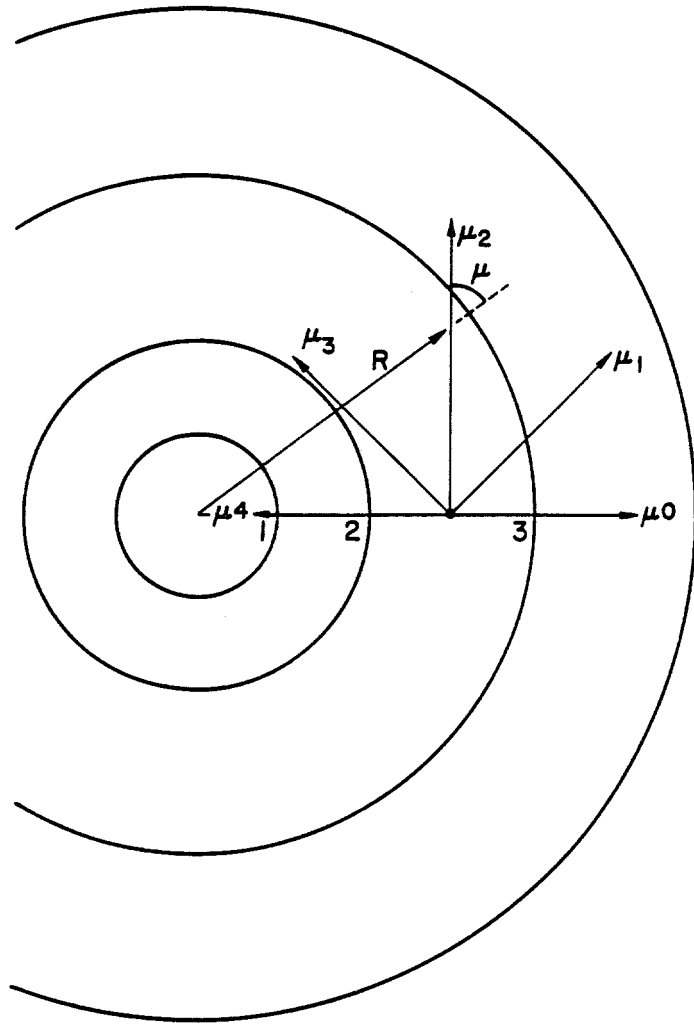


Figure 8.2. Schematic illustration of time-dependent particle tracking.

where the A term is due to scattering on electrons and the B term is due to scattering on ions. The straight line approximation is valid as long as the slowing down is due to collisions with electrons. The plot of Eq. (8.5) in Fig. 8.3 shows that this is generally valid. Equation (8.5) is solved along a ray, between zone boundaries by integrating it along its exact path length:

$$\Delta s = \int_{v_o - \Delta v}^{v_o} g(v) dV, \quad (8.7)$$

where Δs is the distance across the zone along the particle trajectory, v_o is the particle velocity on entering the zone, Δv is the velocity loss in crossing the zone, and

$$g(v) = [K(v)]^{-1}. \quad (8.8)$$

The A and B terms are evaluated using the temperature and density of the zone. Equation (8.7) is an integral equation for Δv and can be solved using a Taylor expansion

$$\begin{aligned} g(v) &= g(v_o) + (v - v_o) g'(v_o) + \dots \\ &= g_o + (v - v_o) g'_o. \end{aligned} \quad (8.9)$$

Substitution into Eq. (8.7) yields

$$\Delta s \simeq g_o \Delta v - 1/2 g'_o (\Delta v)^2. \quad (8.10)$$

This expression can be inverted and solved to second order for Δv as

$$\Delta v = \Delta s / [g_o (1 - 1/2 g'_o / g_o^2 \Delta s)], \quad (8.11)$$

or equivalently

$$\Delta v = K(v_o) \Delta s / [1 + 1/2 k'(v_o) \Delta s]. \quad (8.12)$$

This procedure is accurate for $\Delta v / v_o \ll 1$; however, should $\Delta v / v_o \geq 1$, then the particles have thermalized within the zone so again the error to energy redeposition will not be serious. Only the partition of energy to the electrons and ions will be important. The total energy lost in a zone is simply

$$\Delta E = 1/2 m [v_o^2 - (v_o - \Delta v)^2] N, \quad (8.13)$$

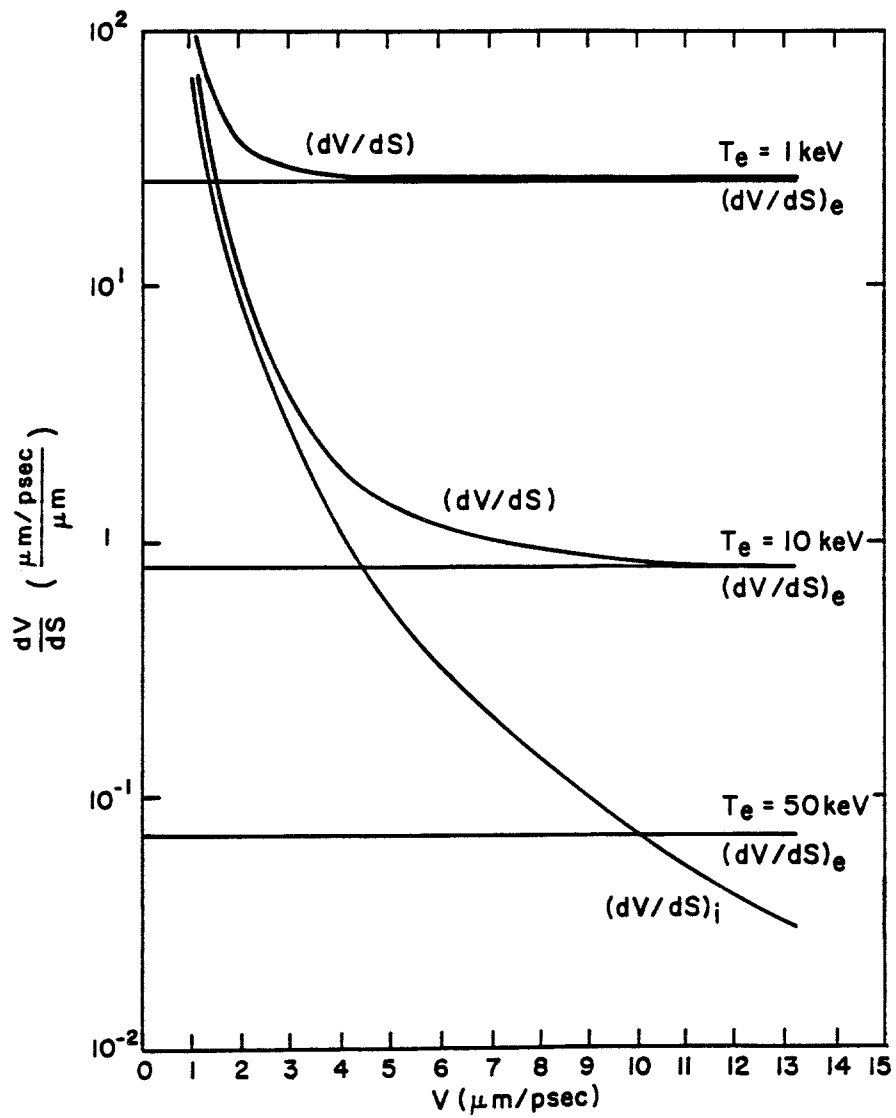


Figure 8.3. Slowing of α particles in D-T at $5 \times 10^{26} \text{ cm}^{-3}$.

where N is the number of ions in the bunch streaming along a given ray. The fraction of this energy going to the electrons is

$$\Delta E^{(e)} = A(\Delta s/\Delta v) \Delta E. \quad (8.14)$$

Should the particles slow to thermal energy in the zone ($\Delta v/v_o \sim 1$), then the fraction of energy going to electrons can be obtained from the results of an infinite medium calculation, tabulated as a function of electron temperature. Then the loss to ions in either case is

$$\Delta E^{(i)} = \Delta E - \Delta E^{(e)}. \quad (8.15)$$

In addition to energy redeposition, the nonthermal ions also impart momentum to the zone:

$$m \Delta v N \cos \alpha = M \Delta u, \quad (8.16)$$

where M is the zone mass, m is the nonthermal particle mass, and α is the angle between the trajectory of the ions and the outward radial direction.

A “bunch” of particles (say, alphas) created at position $r_{j-1/2}$ at time $t^{n+1/2}$ and traveling along a ray in direction μ_m can be totally characterized by four numbers: the number of particles in the “bunch”, N ; the position of this bunch of particles, R ; the direction of these particles with respect to the radius vector to position R , μ ; and the velocity of the particles, V . Particles can be “tracked” from their origin or birthplace to the position that they reach after a time Δt , the time step. At this time their new position, direction, velocity, and number of them can be stored until the next time step. Such an algorithm requires that the energy-time relationship be integrated along the rays:

$$-\frac{dv}{dt} = \frac{-v dv}{ds} = Av + B/v^2 = J(v). \quad (8.17)$$

In exact analogy to the solution of Eq. (8.5), Eq. (8.17) can be integrated to give

$$\Delta v = J_o \Delta t / [1 + 1/2 J'_o \Delta t]. \quad (8.18)$$

In addition to these relations, we must also know the distance travelled in a time Δt and the time taken to move a distance Δs . These are given by

$$\Delta t_{\Delta s} = (\Delta v/J_o) + 1/2 J'_o(\Delta v/J_o)^2 \quad (8.19)$$

$$\Delta s_{\Delta t} = (\Delta v/K_o) + 1/2 K'_o(\Delta v/K_o)^2. \quad (8.20)$$

Storing the numbers, positions, directions, and velocities of particles created on previous time steps that are still streaming requires N_s words of computer memory, where

$$N_s = N_Z \times (N_A^+ N_T^+ + N_A^- N_T^-) \times N_p \times 4 \quad (8.21)$$

and

N_Z = number of zones

N_A^+ = number of directions with $\mu > 0$

N_A^- = number of directions with $\mu \leq 0$

N_T^+ = number of time steps to remember particles starting in a $\mu > 0$ direction

N_T^- = number of time steps to remember particles starting in a $\mu < 0$ direction

N_p = number of different kinds of particles to be tracked.

The number of time steps necessary to follow particles starting in an outward direction will be less than the number required for inward directed particles so provision is made to optimize the amount of necessary storage by utilizing this fact. Also, with such a scheme, there is always the possibility that a bunch of particles that have been remembered for N_T^\pm future time steps will neither have thermalized or escaped the plasma. In such a case, these particles are forced to thermalize or escape by using a time-independent tracking. In practice, enough storage can usually be provided to minimize the effects of this problem. The advantage of this time-dependent particle tracking algorithm is the reasonably accurate

treatment of the slowing down process and energy redeposition at a very reasonable cost. The disadvantage is the rather complex logic required to execute the algorithm, necessitating very careful programming.

8.2.2. Implementation of TDPT

With the physics description of the time dependent particle tracking algorithm given in the previous section, this section will deal with the implementation of this algorithm in BUCKY-1.

Subroutine TNBURN is the first routine called by the hydrodynamics part of BUCKY-1 (called in subroutine PLSCF2). The major results of the thermonuclear burn calculation, so far as the hydrodynamics is concerned, are the electron and ion energy sources due to charged particle reaction products (SETN2B and SNTN2B), the ion source term due to neutron energy deposition (SNEU2B), and the momentum source term (DUTN). TNBURN first determines whether a thermonuclear burn calculation will be done on this hydrodynamic time cycle by calling the logical function DOTN. If a calculation is to be done on this cycle the variables that tally up the energy and momentum deposited in each zone for this cycle are set to zero. Then the “starting points” for the reaction products are computed. Although the number of reactions in each zone are computed, the resultant reaction products from several zones may be grouped together and started from the same point in order to save computation time, as shown in Fig. 8.4. Next the number of reactions in each zone are computed by calling the subroutine TNREAC. If only DT reactions are to be computed (ITN=1) then only the 3.5 MeV alpha particle need be transported. Two transport options exist for each reaction product. These are determined by the switches (LHE4, LP, LT, LHE3, LPS, LHE4S). LHE4=1 means that a simple local energy deposition of the DT alpha energy is made where the user can specify the fraction of energy deposited and the remaining energy is lost. The fraction of alphas corresponding to the fraction of energy deposited are returned to the background plasma in the zone where they were created. If the alphas are

GROUPING ZONES FOR CHARGED PARTICLE
REACTION PRODUCT TRANSPORT

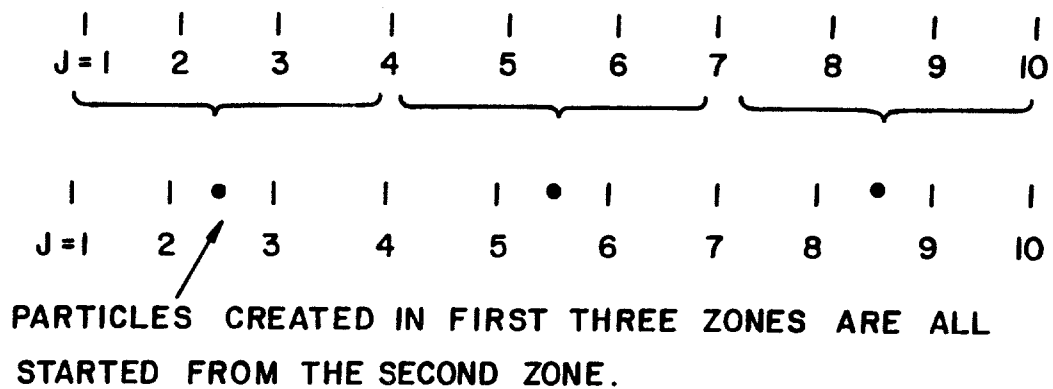


Figure 8.4. Grouping zones for charged particle reaction product transport.

to be transported using TDPT (LHE4=2) then DIRECT is called to determine the number of alphas traveling in each initial direction. This is not straightforward because zones may be grouped together at one starting point. TRANSP is then called to transport 3.5 MeV alphas. Once this is done the subroutine CPSPEC is called if the option is set to compile a charged particle spectrum escaping from the plasma surface. Control then goes to the end of the subroutine, which will be explained later. The other branch at the computed GOTO calls for DD and DT thermal reactions (ITN=2) or DD, DT, and DHe³ thermal reactions (ITN=3). First the 1.01 MeV tritons from the DD reaction are allowed to react nonthermally with deuterium. This is crudely approximated by assuming a fraction of the triton energy (1.01 MeV) is deposited locally and the resultant 3.5 MeV alpha particles are added to the source of alphas that will be transported later. The remaining tritons that have not reacted nonthermally are now transported using either the local deposition approximation (LT=1) or the TDPT method (LT=2). Next the 0.82 MeV He³ reaction product from the DD reaction is treated. The nonthermal He³ reactions with deuterium are computed in the same way as the tritons and the remaining He³ is transported using either local deposition (LHE3=1) or TDPT (LHE3=2). Next the DD 3.02 MeV proton reaction product is transported using local deposition (LP=1) or TDPT (LP=2). Then the DT 3.5 MeV alpha reaction product is transported using local deposition (LHE4=1) or TDPT (LHE4=2). If ITN=2 then only DD and DT thermal reactions are computed and control goes to the end of TNBURN. If ITN=3, then DHe³ reaction products are also transported and DHe³ thermal reactions may also be computed. The 14.7 MeV proton reaction product is transported by either local deposition (LPS=1) or TDPT (LPS=2). Then the 3.6 MeV alpha particle reaction product is transported using local deposition (LHE4S=1) or TDPT (LHE4S=2). At the end of TNBURN thermonuclear energy source terms for the temperature equations, SETN2B and SNTN2B, are computed from the energy tallying variables, DEPETN and DEPNTN, and the thermonuclear time step, DTTN. The momentum transfer term, DUTN, is calculated and the depletion of the numbers of D, T, and He³ in each zone, due to reactions is computed.

Next, the total numbers of reactions on this cycle, DTREAC, DDREAC, and DHE3RE are divided by the time step to give a reaction rate.

The next routine discussed is the logical function DOTN. This routine determines whether a thermonuclear burn calculation is to be done on the current hydrodynamic time cycle and also determines the thermonuclear burn time step, DTTN, which may be greater than or equal to the hydrodynamic time step, DTB. If ITN=0 then no thermonuclear calculation is being done in this PHD-IV computation. If $ITN < 0$ then a thermonuclear calculation will start when the ion temperature exceeds CONTN(1). For instance, if a full implosion and burn calculation is done, then the burn part won't start until the ignition conditions are met. If $ITN > 0$ then a burn calculation is underway. If the hydrodynamic simulation time (TC) is less than the thermonuclear time, TTN, then this hydrodynamic time step is still within the last thermonuclear time step and the rate of thermonuclear energy production, SETN2B and SNTN2B, computed from the last burn time step is still used. If $TC > TTN$ then the rate of thermonuclear energy production must be updated by doing another burn calculation. The thermonuclear time step is computed using the formula

$$\Delta t_{TN} = \text{Max}(\Delta t^{n+1/2}, \Delta t_{TN_{MIN}}).$$

The thermonuclear time step can never be less than the hydrodynamic time step but it may be greater if the hydrodynamic time step becomes less than $\Delta t_{TN_{MIN}}$, an input variable. This lower limit for the burn time step can be adjusted to give the best results with the least computing cost. These varying time steps are illustrated in Fig. 8.5. The energy and momentum redeposition are computed as rates so they are proportionally distributed over the several hydrodynamic time steps that fall within one burn time step. The redeposition of the reaction products and the depletion of the reactant is done all at once on each thermonuclear calculation and this of course is an approximation.

Whereas the subroutine TNBURN contains the logic of choosing the transport technique for each of the six possible reaction products (3.5 MeV alpha, 1.01 MeV triton,

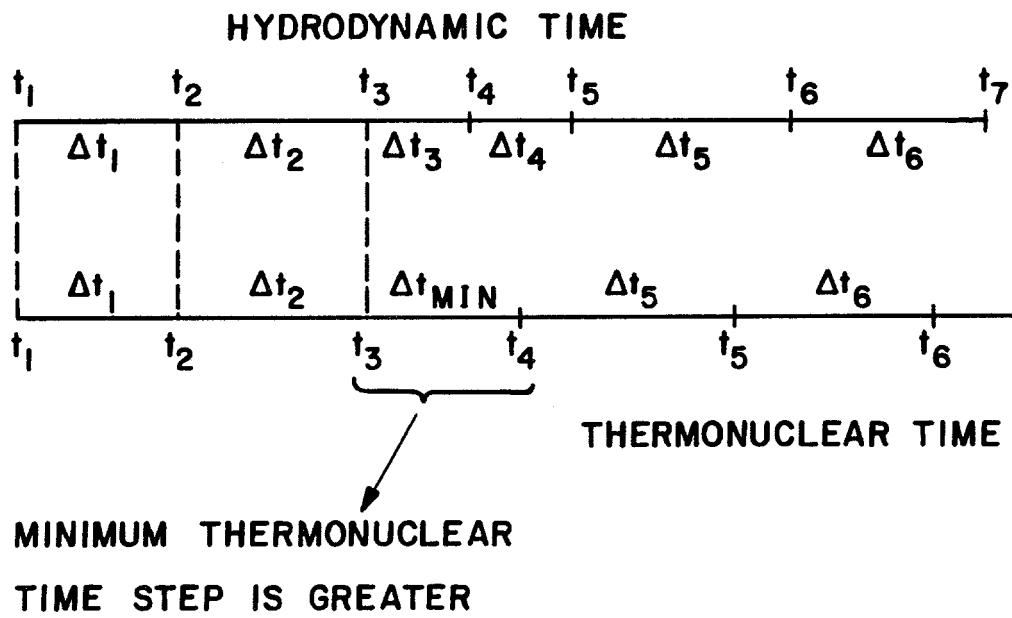


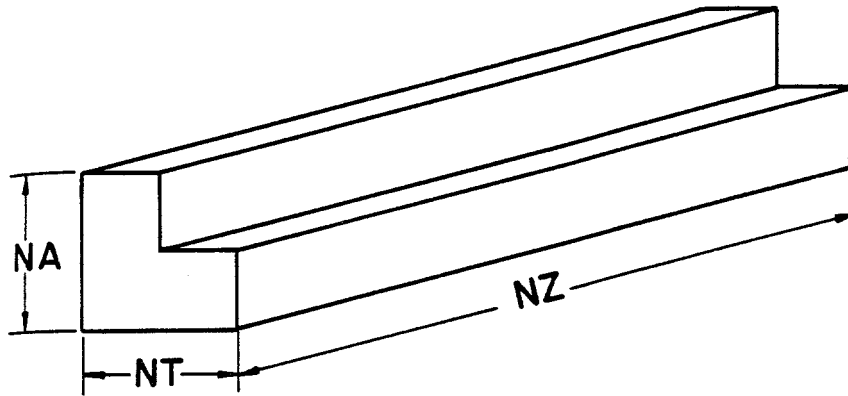
Figure 8.5. Hydrodynamic and thermonuclear time steps.

3.02 MeV proton, 0.82 MeV He³, 14.7 MeV proton, and 3.6 MeV alpha), the subroutine TRANSP contains the logic of transporting a particular reaction product from all previous time cycles and the newborn reaction products on the current cycle. TNBURN passes the vectors in the data structure which correspond to the number (N), position (R), direction (μ), and velocity (V) of this reaction product from the past remembered time cycles. TRANSP does not distinguish the type of charged particle it is transporting; from this point on all of the transport calculation is generally applicable for any fast ion with properties given by TNMASS, ZTN, and CAB. The call to ABCSLO computes the A and B coefficients in the ion range-energy relation (Eq. 8.5) for this type of reaction product. The outer loop is indexed over the zone numbers (IZ). This is not strictly true, for this index is over the starting points of the reaction products (remember that the products from several zones may be grouped together). The next inner loop indexes over the initial directions or angles of the rays along which particles stream (IA). The innermost loop indexes over all of the remembered particle bunches from previous time cycles (IT). The oldest particles are transported first (IT=1) and the function IZIAIT is called to get the index into the vectors of N , R , U , and V that corresponds to these particles. The subroutine SLOW is called to transport and slow down these particles. The new values of N , R , U , and V are returned by SLOW into the variables NDUM, RDUM, UDUM, and VDUM. These are the oldest particles and there is no more room left in the data structure to save them for another cycle. If they have not been thermalized after this last transport calculation then they must be forced to slow down or escape the plasma or they must be forgotten. Either of these choices is available but the first one is the best. To force them to thermalize or escape, the thermonuclear time step, DTTN, is set to a very high value and SLOW is called again. After this the time step is restored to its correct value. The inner loop indices (IT) over all of the remaining “remembered” bunches of particles that originally started in direction μ_{IA} from starting position R_{IZ} . The total number of previous bunches that are remembered is a function of the direction in which they start out (NT(IA)). Those bunches of particles that start in an

inward direction, $\mu \leq 0$, are remembered for more cycles than those that start in an outward direction. Typically the inward directed particles are remembered for twice as many cycles; however, this number can be inputted by the user. The index of each of these bunches of particles (I) is computed by IZIAIT, and SLOW is called to transport them. SLOW returns the results through its argument list to the next lower index (I - 1). In this way the bunches of particles age. A bunch of particles starts out newborn at index $IT=NT(IA)$ and works its way down to $IT=1$ as it grows older. Presumably they will thermalize before reaching $IT=1$ and will be removed from the calculation. The last call to SLOW by TRANSP transports the new reaction products that have been created on the current time step.

The function IZIAIT is necessary because the data structure elements are not simple three-dimensional FORTRAN arrays $R(IZ,IA,IT)$ because the maximum value of IT depends on IA . Consequently the formula given in Fig. 8.6 is used to compute the index.

The subroutine SLOW is the workhorse of the transport calculation and is also the most complex. It has the task of transporting one bunch of particles for a time $\Delta t_{TN(DTTN)}$ and then returning the new position, direction, and velocity of these particles. The values that it receives are NOLD, ROLD, UOLD, and VOLD and the values that it returns are NNEW, RNEW, UNEW, and VNEW. First SLOW determines whether there really are any particles to transport in this bunch; they may have thermalized on a previous time cycle. If there are none then NNEW is also set to zero and SLOW returns to TRANSP. If there are particles, then the inputted values are saved in local variables because the variables in the data structure are saved in single precision while all computations done by the burn calculation are in double precision, therefore the transfer of the data structure values to the local variables is a change in variable type. Next the zone index (J) that corresponds to the zone in which this bunch of particles resides is computed by the function JZONE. If $J < JMAX$ then the particles are still within the plasma boundary but if $J=JMAX$ then the particles may either be within the outer zone or on its boundary. If $RSAVE \geq R1B (JMAX)$



FOR $\mu_I(I_A) \leq 0$ or $IA \leq NA^-$

$$I = [(IZ-1)NA^- + (IA-1)] NT^- + IT$$

FOR $\mu_I(I_A) > 0$ or $IA > NA^-$

$$I = B + [(IZ-1)NA^+ + (IA-NA^- - 1)] NT^+ + IT$$

$$B = NA^- NT^- NZ$$

Figure 8.6. Data structure indexing algorithm.

then the particles have escaped from the plasma and the number of them and their energy is tallied. If a charged particle spectrum is requested then they are added into the appropriate energy group in the CPN vector for later processing by CPSPEC. If they have not escaped from the plasma then FDS is called to compute the distance from their current position (RSAVE) to the next zone boundary that they will intersect, index JNEXT. This distance is DS. Then DELTAV is called to compute the velocity lost (DVDS) in traversing this distance (DS) and also the velocity lost (DVDT) in transporting for a time DTSAVE. Whichever velocity loss is smallest is set equal to DV. If DVDT is smallest, then the bunch of particles does not reach the next zone boundary before the time step is over so FSDST is called to compute the distance traveled DSDT in the time DTSAVE. The subroutine ENEMA is called to tally the energy deposited in zone J as a result of this loss in velocity. RMUV is called to compute the new velocity, position, and direction of this bunch of particles after they have moved this distance. These new values are stored into NNEW, RNEW, UNEW, and VNEW and SLOW returns to TRANSP. If DVDS is smallest, then the bunch of particles reaches the zone boundary before the end of the time step so FDTDS is called to compute the time required (DTDS) to travel the distance DS. The time remaining in the thermonuclear time step is then computed:

$$DTSAVE = DTSAVE - DTDS, \quad (8.22)$$

and ENEMA is called to tally the energy deposited in zone J by the velocity loss DV. RMUV is called to get the new position, direction, and velocity of these particles. The particles' velocity must now be adjusted relative to the fluid velocity of the new zone that they are entering:

$$VSAVE = VSAVE - \frac{1}{2} [U1B(JJ + 1) - U1B(JJ - 1)] * USAVE \quad (8.23)$$

and the new zone index JNEXT (which was saved from the FDS computation) is put into the working index, J. A test is made to insure that the relative velocity of the particles, after the above adjustment, is still positive and if it is, control goes back to the beginning of the subroutine to transport the particles through the next zone or until the time step runs out. If

in either of the cases, DV=DVDS or DV=DVDT, the relation $DV \geq VSAVE$ is encountered, then the bunch of particles have lost all of their energy (i.e. they have thermalized). In this case, the difference between their initial velocity (VSAVE) and their thermal velocity at the ion temperature in zone J is used for DV in the computation of the energy deposited by ENEMA and the particles are added to the thermal background plasma in zone J. NNEW is set to zero and SLOW returns to TRANSP.

The function JZONE very simply determines the zone index corresponding to the zone in which a bunch of particles at radius RSAVE are residing. The subroutine FDS is much more complex, and computes the distance to the next boundary that a bunch of particles at position R and moving in direction μ will intersect. If $\mu = 1$, then the problem is trivial. If $\mu = -1$, then the problem is trivial except that a special case must be made for particles in the center zone for they will go through the origin. If $\mu \neq 1$ and $\neq -1$ and is greater than 0 then they must certainly intersect the outer boundary of the zone in which they reside

$$DS = -R\mu + (R_j^2 - R^2 + (R\mu)^2)^{1/2}. \quad (8.24)$$

If $\mu \leq 0$ then they may or may not intersect the inner boundary of the zone J. If

$$1 - \mu^2 < (R_{j-1}/R)^2 \quad (8.25)$$

then they intersect the inner boundary and

$$DS = -R\mu + (R_{j-1}^2 - R^2 + (R\mu)^2)^{1/2}, \quad (8.26)$$

otherwise they miss the inner boundary and intersect the outer boundary and Eq. (8.24) applies. In slab geometry the calculations are trivial.

The next subroutine called by SLOW is DELTAV and it computes the velocity loss in traveling the distance to the next zone boundary (DS) and the velocity loss in traveling for the time step (DTSAVE). These values are computed according to Eqs. (8.12) and (8.18). The subroutine also has two additional entry points, FDSDT and FDTDS, where the distance

travelled in time DTSAVE and time taken to travel the distance DS are computed according to Eq. (8.20) and Eq. (8.19).

The subroutine RMUV is called to compute the new position, direction and velocity of a bunch of particles after they have been transported. It first computes the new velocity and then skips to the end if slab or planar geometry is used. If spherical geometry is used then it tests to see if $\mu = 1$. If it is, then the calculation is trivial. If $\mu = -1$, then a special case must be made for the center zone, otherwise the calculation is also trivial. If $\mu \neq 1$ and $\mu \neq -1$, then the calculation is slightly less trivial and the law of cosines must be used to compute the new position and direction:

$$R_1 = (R_o^2 + \Delta s^2 - 2R_o \Delta s \mu_o)^{1/2} \quad (8.27)$$

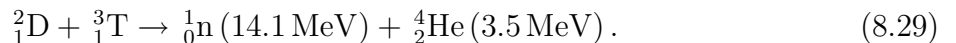
$$\mu_1 = \frac{\Delta s^2 + R_1^2 - R_o^2}{2R_1 \Delta s}. \quad (8.28)$$

If the transport was the result of moving a distance Δs (DS) then the new position of the bunch of particles must be on a zone boundary. In this case (I=0) the new position is not computed but is set equal to RIB(JNEXT) to avoid any roundoff error in the computation.

The last routine called by SLOW is ENEMA. This subroutine computes the energy lost by the bunch of particles and partitions it between the electrons and ions, according to Eqs. (8.13) to (8.15). It then tallies these energies deposited in zone J into the variables DEPETN(J) and DEPNTN(J). It then computes the change in fluid velocity as a result of the momentum deposition (DELTAV) according to Eq. (8.16) and tallies this into the vector DUTN(J).

8.3. Nuclear Energy Deposition Model

The release of energy in a DT fusion reaction is split between the neutron and alpha particle reaction products:



The 3.5 MeV charged alpha particle has a short range in highly compressed DT, with a range of about 0.3 g/cm². The neutral 14 MeV neutron has a much longer range of ≈ 4.15 g/cm². The total cross section for 14 MeV neutrons on D, T, and ${}^4_2\text{He}$ is dominated by elastic scattering, and has a value of $\sigma_{\text{total}} \simeq 1$ barn for each of D, T, and He.

Thus, the range of 14 MeV neutrons is roughly comparable to the ρR -value of a highly compressed high gain ICF target. Detailed neutron transport analyses of neutron energy loss through collisions with DT nuclei show that roughly 3-4 MeV per fusion neutron is deposited in the target by collisions. This is comparable to the energy deposition by the charged alpha particles. Thus, treatment of neutron collisions in the target is important to the high yield target energetics even if it is not critical to the ignition process itself.

In elastic collisions between neutrons and nuclei the average energy loss is given by

$$\overline{\Delta E} = \left(\frac{1 - \alpha}{2} \right) E_i,$$

where

$$\alpha \equiv \left(\frac{A - 1}{A - 2} \right)^2$$

assuming the elastic scattering is isotropic. Thus for D, T, and He:

$$\overline{\Delta E}^{\text{D}} = 6.27 \text{ MeV}$$

$$\overline{\Delta E}^{\text{T}} = 5.29 \text{ MeV}$$

$$\overline{\Delta E}^{\text{He}} = 6.27 \text{ MeV}.$$

At present, we neglect He and average the D and T contributions to get

$$\overline{\Delta E}^{\text{DT}} = 5.78 \text{ MeV}.$$

If Y_{neutron} is the neutron yield on a particular time step, then the neutron energy deposited is

$$E_{\text{neutron}} = Y_{\text{neutron}} (1 - e^{-\tau}) \overline{\Delta E}^{\text{DT}}, \quad (8.30)$$

where τ is a measure of the likelihood that a neutron will escape without a collision. We can estimate τ as:

$$\tau = \frac{\rho R}{\rho R_o},$$

where ρR is the ρR -value of the DT fuel, and ρR_o is related to the 14.1 MeV neutron mean free path in DT.

A previous escape probability analysis [42] shows that for $\rho R \geq 3 \text{ g/cm}^2$, at least two collisions should be treated, while for $\rho R = 2 \text{ g/cm}^2$ one collision is a good approximation. They also compute the average energy deposited per fusion neutron and find it to be nearly linear over the ρR range of interest. Thus, we can approximate

$$(1 - e^{-\tau}) \approx \tau$$

to get

$$E_{\text{neutron}}^{\text{Dep}} = \frac{Y_{\text{neutron}} \overline{\Delta E}^{\text{DT}}}{\rho R_o} \rho R.$$

Using their results, one obtains

$$E_{\text{neutron}}^{\text{Dep}} (\text{MeV}) = Y_{\text{neutron}} (0.64) \rho R (\text{g/cm}^2).$$

We then distribute the deposited energy in the fuel zones by using a $\rho \Delta R$ scaling. Then, the neutron deposition rate is given by:

$$(S_n)_{j-1/2}^n = (1.602 \times 10^{-13} \text{ J/g/s}) Y_{\text{neutron}} (\text{s}^{-1}) \cdot 0.64 (\text{MeV cm}^2 \text{g}) \cdot \frac{(\rho \Delta r)_{j-1/2}}{\Delta m_{j-1/2}}, \quad (8.31)$$

where $\Delta m_{j-1/2}$ is the zone mass. This deposition rate is calculated at the end of subroutine TNBURN.

9. Rapid X-ray Deposition in Cold Media

A rapid x-ray deposition model is used to determine the heating of an ICF target chamber buffer gas and first surface material due to the x-rays emitted from a high gain target. An exponential x-ray attenuation model [43] is used for this purpose. A table of attenuation coefficients [44] for elements with atomic numbers ranging from 1 to 100 and x-ray energies ranging from 0.01 to 1000 keV is provided with the code. These cross sections are valid for cold (unionized) materials. As the code is presently written, gases composed of only one element can be used to attenuate the x-rays.

The initial x-rays that are photo-absorbed by the gas reduce the number of bound electrons available to interact with subsequent x-rays, so the attenuation coefficient decreases as x-rays are deposited. A method of modifying the photoelectric attenuation coefficient of the gas to account for increasing ionization has been developed for this purpose [43]. By counting the number of electrons ejected from each electron shell as the x-rays are deposited, the contribution to the photoelectric attenuation coefficient from each shell can be reduced by an amount proportional to the number of missing electrons. Additionally, the number of electrons lost due to the initial gas temperature is included even though this effect is usually very small. Although simple, this model does at least give the correct attenuation for the limiting cases of a completely neutral and completely ionized atom. The accuracy of this model at intermediate levels of ionization has not been determined. In this version of the code, the model for computing the reduction in photoelectric absorption can only be used with neon, argon, xenon, lithium, carbon, beryllium, oxygen, silicon, helium or nitrogen gas. To extend the model to other gases, the number of electrons in each shell of the neutral atom and the energies of the K, L, and M shells must be added to the EDATA subroutine.

The x-rays emitted by the target can be assumed to be Planckian or an inputted multigroup spectrum. In either case, the code divides the x-ray spectrum into energy groups. The x-rays in each group are then attenuated frequency by frequency.

This code is written to treat the incident x-rays as either an instantaneous or time-dependent source. In both cases, the x-rays are treated as having an infinite propagation speed.

10. Vaporization and Condensation Modeling

BUCKY-1 simulates the vaporization, hydrodynamic motion, and condensation of the first surface material. Under normal conditions, this material is in the form of a liquid or solid. We will refer to it as the “condensed region” or “condensate”. Vaporization effectively occurs in two phases. During the first phase, hard X-rays from the target travel at the speed of light to the wall and, because of their long mean free paths, deposit their energy volumetrically in the condensed region. During the second phase, thermal radiation – i.e., energy absorbed by the background gas and reemitted by the microfireball – deposits its energy near the surface of the condensed region. In BUCKY-1, we model both of these phenomena, using a “volumetric” vaporization model at very early times and a “surface” vaporization model at later times.

For this model, the Lagrangian mesh extends beyond the cavity (vapor region) into the condensed (wall) region. As material is vaporized, the Lagrangian cells undergo hydrodynamic motion. Later, as each cell recondenses, hydrodynamic motion ceases. No mixing occurs between the background gas, which is assumed to be a noncondensable gas, and the vaporized wall material. This approach eliminates the need for rezoning, and allows for better numerical energy conservation.

The hard X-rays that are deposited “volumetrically” in the condensed region vaporize material during the first time cycle of a BUCKY-1 simulation (or during the first several cycles if the time-dependent X-ray deposition option is used). A typical energy deposition profile is illustrated in Figure 10.1, where the energy density is plotted as a function of distance behind the vapor/condensate interface. The condensed layer is divided into 3 regions. In region A, the energy density is higher than the vaporization energy density. All material in this region becomes superheated vapor ($T > T_{\text{vap}}$, the vaporization temperature). In region C, the energy density remains lower than the “sensible” energy density. None of this material is vaporized during the volumetric vaporization phase, and the temperature

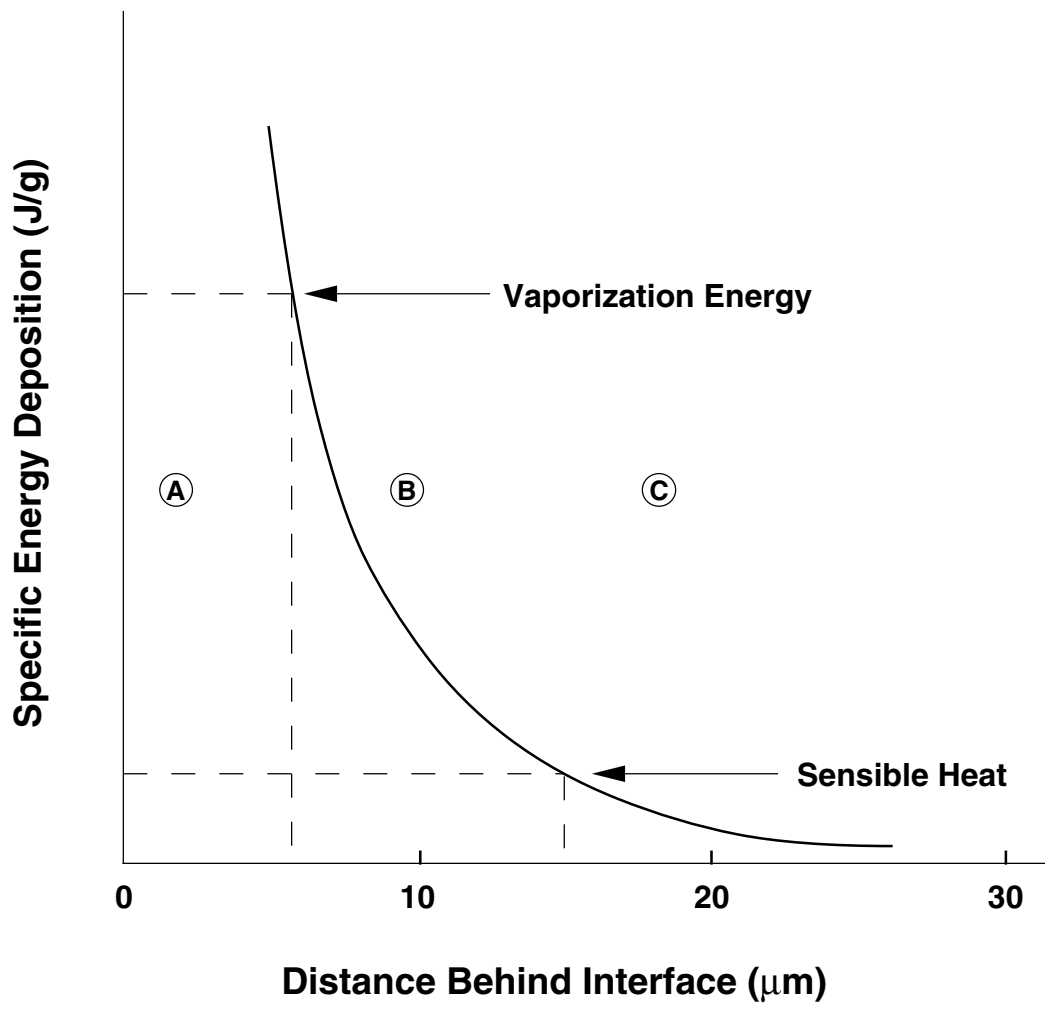


Figure 10.1. Condensed layer vaporization regions.

remains below T_{vap} . In region B, the energy density lies between the vaporization and sensible energies, and the temperature throughout the region is equal to T_{vap} . To determine the amount of material from region B that gets vaporized, we redistribute the energy so that: (1) none of the condensed region has an energy density between the vaporization and sensible values, and (2) energy is conserved.

After material is vaporized, the pressure in the vapor region near the interface becomes very high because of the high density. This causes material to be rapidly accelerated away from the interface, and provides a “recoil” impulse to the wall. BUCKY-1 monitors the pressure at the interface and computes the impulse on the wall directly.

The amount of material vaporized during the volumetric phase can be adjusted by setting $\text{ISW}(25) = 2$. This allows only material with energy densities greater than the vaporization energy density to be vaporized. That is, none of the material in region B is vaporized. This model is less reliable, however, because energy is not conserved.

The primary distinction between the vapor and condensed phases is that vapor cells undergo hydrodynamic motion. The condensed region cells remain stationary due to chemical bonding. In addition, the conservation of momentum and energy equations are solved over all vapor cells. In the condensed region, a one-dimensional conduction equation is solved to determine the energy transport within the region.

After the volumetric deposition phase, radiant energy transported to the condensed region will be effectively deposited at the surface of the interface because of the shorter photon mean free paths. The vaporization and condensation rates are calculated using the kinetic theory model described by Labuntsov and Kryukov [45]. The mass vaporization rate is given by:

$$(dm/dt)_v = \frac{2}{3} P_{\text{sat}} A_{\text{wall}} \left(\frac{\mu}{RT_v} \right)^{1/2} \quad (10.1)$$

where A_{wall} is the surface area of the wall, T_v is the vapor temperature, R is the gas constant, μ is the mean atomic weight of the condensable material, and P_{sat} is the saturation vapor

pressure:

$$P_{\text{sat}} = \exp \left\{ \frac{\Delta H_v}{kT_{\text{vap},o}} \left(1 - \frac{T_{\text{vap},o}}{T_c} \right) \right\} \text{ bar} . \quad (10.2)$$

ΔH_v is the specific heat of vaporization, k is Boltzmann's constant, T_c is the condensate temperature at the interface, and $T_{\text{vap},o}$ is the vaporization temperature at 1 bar. The mass condensation rate is:

$$(dm/dt)_c = \frac{2}{3} f_s f_{NC} P_{\text{vap}} A_{\text{wall}} \left(\frac{\mu}{RT_v} \right)^{1/2} \quad (10.3)$$

where f_s is the sticking coefficient, F_{NC} is a correction factor for noncondensable gas effect, and P_{vap} is the vapor pressure given by the ideal gas law:

$$P_{\text{vap}} = \rho_v \frac{RT_v}{\mu} \quad (10.4)$$

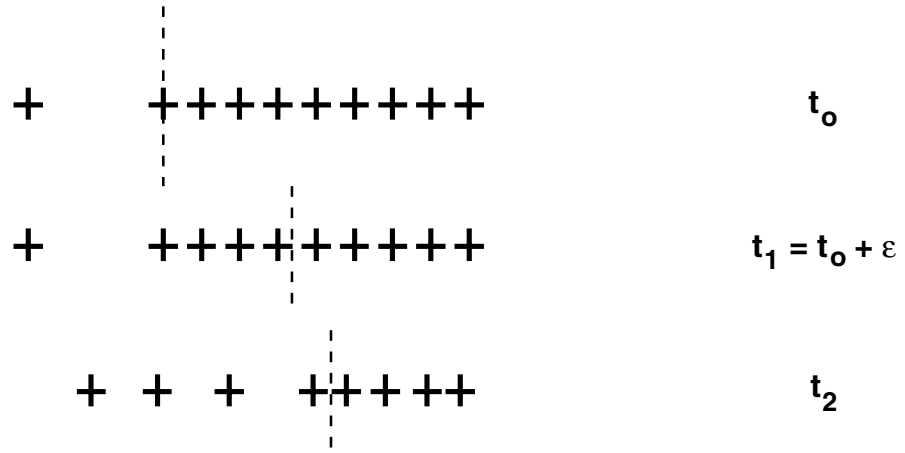
where ρ_v is the vapor density.

Lagrangian cells undergo hydrodynamic motion only after an entire cell is vaporized. Figure 10.2 illustrates the evolution of mesh points during a typical simulation. Vapor cells are to the left of the dashed line and the condensed region is to the right of it. The “+”s represent the cell boundaries and the vertical dashed line represents the vapor/condensate interface. A short time after the target explodes ($t_1 = t_o + \varepsilon$), the target's hard X-rays are deposited in the condensed region, vaporizing a number of cells. Since the vaporized mass is not in general an integral number of cells, the interface is located between cell boundaries. At later times (t_2), the vapor expands away from the wall while thermal radiation from the fireball vaporizes additional cells. No mass is ever exchanged between Lagrangian cells as mixing effects are neglected.

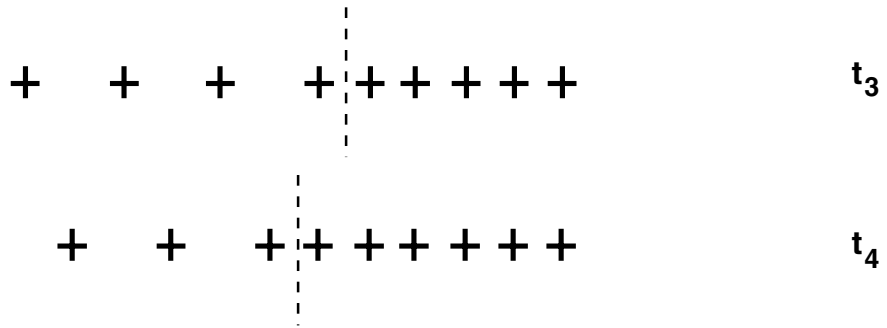
As the radiative flux from within the cavity subsides and the temperature at the surface of the condensed region drops, the condensation rate begins to exceed the vaporization rate. Again, the interface is tracked as condensation occurs. In Figure 10.2 shows vapor moving toward the interface as material recondenses back onto the surface (t_3 and t_4). If any portion of a Lagrangian cell has condensed, it no longer undergoes hydrodynamic motion.

Vapor

Wall



Vaporization



Condensation

Figure 10.2. Evolution of mesh points during a vaporization/condensation calculation.

To calculate energy transport within the condensed region, BUCKY-1 solves the one-dimensional conduction equation:

$$C_P \frac{dT}{dt} = \frac{\kappa}{\rho} \frac{d^2T}{dx^2} + S \quad (10.5)$$

where C_P is the specific heat at constant pressure, κ is the thermal conductivity, ρ is the density in the condensed region, T is the temperature, and x the spatial coordinate. S is a source term which accounts for the energy deposition from the radiative heat flux and debris ions. In practice, only the first cell has a non-zero source term because the heat flux is assumed to be deposited at the surface. The conduction equation is also subject to the following boundary conditions. The temperature at the back of the condensed layer is constant (Dirichlet condition) as heat flows through the back of the condensed region. At the vapor/condensate interface, the conductive heat flux is assumed to be zero (Neumann condition).

11. Energy Conservation Check

Energy conservation is monitored for the plasma and, if applicable, condensate system. At the end of each time step, a check is made to ensure that the difference equations are conserving energy. After integrating the energy equations over time and space, the conservation equations for the plasma, condensate, and radiation can be written as:

$$\text{Ions} \quad e_i + T_P = e_i^o + T_p^o + H_i - X_{e-i} - F_i - G_{i-e} - G_{i-R} - W_i \quad (11.1)$$

$$\text{Electrons} \quad e_e = e_e^o + H_e - E_{R-e} + X_{e-i} - F_e + G_{i-e} - W_e \quad (11.2)$$

$$\text{Radiation} \quad e_R = e_R^o + E_{R-e} - F_R + G_{i-R} + W_R \quad (11.3)$$

$$\text{Total Target} \quad e_{TOT} + T_P = e_{TOT}^o + T_P^o + H_{TOT} - W_{TOT} - F_{TOT} \quad (11.4)$$

$$\text{Condensate} \quad e_c = e_c^o + F_R + F_e + F_i - J_{PT} - Q_B + H_C \quad (11.5)$$

The superscript “o” signifies the initial values. The physical definitions of each term are:

e_x	total internal energy of the ions, electrons, radiation, or condensate
T_p	total kinetic energy of the plasma
H_x	total source of energy to the ions, electrons, radiation, or condensate
E_{R-e}	total radiation energy exchanged between the plasma and radiation field
F_x	total energy conducted across the boundaries from the ions, electrons, or radiation
G_{i-x}	work exchanged between the ions and radiation (x = R) or electrons (x = e)
W_x	work done on the boundary by ions, electrons, or radiation
Q_B	total energy conducted through the back of the condensed region
J_{PT}	total energy exchanged during phase transformation between the plasma and condensate

Equation (11.4) states that the total internal plus fluid kinetic energy at a given time (t^{n+1}) must equal the initial internal and kinetic energy plus all source energy up to this time, minus all heat conducted across the outer boundary, all work done on the outer boundary, and all energy lost to radiation up to this time.

The term, G_e , appears because the electrons and ions have their own temperature and pressure but are constrained to move together at the same fluid velocity. This is the total work done by the ions on the electrons to maintain this constraint. Each of these terms at time step “ n ” is given in finite difference form as follows:

$$e_x^{n+1} = \sum_{j=1}^{\text{JMAX}} (E_x)_{j-1/2}^{n+1} \Delta m_{o_{j-1/2}}, \quad x = e, i, R \quad (11.6)$$

$$T^{n+1} = \frac{1}{2} \sum_{j=1}^{\text{JMAX}} \Delta m_{o_j} (U_j^{n+1/2})^2$$

$$H_x^{n+1} = H_x^n + \Delta t^{n+1/2} \sum_{j=1}^{\text{JMAX}} (S_x)_{j-1/2}^{n+1/2} \Delta m_{o_{j-1/2}} \quad (11.7)$$

$$X_{e-i}^{n+1} = X_{e-i}^n + \Delta t^{n+1/2} \sum_{j=1}^{\text{JMAX}} (R_{e-i})_{j-1/2}^{n+1/2} \Delta m_{o_{j-1/2}} \quad (11.8)$$

$$E_{R-e}^{n+1} = E_{R-e}^n + \Delta t^{n+1/2} \sum_{j=1}^{\text{JMAX}} (\dot{Q}_{R-e})_{j-1/2}^{n+1/2} \Delta m_{o_{j-1/2}} \quad (11.9)$$

$$\begin{aligned} G_{i-R}^{n+1} &= G_{i-R}^n + \Delta t^{n+1/2} \sum_{j=1}^{\text{JMAX}} U_j^{n+1/2} (r^{\delta-1})_j^{n+1/2} (P_{R_{j+1/2}}^{n+1/2} - P_{R_{j-1/2}}^{n+1/2}) \\ &+ \Delta t^{n+1/2} u_{\text{JMAX}}^{n+1/2} (r^{\delta-1})_{\text{JMAX}}^{n+1/2} [P_{R_{\text{JMAX}+1/2}}^{n+1/2} - P_{R_{\text{JMAX}-1/2}}^{n+1/2}] / 2 \\ &+ \text{inner boundary term } (j = 1) \end{aligned} \quad (11.10)$$

$$\begin{aligned} F_P^{n+1} &= F_P^n + \Delta t^{n+1/2} \left[\frac{r^{\delta-1}}{\left(\frac{\Delta r}{\kappa_P} \right)} \right]_{\text{JMAX}}^{n+1/2} (T_{P_{\text{JMAX}+1/2}}^{n+1/2} - T_{P_{\text{JMAX}-1/2}}^{n+1/2}) \quad P = e \text{ or } i \\ &+ \text{inner boundary term } (j = 1) \end{aligned} \quad (11.11)$$

$$\begin{aligned} F_R^{n+1} &= F_R^n + \Delta t^{n+1/2} \left[\frac{r^{\delta-1}}{\left(\frac{\Delta r}{\kappa_R} \right) + \frac{\Delta E_R}{F_R}} \right]_{\text{JMAX}}^{n+1/2} (E_{R_{\text{JMAX}+1/2}}^{n+1/2} - E_{R_{\text{JMAX}-1/2}}^{n+1/2}) \\ &+ \text{inner boundary term } (j = 1) \end{aligned} \quad (11.12)$$

$$W_x^{n+1} = W_x^n + \Delta t^{n+1/2} \left\{ u_{\text{JMAX}}^{n+1/2} (r^{\delta-1})_{\text{JMAX}}^{n+1/2} P_{\text{JMAX}}^{n+1/2} \right\} \quad (11.13)$$

$$J_{PT}^{n+1} = J_{PT}^n + \Delta t^{n+1/2} \left[\left(\frac{dm}{dt} \right)_P^n - \left(\frac{dm}{dt} \right)_c^n \right] \cdot [e_P^{n+1} - e_c^{n+1}] \quad (11.14)$$

$$Q_B^{n+1} = Q_B^n + \Delta t^{n+1/2} \left(\frac{r^{\delta-1}}{\kappa_P} \right)_{JMAXC}^{n+1/2} (T_{eJMAXC+1/2}^{n+1/2} - T_{eJMAXC-1/2}^{n+1/2}) \quad (11.15)$$

BUCKY-1 calculations usually conserve energy to within better than 2-5%.

12. Time Step Control

After each time step, the next time step is determined from a set of stability and accuracy constraints. The new time step is determined by

$$\Delta t^{n+3/2} = \text{Max} \left[\Delta t_{\min}, \text{Min} \left(\Delta t_{\max}, \frac{K_1}{R_1^{n+1}}, \frac{K_2 \Delta t^{n+1/2}}{R_2^{n+1}}, \dots, \frac{K_5 \Delta t^{n+1/2}}{R_5^{n+1}} \right) \right] \quad (12.1)$$

where

$$R_1^{n+1} = \text{Max} \left[(V_{j-1/2}^{n+1} P_{j-1/2}^{n+1})^{1/2} / \Delta r_{j-1/2}^{n+1/2} \right] \quad (12.2)$$

$$R_2^{n+1} = \text{Max} \left[(V_{j-1/2}^{n+1} - V_{j-1/2}^n) / V_{j-1/2}^{n+1/2} \right] \quad (12.3)$$

$$R_3^{n+1} = \text{Max} \left[(E_{R_{j-1/2}}^{n+1} - E_{R_{j-1/2}}^n) / E_{R_{j-1/2}}^{n+1/2} \right] \quad (12.4)$$

$$R_4^{n+1} = \text{Max} \left[(T_{i_{j-1/2}}^{n+1} - T_{i_{j-1/2}}^n) / T_{i_{j-1/2}}^{n+1/2} \right] \quad (12.5)$$

$$R_5^{n+1} = \text{Max} \left[(T_{e_{j-1/2}}^{n+1} - T_{e_{j-1/2}}^n) / T_{e_{j-1/2}}^{n+1/2} \right] \quad (12.6)$$

The maximum values of R_1 through R_5 are found by sweeping over the zones. The input parameters K_1 through K_5 determine the severity of each constraint. The default value for K_1 , K_2 , K_4 , and K_5 is 0.05. The default value of K_3 is set to 0.10.

13. Code Structure

BUCKY-1 is written in FORTRAN 77. The code is written to run primarily on UNIX workstations. At the University of Wisconsin it has been utilized on HP, SUN, and IBM RS6000 workstations. It (in previous forms) has also been run on CRAY X-MP and Y-MP supercomputers. A pre-processor operates on the source code to make FORTRAN (.f) files. During this time, machine-dependent parts of the code (e.g., time and date calls, vector merge operations, etc.) are inserted appropriately into the “.f” files. This allows for the code to be used conveniently on multiple platforms.

13.1. Subroutines

A flow diagram of the BUCKY-1 subroutines is shown in Figures 13.1 through 13.4. Below, each of the subroutines is listed along with brief description of its use. The first 2 listed are the main driver program and a block data subroutine for data initialization. The rest of the subroutines are listed in alphabetical order.

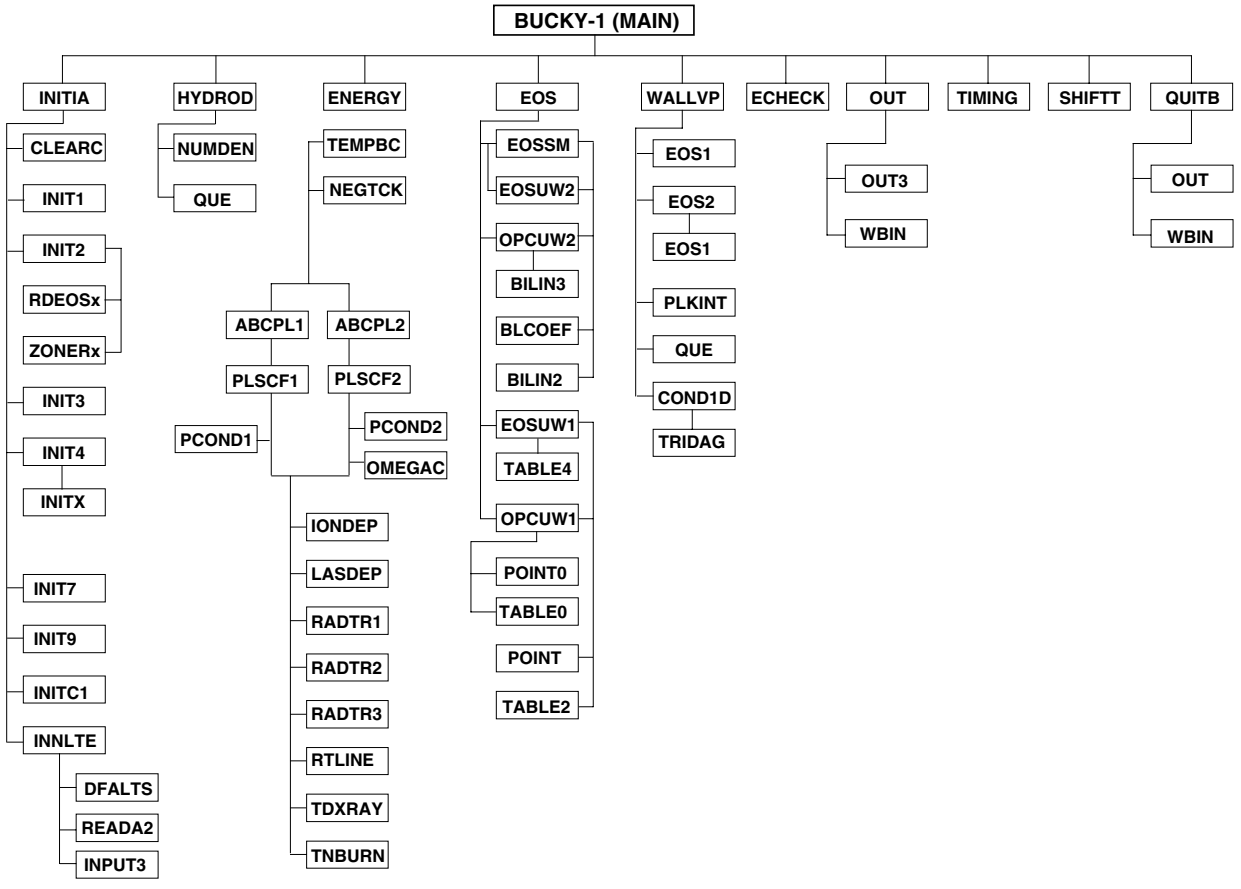


Figure 13.1. Flow diagram for BUCKY-1.

Initialization Routines

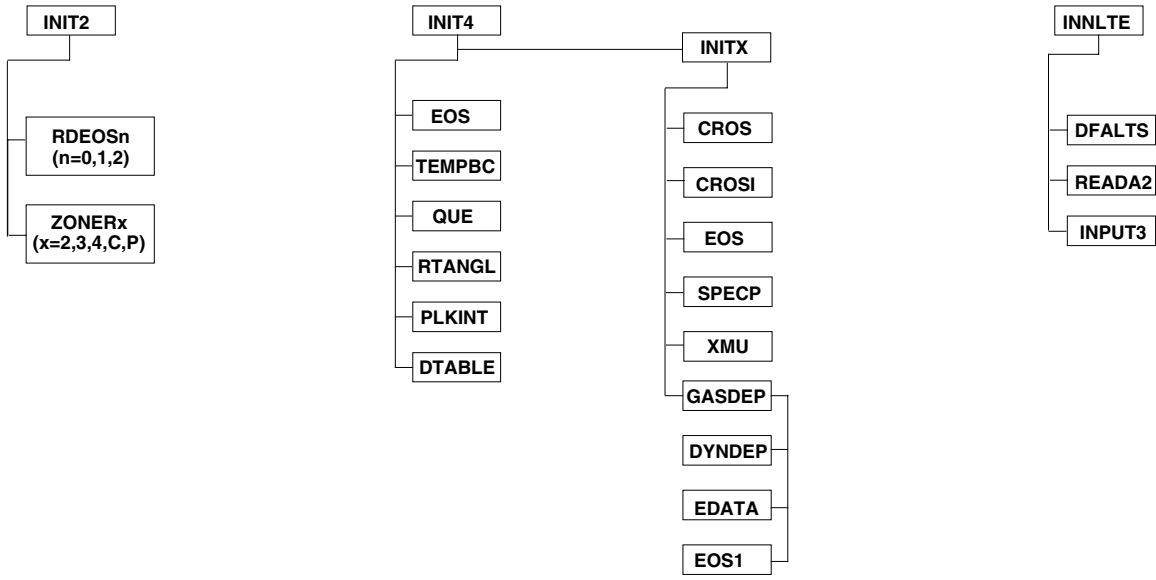


Figure 13.2. Flow diagram for BUCKY-1 initialization routines.

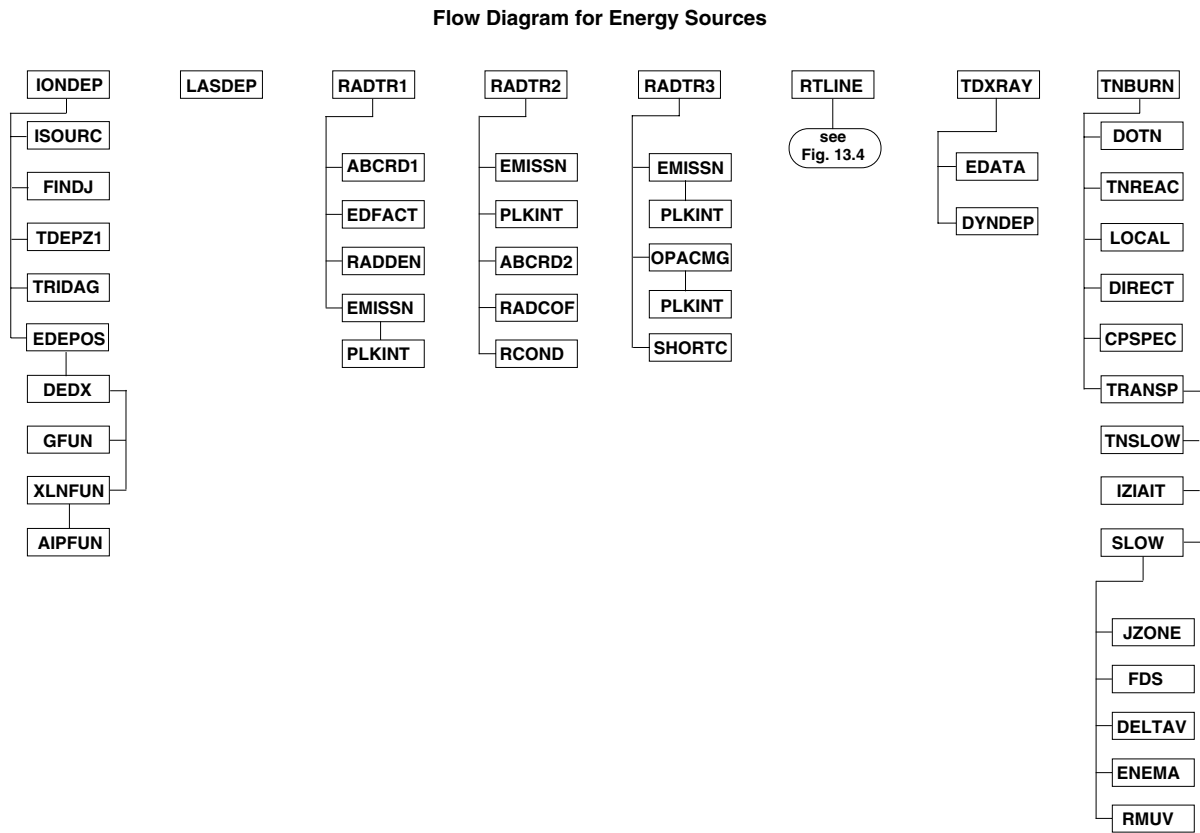


Figure 13.3. Flow diagram for BUCKY-1 energy source routines.

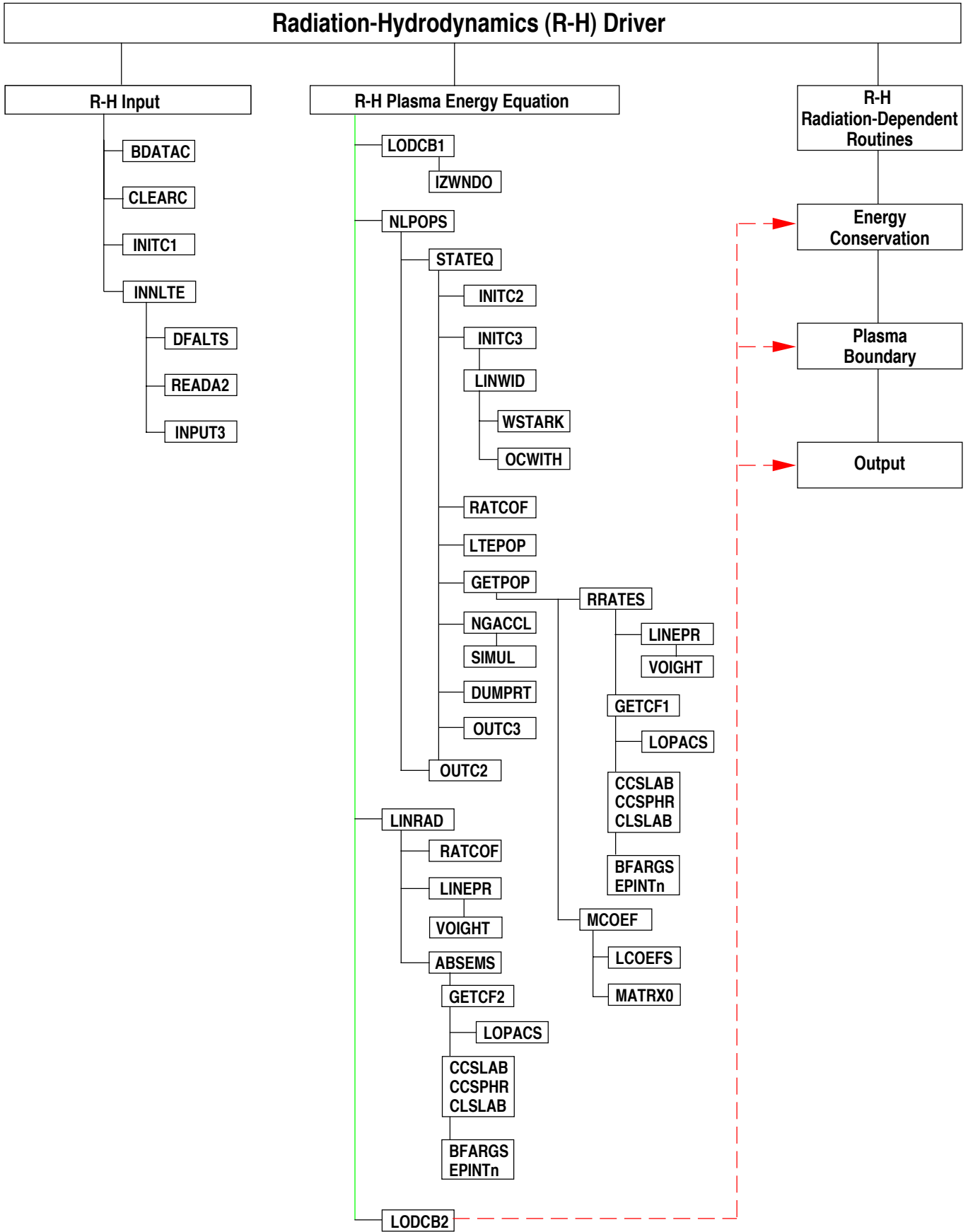


Figure 13.4. Flow diagram for BUCKY-1 CRE line transport routines.

Table 13.1. BUCKY-1 Subroutines

Subroutine Name	Called By	Calls To	Description
MAIN		INITIA, HYDROD, ENERGY, WALLVP, ECHECK, EOS, OUT, QUITB, SHIFTT, TIMING	main driver program
BDATAAC			block data routine for initializing constants
ABCPL1	ENERGY	PLSCF1	computes A, B, C, D, E, and F coefficients used to solve the plasma temperature equation when using the 1- T option ($T_{\text{ion}} = T_e$)
ABCPL2	ENERGY	PLSCF1	same as for ABCPL1, but for 2- T option ($T_{\text{ion}} \neq T_e$)
ABCRD1	RADTR1	—	computes A, B, C, D, E, and F coefficients used to solve the radiation transport equation for a specified frequency group when using the variable Eddington option
ABCRD2	RADTR2	RADCOF	same as for ABCRD1, but for radiation diffusion option
AIPFUN	XLNFUN	—	computes the average ionization potential of the background gas for use in the Bethe stopping power equation
BILIN2	EOSSM, EOSUW2, OPCUW2	—	performs bilinear interpolation on EOS tables
BILIN3	OPCUW2	—	performs bilinear interpolation on multigroup opacity tables
BLCOEF	EOSSM, EOSUW2, OPCUW2	LOCATE	sets up coefficients for bilinear interpolation
COND1D	WALLVP	TRIDAG	solves the 1-dimensional conduction equation for the condensed region

Table 13.1. (Continued)

Subroutine Name	Called By	Calls To	Description
CPSPEC	TNBURN	—	tallies charged particle fusion reaction products escaping outermost Lagrangian zone
CROS	INITX	—	reads the photoionization cross sections for the x-ray attenuation model
CROSI	INITX	—	searches through the x-ray cross section table and computes the cross section of the gas
DEDX	EDEPOS	GFUN, XLNFUN	computes the ion deposition stopping power
DELTAV	SLOW	—	computes change in velocity for a bunch of fast charged particles
DEPLET		—	computes new number densities for the different ionic species that can change due to fusion burning
DIRECT	TNBURN	—	computes the number of particles starting in each angular direction after creation from fusion burn
DOTN	TNBURN	—	determines whether fusion burn calculation is to be done on each hydrodynamic time step
DTABLE	INIT4	—	sets up tables for interpolation using Newton divided difference scheme
DYNDEP	GASDEP, TDXRAY	—	computes the x-ray deposition and the new absorption cross section of each zone
ECHECK	MAIN	—	computes the integrals used in the energy conservation check
EDATA	GASDEP, TDXRAY	—	provides the electron shell structure of the cold gas for the x-ray deposition calculation
EDEPOS	IONDEP	DEDX	computes the ion deposition stopping power
EDFACT	RADTR1	—	computes Eddington factors when using variable Eddington radiation transport model

Table 13.1. (Continued)

Subroutine Name	Called By	Calls To	Description
EMISSN	RADTR(1,2,3)		computes the frequency-dependent radiation emission
ENEMA	SLOW	—	computes energy lost to background electrons and ions by fast charged particles from fusion reactions
ENERGY	MAIN	ABCPL1, ABCPL2, NEGTCCK, TEMPBC	solves electron and ion energy equations
EOS	MAIN, INIT4, INITX	EOSSM, EOSUW1, EOSUW2, OPCUW1, OPCUW2, PRESBC	computes the equation of state quantities
EOS1	EOS2, GASDEP, WALLVP	POINT1, TABLE1	computes the equation of state quantities
EOS2	WALLVP	EOS1	computes the equation of state quantities
EOSSM	EOS	BILIN2, BLCOEFL	looks up equation of state data for SESAME tables
EOSUW1	EOS	POINT, TABLE2, TABLE4	looks up equation of state data from EOSOPA and/or IONMIX tables
EOSUW2	EOS	BILIN2, BLCOEFL	looks up equation of state data from EOSOPA and/or IONMIX tables
FDS	SLOW	—	computes the distance from the position of a bunch of fusion reaction products to the next zone boundary
FINDJ	IONDEP	—	finds the index of the zone an ion bunch is located within
FNEWT	TEMPBC	—	interpolation function using Newton divided difference scheme
GASDEP	INITX	DYNDEP, EDATA, EOS1	computes the temperature of the gas after x-ray deposition

Table 13.1. (Continued)

Subroutine Name	Called By	Calls To	Description
GFUN	DEDX	—	computes the value of a mathematical function used in the stopping power calculation
HYDROD	MAIN	NUMDEN, QUE	solves the equation of motion for the fluid velocity, new zone radii, Δr 's, zone volumes, and specific volumes
INITIA	MAIN	CLEARC, INIT(1,2,3,4,7,9), INITC1, INNLTE	reads namelist input and calls other initialization routines
INITX	INIT4	CROS, CROSI, EOS, GASDEP, SPECPC, XMU	initializes quantities for the x-ray deposition calculation
INIT1	INITIA	—	sets variable default values before reading input
INIT2	INITIA	RDEOS(0,1,2), ZONER(2,3,4,C,P)	computes initial conditions and writes a summary of the initial conditions
INIT3	INITIA	—	computes initial conditions and writes a summary of the initial conditions
INIT4	INITIA	DTABLE, EOS, INITX, PLKINT, QUE, RTANGL, TEMPBC	computes initial conditions and writes a summary of the initial conditions
INIT7	INITIA	—	computes initial conditions and writes a summary of the initial conditions
INIT9	INITIA	—	computes initial conditions and writes a summary of the initial conditions
IONDEP	PLSCF(1,2)	EDEPOS, FINDJ ISOURE, TDEPZ1	computes the ion energy deposition due to all debris ions

Table 13.1. (Continued)

Subroutine Name	Called By	Calls To	Description
ISOURC	IONDEP	—	computes the number of debris ions emitted from the source during a given time interval
IZIAIT	TRANSP	—	determines index in data structure that holds information on fusion reaction products
JZONE	SLOW	—	determines zone index that a bunch of fusion reaction products are residing in
LASDEP	PLSCF(1,2)	—	computes laser energy deposition at each zone
LLAM	OMEGAC, PCOND1, PCOND2	—	computes log Λ for the thermal conductivity
LOCAL	TNBURN	—	computes the energy deposited in the background electrons and ions from fusion reaction products if “local dump” approximation is used
LOCATE	BLCOEF	—	locate indices for EOS bilinear interpolations
NEGTCK	ENERGY	—	checks for negative temperatures after solution of plasma energy equation
NUMDEN	HYDROD	—	computes number densities from the specific volume
OMEGAC	PLSCF2	LLAM	computes the ion-electron energy coupling coefficients
OPACMG	RADTR3	PLKINT	calculates opacity grid for short characteristics radiation transport option
OPCUW1	EOS	POINT, POINT0, TABLE2, TABLE0	looks up multigroup opacities from EOSOPA and/or IONMIX tables
OPCUW2	EOS	BILIN2, BILIN3, BLCOEF	looks up multigroup opacities from EOSOPA and/or IONMIX tables

Table 13.1. (Continued)

Subroutine Name	Called By	Calls To	Description
OUT	MAIN, QUITB	OUT1, OUT3, WBIN	writes output at the end of specified simulation times or number of cycles
OUT1,3	OUT	—	writes output at the end of specified simulation times or number of cycles
PCOND1	PLSCF1	LLAM	computes plasma thermal conductivities for 1- T option
PCOND2	PLSCF2	LLAM	same as PCOND1, but for 2- T option
PLKINT	EMISSN, INIT4, TEMPBC, OPACMG, WALLVP	—	returns the integral of the Planck function
PLSCF1	ABCPL1	IONDEP, LASDEP, PCOND1, RADTR(1,2,3), RTLIN, TDXRAY, TNBURN	computes α , γ , a , and β coefficients used to solve the plasma temperature equation when using the 1- T option
PLSCF2	ABCPL2	IONDEP, LASDEP, PCOND2, OMEGAC, RADTR(1,2,3), RTLIN, TDXRAY, TNBURN	same as PLSCF1, but for the 2- T option.
POINT	EOSUW1, OPCUW1	—	finds pointers in the equation of state tables
POINT1	EOS1	—	finds pointers in the equation of state tables
POINT0	OPCUW1	—	finds pointers in the multigroup opacity tables
QUE	HYDROD, INIT4, WALLVP	—	computes the artificial viscosity

Table 13.1. (Continued)

Subroutine Name	Called By	Calls To	Description
QUITB	MAIN	OUT, WBIN	wraps up the calculation at the end and performs final printouts
PRESBC	EOS		sets pressure boundary conditions
RADCOF	ABCRD2	RCOND	computes α , γ , ω , a , and β coefficients used to solve the radiation energy equation for a specified frequency group when using the multifrequency radiation diffusion
RADDEN	RADTR1	—	computes radiation energy densities in each zone when using variable Eddington radiation transport model
RADTR1	PLSCF(1,2,3)	ABCRD1, EDFACT, EMISSN, RADDEN	computes radiation energy densities when using variable Eddington transport model
RADTR2	PLSCF(1,2,3)	ABCRD2, EMISSN	computes radiation energy densities when using radiation diffusion model
RADTR3	PLSCF(1,2,3)	EMISSN, OPACMG, SHORTC	computes radiation energy densities when using short characteristics transport model
RCOND	RADCOF	—	computes the radiation conductivity for a specified frequency group when using the multifrequency radiation diffusion option
RDEOS0	INIT2	—	read in the equation of state and opacity data (EOSOPA format)
RDEOS1	INIT2	—	read in equation of state and opacity data (IONMIX format)
RDEOS2	INIT2	—	read in equation of state data (SESAME format)
RMUV	SLOW	—	computes new position, direction of motion, and velocity of fast fusion reaction products
RTANGL	INIT4	—	sets up angles and integration weights for multiangle radiation transport option

Table 13.1. (Continued)

Subroutine Name	Called By	Calls To	Description
RTLIN	PLSCF(1,2)	LINRAD, LODCB1, LODCB2, NLPOPS	controls CRE line radiation algorithms
SHIFTT	MAIN	—	shifts values of variables at $(n + 1)$ to variables at (n) at the end of a time step.
SHORTC	RADTR3	—	solves radiation transport equation using method of short characteristics
SIGMAV	TNREAC	—	computes fusion reaction rates
SLOW	TRANSP	DELTA V, ENEMA, FDS, JZONE, RMUV	computes the slowing down of fast fusion reaction products
SPECP	INITX	—	computes the x-ray spectrum
TABLE1	EOS1	—	interpolates in the equation of state tables using the pointers
TABLE2	EOSUW1, OPCUW1	—	interpolates in the equation of state tables
TABLE4	EOSUW1	—	interpolates in the equation of state tables
TABLE0	OPCUW1	—	interpolates in the opacity tables
TDEPZ1	IONDEP	TRIDAG	computes the time-dependent debris ion ionization populations
TDXRAY	PLSCF(1,2)	DYNDEP, EDATA	computes the time-dependent x-ray deposition
TEMPBC	ENERGY, INIT4	FNEWT, PLKINT	computes the plasma temperature and radiation specific energy boundary conditions
TIMING	MAIN	—	computes a new time step and determines whether the calculation is over

Table 13.1. (Continued)

Subroutine Name	Called By	Calls To	Description
TNBURN	PLSCF(1,2)	CPSPEC, DIRECT, DOTN, LOCAL, TNREAC, TRANSP	main routine for fusion burn calculation
TNREAC	TNBURN	SIGMAV	computes the number of DT, DD, and DHe ³ reactions in each zone
TNSLOW	TRANSP	—	sets up coefficients for the slowing down of fast fusion reaction products
TRANSP	TNBURN	IZIAIT, SLOW, TNSLOW	transport solver for fusion reaction products
TRIDAG	COND1D, TDEPZ1	—	tridiagonal matrix solver for the condensed region conduction equation and the rate equations for the time-dependent charge state calculations
WALLVP	MAIN	COND1D, EOS1, EOS2, QUE, PLKINT	computes vaporization/condensation of wall material
WBIN	OUT, QUITB	—	writes binary output to unit 8 for post-processing
XLNFUN	DEDX	AIPFUN	computes log Λ for the stopping power calculations
XMU	INITX	—	calculates the mass attenuation coefficients for the x-ray deposition calculations
ZONERC, ZONERP ZONER2,3,4	INIT2	—	zoning setup routine

Table 13.1. (Continued)

Subroutine Name	Called By	Calls To	Description
ABSEMS	LINRAD	GETCF2	Computes CRE line power densities and fluxes.
BFARGS	CCSLAB, CCSPHR, CLSLAB	—	Sets up bound-free escape probability parameters.
CLSLAB	GETCF1, GETCF2	EPINT1	Computes escape probability coupling coefficients for Doppler profiles in planar geometry.
CLSLAB	GETCF1, GETCF2	EPINT9, BFARGS	Computes escape probability coupling coefficients for bound-free transitions in planar geometry.
CCSPHR	GETCF1, GETCF2	EPINT2, EPINT3, BFARGS	Computes escape probability coupling coefficients for bound-bound and bound-free transitions in planar geometry.
DFALTS	INNLTE	—	Initialize variables and set default values for CRE calculation.
CLEARC	Hydro initialization subroutine	—	Initializes some CRE variables to zero.
DUMPRT	MATRX0, STATEQ	—	Writes CRE radiative transfer parameters to output files.
EPINT1	CLSLAB, CCSPHR	—	Computes escape probability integral for a Doppler profile.
EPINT2	CLSLAB, CCSPHR	—	Computes escape probability integral for a Lorentz profile.
EPINT3	CLSLAB, CCSPHR	—	Compute escape probability integral for a Voigt profile.
EPINT9	CLSLAB, CCSPHR	—	Compute escape probability integral for bound-free transitions.
GETCF1	RRATES	CCSLAB, CCSPHR, CLSLAB, LOPACS	Compute zone-to-zone coupling coefficients for all transitions.

Table 13.1 (Continued)

Subroutine Name	Called By	Calls To	Description
GETCF2	ABSEMS	CCSLAB, CCSPHR, CLSLAB, LOPACS	Compute zone-to-zone coupling coefficients for all transitions.
GETPOP	STATEQ	MCOEF1, RRATES	Computes CRE atomic level populations for all gas species.
INITC1	Hydro initialization subroutine	—	Initialize some atomic parameters and print out control switches and constants for CRE calculation.
INITC2	STATEQ	—	Initialize radiative transfer parameters for CRE calculation.
INITC3	STATEQ	LINWID	Initialize line profile parameters for CRE calculation.
INNLTE	Hydro initialization subroutine	INPUT3, READA2, DFALTS	Input controller routine for CRE calculation.
INPUT3	INPUT	—	Reads in photoionization data for CRE calculation.
IZWDO	LODCB1	—	Sets range of ionization stages to be considered for each spatial zone in CRE calculation.
LCOEFS	MCOEF0	—	Sets up statistical equilibrium matrix coefficients.
LINEPR	LINRAD, RRATES	VOIGT	Computes line profile parameters.
LINWID	INITC3	WSTARK, OCWITH	Sets up line broadening parameters.
LOPACS	GETCF1, GETCF2	—	Computes source functions and opacities for a given line.
LTEPOP	STATEQ	—	Computes LTE populations for each zone.
MATRX0	MCOEF1	LAPACK routines	Inverts statistical equilibrium matrix to get atomic level populations for 1 spatial zone.
MCOEF1	GETPOP	LCOEFS, MATRX0	Sets up and solves statistical equilibrium equations for all zones.
LINRAD	Hydro plasma energy subroutines	RATCOF, LINEPR, ABSEMS	Computes line radiation absorption and emission rates for each spatial zone.

Table 13.1 (Continued)

Subroutine Name	Called By	Calls To	Description
LODCB1	Hydro plasma energy subroutines	IZWNO	Loads hydro parameters into CRE common blocks.
LODCB2	Hydro plasma energy subroutines	—	Loads CRE results into hydro common blocks.
NGACCL	STATEQ	SIMUL	Ng acceleration algorithm.
NLPOPS	Hydro plasma subroutine	STATEQ, OUTC2	Computes non-LTE atomic level populations.
OCWITH	LINWID	—	Sets up line broadening parameters for H-like ions at high density.
OUTC2	STATEQ, NLPOPS	—	Prints out atomic level populations.
OUTC3	STATEQ	—	Prints out transition rates.
RATCOF	STATEQ, LINRAD	—	Calculates collisional and radiative rate coefficients for CRE calculation.
READA2	INNLTE	—	Reads in atomic data for CRE calculation.
RRATES SIMUL	GETPOP NGACCL	LINEPR, GETCF1 —	Computes radiation-dependent rate coefficients. Solves a set of linear equations (for small matrices only).
STATEQ	NLPOPS	INITC2, INITC3, RATCOF, LTEPOP, GETPOP, NGACCL, OUTC3, OUTC2, DUMPRT	Determines distribution of atomic populations from self-consistent solution of statistical equilibrium equations and radiation field.
VOIGT	LINEPR,	—	Compute Voigt line profile.
WSTARK	LINWID	AVG	Computes Stark width for a given line.

13.2. The Common Blocks

Listed below are the common blocks used in BUCKY-1. For each common block, the variable name, type, dimensions, and a brief description of each variable is provided. In most cases, the dimensions of variables are specified by quantities defined in PARAMETER statements. This, when used with the pre-processor, allows the dimensions of all like arrays to be changed quickly by modifying just one line of code.

The parameters defining the array sizes are:

<u>Parameter</u>	<u>Sets the MAXIMUM number of:</u>
MXZONS	spatial zones
MXMATR	materials (i.e., EOS tables)
MXREGN	regions for spatial gridding
MXTTAB	temperatures in EOS tables
MXDTAB	densities in EOS tables
MXTTBO	temperatures in opacity tables
MXDTBO	densities in opacity tables
MXGTAB	frequency groups in opacity tables
MXIDPT	ion bunches for ion deposition model
MXIDPE	ion energy groups for ion deposition model
MXIDPX	ion species for ion deposition model
MAXTDQ	ionization stages for time-dependent ion deposition model
MXSAVE	time-dependent quantities saved for final output
MXLVLS	atomic levels for CRE model
MXIONZ	ionization stages for CRE model
MXGASS	gas species for CRE model
MXDATT	temperatures in atomic data tables used by CRE model
MXDATD	densities in atomic data tables used by CRE model
MXTRNS	atomic transitions in CRE model
MXSSHL	atomic subshells in CRE model
MXLVLI	levels in atomic data tables used by CRE model

For many of the variables, the second to the last letter indicates whether the variable is at a zone center or zone boundary, and the last letter denotes the time level. The suffixes are:

1 – zone boundary

2 – zone center

A – t^{n+1}

B – $t^{n+1/2}$

C – t^n

D – $t^{n-1/2}$

The letter R will appear in a variable name if the quantity is associated with the radiation field, N if the quantity is associated with the ions, and E if associated with the electrons. Thus, TR2B(J) is the radiation temperature in the center of zone j at time $t^{n+1/2}$, and UID(J) is the fluid velocity on the zone j boundary at time $t^{n-1/2}$. The common blocks are listed below along with their meaning and units.

COMMON/TIME/

Variable	Type	Dimensions	Units	Description
TA	R*8	—	sec	t^{n+1} time
TB	R*8	—	sec	$t^{n+1/2}$
TC	R*8	—	sec	t^n
TD	R*8	—	sec	$t^{n-1/2}$
DTB	R*8	—	sec	$\Delta t^{n+1/2}$
DTC	R*8	—	sec	$\Delta t^n = (\Delta t^{n+1/2} + \Delta t^{n-1/2})/2$
DTD	R*8	—	sec	$\Delta t^{n-1/2}$
DT	R*8	—	sec	$\Delta t^{n+3/2}$, the new time step
TMAX	R*8	—	sec	total time for the simulation
DTMIN	R*8	—	sec	minimum allowed time step
DTMAX	R*8	—	sec	maximum allowed time step
DTIONT	R*8	—	sec	time step for updating debris ion deposition properties
DTVAVZ	R*8	—	sec	time step after vaporization of first wall zone
TSPEC	R*8	—	sec	simulation time for specifying user-prescribed time step (DTSPEC)
DTSPEC	R*8	—	sec	time step corresponding to TSPEC

COMMON/TEMPER/

Variable	Type	Dimensions	Units	Description
TN2A	R*8	MXZONS	eV	$(T_P)_{j-1/2}^{n+1}$ plasma, or ion, temperatures
TN2B	R*8	MXZONS	eV	$(T_P)_{j-1/2}^{n+1/2}$
TN2C	R*8	MXZONS	eV	$(T_P)_{j-1/2}^n$
TN1B	R*8	MXZONS	eV	$(T_P)_j^{n+1/2}$
TNSR2B	R*8	MXZONS	eV ^{1/2}	$\sqrt{(T_P)_{j-1/2}^{n+1/2}}$
TE2A	R*8	MXZONS	eV	$(T_e)_{j-1/2}^{n+1}$ electron temperatures
TE2B	R*8	MXZONS	eV	$(T_e)_{j-1/2}^{n+1/2}$
TE2C	R*8	MXZONS	eV	$(T_e)_{j-1/2}^n$
TE1B	R*8	MXZONS	eV	$(T_e)_j^{n+1/2}$
TESR2B	R*8	MXZONS	eV ^{1/2}	$\sqrt{(T_e)_{j-1/2}^{n+1/2}}$
TR2A	R*8	MXZONS	eV	$(T_R)_{j-1/2}^{n+1}$ radiation temperatures
TR2B	R*8	MXZONS	eV	$(T_R)_{j-1/2}^{n+1/2}$
TR2C	R*8	MXZONS	eV	$(T_R)_{j-1/2}^n$
TR1B	R*8	MXZONS	eV	$(T_R)_j^{n+1/2}$
TBC	R*8	MXZONS	eV	temperature boundary condition

COMMON/CNTROL/

Variable	Type	Dimensions	Units	Description
CON	R*8	100	—	real constants (see Table 15.3)
ISW	I*4	100	—	control switches (see Table 15.2)
IEDIT	I*4	100	—	intermediate output cycle frequencies (see Table 15.4)
IO	I*4	31	—	primary output frequency vector
INDEX	I*4	MXZONS	—	a vector used for output indexing
T1	R*8	MXZONS	—	temporary vector
T2	R*8	MXZONS	—	temporary vector
T3	R*8	MXZONS	—	temporary vector
T4	R*8	MXZONS	—	temporary vector
TGROW	R*8	—	—	max. percentage that Δt can increase in one cycle
TEDIT	R*8	—	sec	time at which output freq. switches from 10(1) to 10(11)
GEOFAC	R*8	—	—	a geometry factor; 1, 2π , 4π
R3N	R*8	—	—	worst case for $\Delta T_P/T_P$
TSCC	R*8	—	—	Courant condition time step control
TSCV	R*8	—	—	$\Delta V/V$ time step control
R1	R*8	—	—	worst case for Courant condition
R2	R*8	—	—	worst case for $\Delta V/V$
IDELTA	I*4	—	—	1 = cartesian 2 = cylindrical 3 = spherical
IDELM1	I*4	—	—	0 = cartesian 1 = cylindrical 2 = spherical
NCYCLE	I*4	—	—	time cycle index
NMAX	I*4	—	—	max number of time steps
JMAX	I*4	—	—	max number of spatial zones
JMAXM1	I*4	—	—	JMAX-1
JMAXP1	I*4	—	—	JMAX+1 used for indexing
JMAXP2	I*4	—	—	JMAX+2

COMMON/CNTROL/ (Continued)

Variable	Type	Dimensions	Units	Description
JMAXV0	I*4	—	—	maximum spatial index for vapor phase at $t = 0$
JMAXV	I*4	—	—	maximum spatial index for vapor phase
JMINC	I*4	—	—	minimum spatial index for condensed phase
JMAXT	I*4	—	—	maximum spatial index for condensed phase
NCZONS	I*4	—	—	initial number of zones in condensed phase
ILUNIT	I*4	—	—	output units for flux quantities
JCOUR	I*4	—	—	zone index of Courant condition worst case
JSPVOL	I*4	—	—	zone index of $\Delta V/V$ worst case
JNTEMP	I*4	—	—	zone index of $\Delta T_P/T_P$ worst case
IZONE	I*4	—	—	zone index of worst case of Courant, $\Delta V/V$, $\Delta T_P/T_P$
ITYPE	I*4	—	—	1 = Courant 2 = $\Delta V/V$ 3 = $\Delta E_R/E_R$ 4 = $\Delta T_P/T_P$ worst restriction
NREGNS	I*4	—	—	total number of zoning regions
NVREGN	I*4	—	—	number of plasma (vapor) regions
NCREGN	I*4	—	—	number of condensed matter regions
JMN	MXREGN	—	—	minimum spatial index of each region
JMX	MXREGN	—	—	maximum spatial index of each region
IITYPE	I*4	—	—	0 = physical -1 = min Δt 1 = max Δt
IIZONE	I*4	—	—	zone # of worst case if the Δt is Δt_{\max} or Δt_{\min}
ICOND	I*4	—	—	principal time step constraint
ICOND2	I*4	—	—	secondary time step constraint if primary is Δt_{\min} or Δt_{\max}
IUNIT	I*4	—	—	cm ² , radian-cm, steradian for $\delta = 1, 2, 3$
TSCTN	R*8	—	—	$\Delta T_P/T_P$ time step control

COMMON/CNTROL/ (Continued)

Variable	Type	Dimensions	Units	Description
IOBIN	I*4	—	—	output frequency of binary output
RADIUS	R*8	—	cm	the radius of the first wall
R3R	R*8	—	—	worst case for $\Delta E_R/E_R$
TSCTR	R*8	—	—	$\Delta E_R/E_R$ time step control
JRTEMP	I*4	—	—	zone index of $\Delta E_R/E_R$ worst case
NFG	R*8	—	—	the number of frequency groups
NMAT	I*4	—	—	number of gas types
R3E	R*8	—	—	worst case for $\Delta T_e/T_e$
TPROUT	R*8	500	sec	if ISW(66) > 0, text output times
TPBOUT	R*8	500	sec	if ISW(66) > 0, binary output times
DTPOUT	R*8	—	sec	if ISW(66) > 0, text output time interval
DTBOUT	R*8	—	sec	if ISW(66) > 0, binary output time interval
TPRBEG	R*8	—	sec	if ISW(66) > 0, beginning time of text output
TPBBEG	R*8	—	sec	if ISW(66) > 0, beginning time of binary output
IPROUT	I*4	—	—	index for text output time
IPBOUT	I*4	—	—	index for binary output time
NFDOUT	I*4	—	—	number of text outputs per binary output
IDEOS	I*4	MXMATR	—	EOS material index
IDOPAC	I*4	MXMATR	—	opacity material index

COMMON/CNTROL/ (Continued)

Variable	Type	Dimensions	Units	Description
JINNER	I*4	—	—	innermost hydrodynamic zone
JETEMP	I*4	—	—	zone index of $\Delta T_e/T_e$ worst case
IRAD	I*4	—	—	radiation transport model type
IRADBC	I*4	—	—	radiation boundary condition flag
IRADEF	I*4	—	—	flag for Eddington factor transfer model
ITN	I*4	—	—	fusion burn flag
NRHOR	I*4	—	—	time step number when maximum ρR occurs
NTNMAX	I*4	—	—	time step number when maximum ion temperature occurs
JTNMAX	I*4	—	—	zone index of maximum ion temperature
JVMAX	I*4	—	—	zone index of maximum compression
JTSTEP	I*4	—	—	maximum zone index to assess when calculating new time step
NVMAX	I*4	—	—	time step number when maximum compression occurs
NLTEID	I*4	MXREGN	—	flag for NLTE line transport model
IOCREG	I*4	—	—	region index for writing out results for CRE spectral post-processing
IBEAM	I*4	—	—	ion beam model type
ILASER	I*4	—	—	laser deposition model type
IBENCH	I*4	20	—	array for benchmark calculations

COMMON/HYDROD/

Variable	Type	Dimensions	Units	Description
U1D	R*8	MXZONS	cm/sec	$u_j^{n-1/2}$ fluid velocity
U1B**	R*8	MXZONS		$u_j^{n+1/2}$
DR2B	R*8	MXZONS	cm	$\Delta r_{j-1/2}^{n+1/2}$ zone widths
DR2A	R*8	MXZONS		$\Delta r_{j-1/2}^{n+1}$
R1C	R*8	MXZONS	cm	r_j^n radius
R1B	R*8	MXZONS		$r_j^{n+1/2}$
R1A	R*8	MXZONS		r_j^{n+1}
RS1C	R*8	MXZONS		$(r_j^n)^{\delta-1}$
RS1B	R*8	MXZONS		$(r_j^{n+1/2})^{\delta-1}$
RS1A	R*8	MXZONS		$(r_j^{n+1})^{\delta-1}$
PR2C	R*8	MXZONS	J/cm ³	$(P_R)_{j-1/2}^n$ radiation pressure
PR2B	R*8	MXZONS		$(P_R)_{j-1/2}^{n+1/2}$
PR2A	R*8	MXZONS		$(P_R)_{j-1/2}^{n+1}$
PN2C	R*8	MXZONS	J/cm ³	$(P_P)_{j-1/2}^n$ plasma, or ion, pressure
PN2B	R*8	MXZONS		$(P_P)_{j-1/2}^{n+1}$
PN2A	R*8	MXZONS		$(P_P)_{j-1/2}^{n+1}$
PE2A	R*8	MXZONS	J/cm ³	$(P_e)_{j-1/2}^{n+1}$ electron pressure
PE2B	R*8	MXZONS		$(P_e)_{j-1/2}^{n+1/2}$
PE2C	R*8	MXZONS		$(P_e)_{j-1/2}^n$
P2C	R*8	MXZONS	J/cm ³	$P_{j-1/2}^n$ total pressure
P2A	R*8	MXZONS		$P_{j-1/2}^{n+1}$
V2C	R*8	MXZONS	cm ³ /g	$V_{j-1/2}^n$ specific volume
V2B	R*8	MXZONS		$V_{j-1/2}^{n+1/2}$

COMMON/HYDROD/ (Continued)

Variable	Type	Dimensions	Units	Description
V2A	R*8	MXZONS		$V_{j-1/2}^{n+1}$
V0	R*8	MXZONS	cm^3/g	initial specific volume
COMPR	R*8	MXZONS	—	V0/V compression
VDOT2B	R*8	MXZONS	$\text{cm}^3/\text{g} - s$	$V_{j-1/2}^{n+1/2}$ time derivative of sp. volume
DMASS2	R*8	MXZONS	$\delta = 1: \text{g}/\text{cm}^2$ $\delta = 2: \text{g}/\text{cm}/\text{rad}$ $\delta = 3: \text{g}/\text{ster}$	$\delta m_{o_{j-1/2}}$ Langrangian mass
DMASS1	R*8	MXZONS	see above	$\delta m_{o_j} = (\delta m_{o_{j-1/2}} + \delta m_{o_{j+1/2}})/2$
Q2B	R*8	MXZONS	J/cm^3	$q_{j-1/2}^{n+1/2}$ artificial viscosity
VOL2B	R*8	MXZONS	cm^3	$V_{j-1/2}^{n+1/2}$ zone volume
VOL2A	R*8	MXZONS	cm^3	$V_{j-1/2}^{n+1/2}$
DMOM1C	R*8	MXZONS	cm/sec^2	momentum lost by debris ions during Δt^n
DMASS0	R*8	MXZONS	see above	initial values of DMASS2
VMAX	R*8	MXZONS	—	maximum compression
TAVMAX	R*8	MXZONS	sec	time of maximum compression
TOTMS0	R*8	MXZONS	grams	initial mass
RINNER	R*8	—	cm	inner radius of innermost zone
RHORMX	R*8	—	g/cm^2	maximum value of ρR
RHOR	R*8	—	g/cm^2	current value of ρR
TRHOR	R*8	—	sec	time at which maximum ρR was achieved
TNMAX	R*8	—	eV	maximum ion temperature
TATNMX	R*8	—	sec	time at which maximum ion temperature occurred
PRBC	R*8	—	J/cm^3	pressure at outermost boundary

COMMON/ESCOM/

Variable	Type	Dimensions	Units	Description
ER2C	R*8	MXZONS	J/cm ³	$E_{R_{j-1/2}}^n$ radiation energy density
ENT2B	R*8	MXZONS	J/g/eV	$(C_v)_{j-1/2}^{n+1/2}$ plasma specific heat
EET2B	R*8	MXZONS	J/g/eV	$(C_v)_{j-1/2}^{n+1/2}$ electron specific heat
ER2B	R*8	MXZONS	J/cm ³	$E_{R_{j-1/2}}^{n+1/2}$ radiation energy density
PNT2B	R*8	MXZONS	J/cm ³ /eV	$(P_P)_{T_{j-1/2}}^{n+1/2}$ temperature derivative of ion pressure
PET2B	R*8	MXZONS	J/cm ³ /eV	$(P_e)_T$ temperature derivative of electron pressure
ER2A	R*8	MXZONS	J/cm ³	$(E_R)_{j-1/2}^{n+1}$ radiation energy density
ER2B	R*8	MXZONS	J/cm ³	$(E_R)_{j-1/2}^{n+1/2}$ radiation energy density
EN2A	R*8	MXZONS	J/g	$(E_P)_{j-1/2}^{n+1}$ ion, or plasma, specific internal energy
EE2A	R*8	MXZONS	—	$(E_e)_{j-1/2}^{n+1}$ electron specific internal energy
DE2A	R*8	MXZONS	cm ³	$(n_e)_{j-1/2}^{n+1}$ electron number density
DN2A	R*8	MXZONS	cm ³	$(n_P)_{j-1/2}^{n+1}$ ion number density
DE2B**	R*8	MXZONS	cm ³	$(n_e)_{j-1/2}^{n+1/2}$ electron number density
DN2B*	R*8	MXZONS	cm ³	$(n_P)_{j-1/2}^{n+1/2}$ ion number density
ATW2B*	R*8	MXZONS	amu	$A_{j-1/2}^{n+1/2}$ average ion atomic weight
ATWQ2B	R*8	MXZONS	amu ^{1/2}	square root of ATW2B
ZT2B	R*8	MXZONS	esu/eV	$\partial Z/\partial T_{j-1/2}^{n+1/2}$ temperature derivative of average charge
ENN2B	R*8	MXZONS	J/cm ³	scaled density derivative of specific energy
Z2B**	R*8	MXZONS	esu	$Z_{j-1/2}^{n+1/2}$ average charge

COMMON/ESCOM/ (Continued)

Variable	Type	Dimensions	Units	Description
ZSQ2B	R*8	MXZONS	esu ²	$(Z_{j-1/2}^{n+1/2})^2$ average squared charge
DD2A	R*8	MXZONS	cm ⁻³	number density of deuterium at $(n + 1)$
DD2B	R*8	MXZONS	cm ⁻³	number density of deuterium at $(n + 1/2)$
DT2A	R*8	MXZONS	cm ⁻³	number density of tritium at $(n + 1)$
DT2B	R*8	MXZONS	cm ⁻³	number density of tritium at $(n + 1/2)$
DO2A	R*8	MXZONS	cm ⁻³	number density of non-DT ions at $(n + 1)$
DO2B	R*8	MXZONS	cm ⁻³	number density of non-DT ions at $(n + 1/2)$
ATWO	R*8	MXZONS	amu	atomic weight of non-DT ions
ZO2B	R*8	MXZONS	esu	mean charge of non-DT ions
XNO2A	R*8	MXZONS	—	DO2A * VOL2A
JMAT	I*4	MXZONS	—	material type index
VBC	I*4	MXZONS	cm ³ /g	specific volume boundary condition
AD	I*4	MXZONS	—	
AT	I*4	MXZONS	—	coefficients defining the grid for the equations of state
BD	I*4	MXZONS	—	
BT	I*4	MXZONS	—	
EBC	I*4	MXZONS	—	radiation energy density boundary condition
RAD	I*4	MXZONS	—	1/AD
RAT	I*4	MXZONS	—	1/AT
RBT	I*4	MXZONS	—	1/BT
RBD	I*4	MXZONS	—	1/BD

COMMON/ESCOM1/

Variable	Type	Dimensions	Units	Description
ZTAB	R*8	MXTTAB, MXDTAB, MXMATR	esu	EOS table for mean charge state
DZDTAB	R*8	same as above	esu/eV	EOS table for (dZ/dT)
ENTAB	R*8	same as above	J/g	EOS table for specific ion internal energy
ENTTAB	R*8	same as above	J/g/eV	EOS table for $(\partial E_{\text{ion}}/\partial T)$
ENNTAB	R*8	same as above	eV ⁻¹	EOS table for scaled $(\partial E_{\text{ion}}/\partial \rho)$
EETAB	R*8	same as above	J/g	EOS table for specific electron internal energy
EETTAB	R*8	same as above	J/g/eV	EOS table for $(\partial E_e/\partial T)$
PNTAB	R*8	same as above	J/cm ³	EOS table for ion pressure
PNTTAB	R*8	same as above	J/cm ³ /eV	EOS table for $(\partial E_{\text{ion}}/\partial T)$
PETAB	R*8	same as above	J/cm ³	EOS table for electron pressure
PETTAB	R*8	same as above	J/cm ³ /eV	EOS table for $(\partial P_e/\partial T)$
RRTAB	R*8	MXGTAB, MXTTAB, MXDTAB, MXMATR	cm ² /g	Rosseland opacity table
RPTAB	R*8	same as above	cm ² /g	Planck opacity table (absorption)
RPETAB	R*8	same as above	cm ² /g	Planck opacity table (emission)

COMMON/ESCOM1/ (Continued)

Variable	Type	Dimensions	Units	Description
ADTAB	R*8	MXMATR	—	ρ -increment for EOS table
ATTAB	R*8	MXMATR	—	T -increment for EOS table
BDTAB	R*8	MXMATR	—	\log_{10} of ρ_{\min} in EOS table
BTTAB	R*8	MXMATR	—	\log_{10} of T_{\min} in EOS table
RADTAB	R*8	MXMATR	—	ρ -increment for opacity table
RATTAB	R*8	MXMATR	—	T -increment for opacity table
RBDTAB	R*8	MXMATR	—	\log_{10} of ρ_{\min} in opacity table
RBTTAB	R*8	MXMATR	—	\log_{10} of T_{\min} in opacity table
TMPTAB	R*8	MXTTAB, MXMATR,5	eV	temperature grid for SESAME EOS table
RHOTAB	R*8	MXTTAB, MXMATR,5	g/cm ³	density grid for SESAME EOS table
RADCON	R*8	MXMATR,3	—	multiplier for opacities
NTTAB	I*4	MXMATR	—	number of temperatures in EOS table
NDTAB	I*4	MXMATR	—	number of densities in EOS table
NTTABO	I*4	MXMATR	—	number of temperatures in opacity table
NDTABO	I*4	MXMATR	—	number of densities in opacity table
NTMPTB	I*4	MXMATR,5	—	number of temperatures in SESAME EOS table
NRHOTB	I*4	MXMATR,5	—	number of densities in SESAME EOS table
IZEOS	I*4	MXMATR	—	file identifier for EOS/opacity tables

COMMON/COEFF/

Variable	Type	Dimensions	Units	Description
OMC2B	R*8	MXZONS	J/eV/g/s	$(\omega_c)_{j-1/2}^{n+1/2}$ energy exchange between electrons and ions
XKNM1B	R*8	MXZONS	J/cm/eV/s	$(K_P^-)_j^{n+1/2}$ ion, or plasma, thermal conductivity
XKNP1B	R*8	MXZONS	J/cm/eV/s	$(K_P^+)_j^{n+1/2}$ ion, or plasma, thermal conductivity
XKEM1B	R*8	MXZONS	J/cm/eV/s	$(K_e^-)_j^{n+1/2}$ electron thermal conductivity
XKEP1B	R*8	MXZONS	J/cm/eV/s	$(K_e^+)_j^{n+1/2}$ electron thermal conductivity
XKRM1B	R*8	MXZONS	cm ² /s	$(K_R^-)_j^{n+1/2}$ radiation thermal conductivity
XKRP1B	R*8	MXZONS	cm ² /s	$(K_R^+)_j^{n+1/2}$ radiation thermal conductivity
SION2B	R*8	MXZONS	J/g/s	ion energy deposition rate
SHOK2B	R*8	MXZONS	J/g/s	shock heating rate
SLAS2B	R*8	MXZONS	J/g/s	laser energy deposition rate
SNTN2B	R*8	MXZONS	J/g/s	fusion charged particle deposition rate to ions
SETN2B	R*8	MXZONS	J/g/s	fusion charged particle deposition rate to electrons
SNEU2B	R*8	MXZONS	J/g/s	neutron energy deposition rate
SLIN2B	R*8	MXZONS	J/g/s	energy deposition rate from CRE line transport
XLMN2B	R*8	MXZONS	—	Spitzer log Λ for ions
XLME2B	R*8	MXZONS	—	Spitzer log Λ for electrons
FLIM1B	R*8	MXZONS	J/cm ² /s	radiation flux limit
FLMC1B	R*8	MXZONS	J/cm ² /s	conduction flux limit
RFLU1B	R*8	MXZONS	J/cm ² /s	diffusion flux
TDXRED	R*8	MXZONS	J/g/s	time-dependent x-ray source term

COMMON/COEFF1/

Variable	Type	Dimensions	Units	Description
BET12B	R*8	MXZONS	—	$(\beta_1)_{j-1/2}^{n+1/2}$ beta vector
BET22B	R*8	MXZONS	—	$(\beta_2)_{j-1/2}^{n+1/2}$ beta vector
AL112B	R*8	MXZONS	—	$(\alpha_{11})_{j-1/2}^{n+1/2}$ diagonal elements of alpha matrix
AL222B	R*8	MXZONS	—	$(\alpha_{22})_{j-1/2}^{n+1/2}$ diagonal elements of alpha matrix
OM112B	R*8	MXZONS	—	$(\omega_{11})_{j-1/2}^{n+1/2}$ diagonal elements of omega matrix
OM222B	R*8	MXZONS	—	$(\omega_{22})_{j-1/2}^{n+1/2}$ diagonal elements of omega matrix
GM112B	R*8	MXZONS	—	$(\gamma_{11})_{j-1/2}^{n+1/2}$ diagonal elements of gamma matrix
GM222B	R*8	MXZONS	—	$(\gamma_{22})_{j-1/2}^{n+1/2}$ diagonal elements of gamma matrix
AA111B	R*8	MXZONS	—	$(a_{11})_j^{n+1/2}$ diagonal elements of “a” matrix
AA221B	R*8	MXZONS	—	$(a_{22})_j^{n+1/2}$ diagonal elements of “a” matrix
OM122B	R*8	MXZONS	—	$(\omega_{12})_{j-1/2}^{n+1/2}$ off diagonal elements of omega matrix
OM212B	R*8	MXZONS	—	$(\omega_{21})_{j-1/2}^{n+1/2}$ off diagonal elements of omega matrix

COMMON/COEFF2/

Variable	Type	Dimensions	Units	Description
E11	R*8	MXZONS	—	(E ₁₁) all elements of the “E” matrix
E12	R*8	MXZONS	—	(E ₁₁)
E21	R*8	MXZONS	—	(E ₂₁)
E22	R*8	MXZONS	—	(E ₂₂)
F1	R*8	MXZONS	—	(F ₁) both components of the “F” vector
F2	R*8	MXZONS	—	(F ₂)
B11	R*8	MXZONS	—	(B ₁₁) all elements of the “B” matrix
B12	R*8	MXZONS	—	(B ₁₂)
B21	R*8	MXZONS	—	(B ₂₁)
B22	R*8	MXZONS	—	(B ₂₂)
D1	R*8	MXZONS	—	(D ₁) both elements of the “D” vector
D2	R*8	MXZONS	—	(D ₂)

COMMON/ECKCOM/

Variable	Type	Dimensions	Units	Description
T1A	R*8	MXZONS	J/x	$(T)_j^{n+1}$ kinetic energy of fluid
GGGE2A	R*8	MXZONS	J/x	$(G_e)_{j-1/2}^{n+1}$ radiation-gas work
HHHR2B	R*8	MXZONS	J/x	$(H_R)_{j-1/2}^{n+1/2}$ radiation source
HHHH2B	R*8	MXZONS	J/x	$(H_P)_{j-1/2}^{n+1/2}$ ion source term
HHHE2B	R*8	MXZONS	J/x	$(H_e)_{j-1/2}^{n+1/2}$ electron source term
EEEC2A	R*8	MXZONS	J/x	$(E_c)_{j-1/2}^{n+1}$ electron-ion energy exchange
EEER2A	R*8	MXZONS	J/x	$(E_R)_{j-1/2}^{n+1}$ radiation-electron energy exchange
FSAVE	R*8	MXSAVE	J/cm ² /s	heat fluxes at first wall
PSAVE	R*8	MXSAVE	J/cm ²	pressures at first wall
TSAVE	R*8	MXSAVE	s	times of heat fluxes and pressures
EEEEER0	R*8	—	J/x	E_{R_o} total initial radiation internal energy
EEEEEN0	R*8	—	J/x	E_{P_o} total initial ion internal energy
EEEEEO	R*8	—	J/x	E_{e_o} total initial electron energy
EEEEER	R*8	—	J/x	$(E_R)^{n+1}$ total radiation internal energy
EEEEEN	R*8	—	J/x	$(E_P)^{n+1}$ total ion internal energy
EEEEEO	R*8	—	J/x	$(E_e)^{n+1}$ total electron internal energy
TTTTTT	R*8	—	J/x	$(T)^{n+1}$ total fluid kinetic energy
HHHHHR	R*8	—	J/x	$(H_R)^{n+1}$ total radiation source term
HHHHHN	R*8	—	J/x	$(H_P)^{n+1}$ total ion source term
HHHHHE	R*8	—	J/x	$(H_E)^{n+1}$ total electron source term
EEEEEC	R*8	—	J/x	$(E_c)^{n+1}$ total radiation-gas energy exchanged
GGGGGE	R*8	—	J/x	$(G_e)^{n+1}$ total work done by ions on electrons

COMMON/ECKCOM/ (Continued)

Variable	Type	Dimensions	Units	Description
WWWWWR	R*8	—	J/x	$(W_R)^{n+1}$ total work done on radiation
WWWWWN	R*8	—	J/x	$(W_P)^{n+1}$ total work done on ions
WWWWW	R*8	—	J/x	$(W_E)^{n+1}$ total work done on electrons
FFFFFR	R*8	—	J/x	$(F_R)^{n+1}$ total radiation heat lost across outer boundaries
FFFFFN	R*8	—	J/x	$(F_P)^{n+1}$ total ion heat loss across outer boundaries
FFFFFE	R*8	—	J/x	$(F_e)^{n+1}$ total electron heat loss across outer boundaries
WWWWR	R*8	—	J/x	$(W_R)^{n+1}$ total work done on radiation on last cycle
WWWWN	R*8	—	J/x	$(W_P)^{n+1}$ total work done on ions on last cycle
WWWWE	R*8	—	J/x	$(W_E)^{n+1}$ total work done on electrons on last cycle
FFFFR	R*8	—	J/x	$(f_R)^{n+1}$ total radiation lost at outer bd. on last cycle
FFFFN	R*8	—	J/x	$(f_P)^{n+1}$ total ion energy lost at outer bd. on last cycle
FFFFE	R*8	—	J/x	$(f_e)^{n+1}$ total electron energy lost at outer bd. on last cycle
HHHR	R*8	—	J/x	$(h_R)^{n+1}$ total radiation source term on last cycle
HHHN	R*8	—	J/x	$(h_P)^{n+1}$ total ion source term on last cycle
HHHE	R*8	—	J/x	$(h_e)^{n+1}$ total ion source term on last cycle
GGGGE	R*8	—	J/x	$(g_e)^{n+1}$ total work to maintain one fluid on last cycle
ENLHS	R*8	—	J/x	left side of ion energy balance equation
ENLHS	R*8	—	J/x	left side of electron energy balance equation
ETLHS	R*8	—	J/x	left side of total energy balance equation
ERRHS	R*8	—	J/x	right side of radiation energy balance equation
ERLHS	R*8	—	J/x	left side of radiation energy balance equation
ENRHS	R*8	—	J/x	right side of ion energy balance equation
EERHS	R*8	—	J/x	right side of electron energy balance equation
ETRHS	R*8	—	J/x	right side of total energy balance equation
TTTTN0	R*8	—	J/x	initial kinetic energy
PMAX	R*8	—	J/cm ³	maximum pressure at the wall

COMMON/ECKCOM/ (Continued)

Variable	Type	Dimensions	Units	Description
TIMP	R*8	MXSAVE	J/s/cm ³	pressure impulse at first wall
HFINTG	R*8	MXSAVE	J/cm ²	heat fluence at first wall
VMSAVE	R*8	MXSAVE	g	mass vaporized from first wall
DMSAVE	R*8	MXSAVE	g/s	mass vaporization rate
TSKNSV	R*8	MXSAVE	eV	first wall skin temperature
TBLSAV	R*8	MXSAVE	eV	average temperature in boundary layer
PSATSV	R*8	MXSAVE	erg/cm ³	saturation vapor pressure at first wall
PVAPSV	R*8	MXSAVE	erg/cm ³	vapor pressure at first wall
ERAD2A	R*8	MXZONS	J	radiation energy in each zone
FFFFFL	R*8	—	J	total line radiation lost across boundaries
FFFFL	R*8	—	J	line radiation lost across bd. on last cycle
COOLCR	R*8	MXREGN	J/s/cm ^{3-δ}	continuum radiation cooling rate
COOLLR	R*8	MXREGN	J/s/cm ^{3-δ}	line radiation cooling rate
FLXBDC	R*8	MXREGN+1	J/cm ² /s	continuum radiation flux at region interfaces
FLXBDL	R*8	MXREGN+1	J/cm ² /s	line radiation flux at region interfaces
RFLINT	R*8	MXREGN+2	J/cm ²	time-integrated radiation energy lost across inner and outer boundaries
RFLOUT	R*8	MXREGN+2	J/cm ²	time-integrated radiation energy lost across inner and outer boundaries
EEERAD	R*8	—	J	total radiation energy
ETN	R*8	—	J	total energy generated from fusion reactions
ECPT	R*8	—	J	total charged particle energy generated from fusion reactions
EDTTN	R*8	—	J	total energy generated from DT reactions
EDDTN	R*8	—	J	total energy generated from DD reactions
EDHE3T	R*8	—	J	total energy generated from D-HE ³ reactions

COMMON/ECKCOM/ (Continued)

Variable	Type	Dimensions	Units	Description
EDTCP	R*8	—	J	total charge particle energy generated from DT reactions
EDDCP	R*8	—	J	total charge particle energy generated from DD reactions
EATN	R*8	—	J	total charge particle energy reabsorbed by the plasma
ETOT1B	R*8	—	J	total ion beam energy deposited in the plasma
ETOTLZ	R*8	—	J	total laser beam energy deposited in the plasma
GGGGGR	R*8	—	J/x	total work done by ions on radiation
GGGGR	R*8	—	J/x	work done by ions on radiation for last cycle
GGGR2A	R*8	MXZONS	J/x	work done by ions on radiation
EEEEEX	R*8	—	J/x	total energy exchanged between ions and electrons
EEEEEX	R*8	—	J/x	energy exchanged between ions and electrons for last cycle
EEEX2A	R*8	MXZONS	J/x	energy exchanged between ions and electrons
TPMAX	R*8	—	s	time of maximum pressure
FMAX	R*8	—	J/cm ² /s	maximum radiation heat flux at the wall
TFMAX	R*8	—	s	time of maximum heat flux
NPMAX	I*4	—	—	time step of max. pressure
NSAVE	I*4	—	—	index into FSAVE, PSAVE, and TSAVE
NFMAX	I*4	—	—	time step of max. heat flux
HFINTGL	R*8	—	J/cm ²	time-integrated heat flux at the wall
TIMPLS	R*8	—	J/s/cm ³ /s	time-integrated pressure at the wall

Planar: x = cm²; cylindrical: x = cm-radian; spherical: x =steradian

COMMON/IONCOM/

Variable	Type	Dimensions	Units	Description
ATN2B	R*8	MXZONS	esu	atomic number of the background plasma
DIMASS	R*8	MXZONS	g	debris ion mass deposited in each Lagrangian cell during one time step
XIKE2B	R*8	MXZONS	J	debris ion energy deposited in the plasma
TOTION	R*8	MXZONS	J	total debris energy deposited in each Lagrangian cell
XIONIN	R*8	MXIDPT, MXIDPE, MXIDPX	ions/s	ion flux array
BEAMCD	R*8	MXZONS	ions/cm ² /s	ion beam particle current density
BEAMEN	R*8	MXZONS	keV	ion energy kinetic energy
EIONIN	R*8	MXIDPT, MXIDPE, MXIDPX	keV	ion flux array
TIONIN	R*8	MXIDPT	sec	ion time array
AWION	R*8	MXIDPX	amu	atomic weight of the debris ions
ANION	R*8	MXIDPX	—	atomic number of the debris ions
Q1INIT	R*8	MXIDPX	esu	initial charge state of the debris ions
CDEPCN	R*8	MXIDPX,5	—	constants used in stopping power calculation

COMMON/IONCOM/ (Continued)

Variable	Type	Dimensions	Units	Description
ATNION	R*8	MXIDPX	—	debris ion atomic number
ATWION	R*8	MXIDPX	amu	debris ion atomic weight
WALION	R*8	—	J	debris ion energy deposited in the wall
TIONEN	R*8	—	sec	estimated ending time of ion energy deposition
SRCION	R*8	—	J	total ion energy emitted by the source
NIX	R*8	—	—	number of debris ion species
NIE	R*8	—	—	number of debris ion energy bins
NIT	R*8	—	—	number of debris ion time bins
PLSION	R*8	—	J	time-integrated ion energy deposited in the entire background plasma
PLSIKE	R*8	—	J	time-integrated ion energy deposited in the background plasma by stopped ions
Z1EFF	R*8	—	esu	effective charge state of debris ions
WALIEB	R*8	—	J/s	ion energy deposition rate at the wall
Z1MIN	R*8	MXIDPT	esu	minimum projectile charge

COMMON/XRAY/

Variable	Type	Dimensions	Units	Description
EXRAY	R*8	MXZONS	keV	the energy of the x-rays in each group
FXRAY	R*8	MXZONS	J/keV	the energy in each x-ray group
UXRAY	R*8	MXZONS	cm ² /g	x-ray attenuation coefficients computed from tables
IZ	I*4	MXZONS	—	the atomic number of the plasma
TDXAMP	R*8	(100,20)	—	time-dependent x-ray amplitudes
ATTENC	R*8	(100,5)	—	attenuation coefficients
COEF	R*8	(100,4)	—	coefficients computed from x-ray cross section tables
ELIM	R*8	100	—	a vector used in computing the x-ray cross sections
XRTIM	R*8	20	sec	times at which x-ray amplitudes are specified
XAMP	R*8	100	J/keV	the amplitude of an input x-ray spectrum
XEHIST	R*8	101	keV	the energy of the x-rays in each group of the input spectrum
CRLOC	I*4	100	—	data for x-ray stopping cross sections
CRA	R*8	3884	—	data for x-ray stopping cross sections
CRB	R*8	971	—	data for x-ray stopping cross sections
CRHD	R*8	10	—	data for x-ray stopping cross sections
CRZOA	R*8	100	—	data for x-ray stopping cross sections
CONFAC	R*8	(2,2)	—	data for x-ray stopping cross sections

COMMON/XRAY/ (Continued)

Variable	Type	Dimensions	Units	Description
IATTEN	I*4	6	—	data for x-ray stopping cross sections
EDGE	R*8	5	keV	the minimum x-ray energy required for absorption by electrons in each shell
SHELEL	R*8	5	—	the number of electrons in each shell
KEDGE	I*4	—	—	the number of shells the plasma atoms have
ONEZOA	R*8	—	—	a coefficient used in computing the x-ray scattering cross section
NXRG	I*4	—	—	number of x-ray groups
KEV	R*8	—	keV	the blackbody temperature of a blackbody x-ray spectrum
FLUX	R*8	—	J	the total energy in x-rays input by the user
SUMFLU	R*8	—	J	the energy in the x-ray spectra
NXRT	I*4	—	—	the number of times at which the input intensity is given
NUM	I*4	—	—	a number generated by the code in searching through the x-ray cross section tables
TXRED	R*8	—	J	the x-ray energy absorbed by the plasma
ETXR	R*8	—	—	
EETXR	R*8	—	—	
STDXR	R*8	—	—	
SSTDXR	R*8	—	—	
EXRW	R*8	—	—	
EEXRW	R*8	—	—	
NIZJ	I*4	—	—	

COMMON/MFRAD/

Variable	Type	Dimensions	Units	Description
ERFD2A	R*8	MXGTAB, MXZONS	J/g	frequency dependent radiation specific energy at t^{n+1}
ERFD2C	R*8	MXGTAB, MXZONS	J/g	frequency dependent radiation specific energy at t^n
SRFD2B	R*8	MXGTAB, MXZONS	J/g/s	frequency dependent radiation emission energy at $t^{n+1/2}$
SR2B	R*8	MXGTAB, MXZONS	cm ² /g	frequency dependent Rosseland opacity
SP2B	R*8	MXGTAB, MXZONS	cm ² /g	frequency dependent Planck absorption opacity
SPE2B	R*8	MXGTAB, MXZONS	cm ² /g	frequency dependent Planck emission opacity
SER2B	R*8	MXZONS	J/g/s	frequency integrated radiation absorption
SRE2B	R*8	MXZONS	J/g/s	frequency integrated radiation emission term
HNU1	R*8	MXGTAB+1	keV	boundaries of frequency groups
HNU2	R*8	MXGTAB	keV	centers of frequency groups
RFDOUT	R*8	MXGTAB,2	J	frequency dependent radiation energy flux at first wall on a given time cycle
RFDINT	R*8	MXGTAB,2	J	time integrated frequency dependent radiation energy flux at first wall up through a given time cycle

COMMON/WALVAP/

Variable	Type	Dimensions	Units	Description
DELXC	R*8	MXZONS	cm	cell sizes in the condensed region
TCN2A	R*8	MXZONS	eV	temperature in the condensed region
TCN2B	R*8	MXZONS	eV	temperature in the condensed region
TCN2C	R*8	MXZONS	eV	temperature in the condensed region
XKCOND	R*8	MXZONS	J/cm/s/eV	thermal conductivity in the condensed region
RHOCND	R*8	—	g/cm ³	mass density of the condensed region
QHEATV	R*8	—	J/g	specific heat of vaporization of the condensed region
CPHEAT	R*8	—	J/g/eV	specific heat of the condensed region
TVAPO	R*8	—	eV	vaporization temperature at 1 bar
TWALLB	R*8	—	eV	temperature at the back of the condensed region
DELXCT	R*8	—	cm	total width of the condensed region
UNSENS	R*8	—	J/g	specific internal energy at the vaporization temperature
UNVAP	R*8	—	J/g	specific internal energy required to vaporize (UNSENS + QHEATV)
TVAP	R*8	—	eV	vaporization temperature
DMVCDT	R*8	—	g/sec	net vaporization rate
IZFILM	R*8	—	amu	atomic number of the condensed region
TMASVP	R*8	—	g	total mass vaporized
FRACMV	R*8	—	—	mass fraction of the interface zone in the vapor phase
FRACMC	R*8	—	—	mass fraction of the interface zone in the condensed phase
UNFINP	R*8	—	J	time-integrated radiation and debris ion energy added to the condensed region
DUFINP	R*8	—	J	radiation and debris ion energy added to the condensed region
HVSTOR	R*8	—	J	time-integrated energy stored in the heat of vaporization
DHVSTO	R*8	—	J	energy stored in the heat of vaporization
WVSTOR	R*8	—	J	time-integrated work energy due to phase change

COMMON/WALVAP/ (Continued)

Variable	Type	Dimensions	Units	Description
DWVSTO	R*8	—	J	work energy due to phase change
HVSTO0	R*8	—	J	energy stored in the heat of vaporization due to prompt x-rays
UNFLM0	R*8	—	J	initial internal energy of the condensed region
UNFLMT	R*8	—	J	total internal energy of the condensed region
UNBACK	R*8	—	J	time-integrated energy conducted through the back of the condensed region
DUNBAK	R*8	—	J	energy conducted through the back of the condensed region
UVAPMT	R*8	—	J	time-integrated energy added to the vapor phase due to phase change
DUVPMT	R*8	—	J	energy added to the vapor phase due to phase change
UCNDMT	R*8	—	J	time-integrated energy added to the condensed region due to phase change
DUCNMT	R*8	—	J	energy added to the condensed region due to phase change
VAPMAS	R*8	—	J	vapor mass of the non-condensable and condensable gases
QRAD	R*8	—	J/cm ²	radiant heat for last cycle
QCOND	R*8	—	J/cm ²	condensation heat for last cycle
AWFILM	R*8	—	amu	atomic weight of solid/liquid
TOTMSN	R*8	—	g	total mass of condensed region
FSTICK	R*8	—	—	sticking coefficient for condensation
QVOL	R*8	MXZONS	J/cm ³ /s	rate of radiation energy deposition
UNFLM	R*8	MXZONS	J/g	specific internal energy in condensed region
QINT	R*8	100	J/cm ² /s	x-ray flux onto first wall
FXMU	R*8	100	cm ² /g	x-ray attenuation coefficient
PSAT	R*8	—	erg/cm ³	saturation vapor pressure
PVAP	R*8	—	erg/cm ³	vapor pressure
AVGTMP	R*8	—	eV	average temperature of boundary layer
TSKIN	R*8	—	eV	skin temperature of condensed region

COMMON/DEBUGCM/

Variable	Type	Dimensions	Units	Description
NOBUG	I*4	—	—	logical flag; true if no debug output requested
NAMEDB	I*4	10	—	subroutine names for which debug output is requested
NCYCLD	I*4	10	—	beginning cycle number for debug output
ICYCLD	I*4	10	—	cycle increment for debug output
TBEGDB	R*8	10	sec	simulation time at which debug output begins
TENDDB	R*8	10	sec	simulation time at which debug output ends

COMMON/TDION/

NQTDEP	I*4	—	—	maximum number of ionization states tracked in a time-dependent debris ion calculation
IQMIN	I*4	MXIDPX	—	minimum charge state for debris ions in rate equation solution
IQMAX	I*4	MXIDPX	—	maximum charge state for debris ions in rate equation solution
Q1MIN	R*8	MXIDPX	esu	minimum allowable charge state for debris ions
POTEN	R*8	MAXTDQ, MXIDPX	—	ionization potentials for debris ions
FRTDIZ	R*8	MAXTDQ MXIDPT MXIDPE MXIDPX	—	fractional ionization abundances of the debris ions
BGPOTN	R*8	50	eV	ionization potentials for the background plasma
RATCN	R*8	7,MAXTDQ, MXIDPX	—	constants used in rate equations for debris ions
Z1AVER	R*8	MXIDPT MXIDPE MXIDPX	esu	average charge state for each debris ion group

COMMON/TNCOM/

Variable	Type	Dimensions	Units	Description
CONTN	R*8	20	—	constants used by the thermonuclear burn part of the code (see Table 15.5)
DEPETN	R*8	MXZONS	Jk	the accumulated energy deposited into the electrons in each zone by the streaming reaction products on a TN burn time step
DEPNTN	R*8	MXZONS	Jk	save as above except for ions
DTTN	R*8	—	sh	the thermonuclear burn time step
TTN	R*8	—	sh	the thermonuclear burn time
ZHE4	R*8	—	esu	the charge of He ⁴
ZHE3	R*8	—	esu	the charge of He ³
ZP	R*8	—	esu	the charge of a proton
ZT	R*8	—	esu	the charge of a triton
VSAVE	R*8	—	cm/sh	a working variable in SLOW that contains the velocity of the transporting bunch of particles
USAVE	R*8	—	—	a working variable in SLOW that contains the cosine of the angle μ that specifies the direction of the transporting particles
RSAVE	R*8	—	cm	a working variable in SLOW that contains the radius of the transporting particles
DTSAVE	R*8	—	sh	a working variable in SLOW that contains the time remaining in the transport of the particles
DVDT	R*8	—	cm/sh	$\Delta V_{\Delta t}$ — the velocity lost by the transporting particles during the thermonuclear time step
DV	R*8	—	cm/sh	ΔV — the smaller of $\Delta V_{\Delta T}$ and $\Delta V_{\Delta S}$
DVDS	R*8	—	cm/sh	$\Delta V_{\Delta S}$ — the velocity lost by the transporting particles in the distance ΔS to the next zone boundary
DS	R*8	—	cm	ΔS — the distance from the transporting particles current position to the next zone boundary that they will cross
DSDT	R*8	—	cm	$\Delta S_{\Delta t}$ — the distance that the particles would travel during the TN time step
DTDS	R*8	—	cm	$\Delta t_{\Delta s}$ — the time that it will take the particles to move the distance Δs to the next zone boundary

COMMON/TNCOM/ (Continued)

Variable	Type	Dimensions	Units	Description
RNEXT	R*8	—	cm	the radius of the next zone boundary that the transporting particles will cross
AN14	R*8	—	—	the number of 14.1 MeV neutrons created during the current TN time step
AN14T	R*8	—	—	the total number of 14 MeV neutrons created up to the current time
EN14T	R*8	—	J	total energy of 14 MeV neutrons created
AN245	R*8	—	—	the number of 2.45 MeV neutrons created on the current TN time step
AN245T	R*8	—	—	the number of 2.45 MeV neutrons created up to the current time
PESCTN	R*8	—	—	total number of charged particle reaction products that have escaped the plasma
EESCTN	R*8	—	Jk	total energy of charged particle reaction products that have escaped the plasma
AESCAP	R*8	—	—	not used
ZTN	R*8	—	esu	charge of the particles being transported
TNMASS	R*8	—	g	mass of the particle being transported
HE4M	R*8	—	g	mass of He ⁴
HE3M	R*8	—	g	mass of He ³
TM	R*8	—	g	mass of a triton
PM	R*8	—	g	mass of a proton
KO	R*8	—	—	terms in the solution of the integral equation used to compute the slowing down
JO	R*8	—	—	terms in the solution of the integral equation used to compute the slowing down
KOP	R*8	—	—	terms in the solution of the integral equation used to compute the slowing down
JOP	R*8	—	—	terms in the solution of the integral equation used to compute the slowing down
SLOWE	R*8	MXZONS	sh ⁻¹	the electron, ion, and nuclear contributions to the slowing
SLOWI		MXZONS	cm ³ /sh ⁴	down of charged particle reaction products
SLOWN		MXZONS	sh ⁻¹	$-\frac{dv}{dS} = \text{SLOWE} + \text{SLOWI}/V^3 + \text{SLOWN}$
ENERG	R*8	—	Jk	total energy lost by one bunch of transporting particles in a zone, used in ENEMA
ENERGE	R*8	—	Jk	energy lost by one bunch of transporting particles in a zone to electrons
ENERGN	R*8	—	Jk	energy lost by one bunch of transporting particles in a zone to ions

COMMON/TNCOM/ (Continued)

Variable	Type	Dimensions	Units	Description
DELTAU	R*8	—	cm/sh ²	change in fluid velocity of a zone due to one bunch of particles transporting through it, used by ENEMA
DS1	R*8	—	cm	same as DS used in RMUV
DUTN	R*8	MXZONS	cm/sh ²	change in fluid velocity of a zone due to the combined effect of all particles that transport through it on a TN time step
HE4MSQ	R*8	—	g	square root of He ⁴ mass
HE3MSQ	R*8	—	g	square root of He ³ mass
TMSQ	R*8	—	g	square root of T mass
PMSQ	R*8	—	g	square root of p mass
TNMSQ	R*8	—	g	square root of mass of particle being transported
DTTNMN	R*8	—	sh	minimum TN time step
DTTNM	R*8	—	sh	previous TN time step
UO	R*8	MXZONS	—	μ_o cosines of angles that particles are started onto
VOHE4	R*8	—	cm/sh	initial velocity of 3.5 MeV He ⁴
VOHE3	R*8	—	cm/sh	initial velocity of 0.82 MeV He ³
VOT	R*8	—	cm/sh	initial velocity of 1.01 MeV triton
VOP	R*8	—	cm/sh	initial velocity of 3.02 MeV proton
NZBURN	I*4	—	—	number of zones in burn calculation
NABURN	I*4	—	—	number of directions in particle tracking calculation
NT	I*4	15	—	maximum number of time levels for each direction
NAM	I*4	—	—	number of directions with $\mu \leq 0$
NAP	I*4	—	—	number of directions with $\mu > 0$
NTM	I*4	—	—	number of time levels for directions with $\mu \leq 0$
NTP	I*4	—	—	number of time levels for directions with $\mu > 0$

COMMON/TNCOM/ (Continued)

Variable	Type	Dimensions	Units	Description
IBASE	I*4	—	—	used to index into TND, actually = 0
IBETA	I*4	—	—	NTM = NTP * IBETA
LHE4	I*4	—	—	switch to determine transport technique for 3.5 MeV He ⁴
LHE3	I*4	—	—	switch to determine transport technique for 0.82 MeV He ³
LT	I*4	—	—	switch to determine transport technique for 1.01 MeV triton
LP	I*4	—	—	switch to determine transport technique for 3.02 MeV protons
NBORN	R*8	MXZONS	—	the number of particles born in each zone
RBORN	R*8	MXZONS	—	the radius where the particles born in each zone are started
JSAVE	I*4	—	—	the index of the zone where a transporting bunch of particles currently reside
JMAXTN	I*4	—	—	the index of the outer most zone where TN fuel is found
JNEXT	I*4	—	—	the index of the next zone boundary that a transporting bunch of particles will cross
LDOTN	L*4	—	—	logical variable that tells UEPLET that a thermonuclear calculation was done on the current time step
IMAXTN	I*4	—	—	the maximum number of words used in the vector TND; must be less than 16000
LLEFTO	L*4	—	—	logical variable that tells TRANSP that a bunch of particles have run out of time levels and must be forced to stop or escape
NG	I*4	—	—	number of energy groups used to accumulate the spectrum of escaping charged particles
IRBORN	I*4	MXZONS	—	index to choose the zones where charged particles will start
INBORN	I*4	MXZONS	—	index to choose the zone where particles from a given zone will start
VOPS	R*8	—	cm/sh	initial velocity of 14.7 MeV proton
VOHE4S	R*8	—	cm/sh	initial velocity of 3.6 MeV He ⁴
LHE4S	I*4	—	—	switch to determine transport technique for 3.6 MeV He ⁴
LPS	I*4	—	—	switch to determine transport technique for 14.7 MeV proton

COMMON/TNCOM1/

Variable	Type	Dimensions	Units	Description
NHE42A	R*8	MXZONS	—	number of He ⁴ in each zone at (n + 1)
NHE32A	R*8	MXZONS	—	number of He ³ in each zone at (n + 1)
NP2A	R*8	MXZONS	—	number of protons in each zone at (n + 1)
NT2A	R*8	MXZONS	—	number of tritons in each zone at (n + 1)
ND2A	R*8	MXZONS	—	number of deuterons in each zone at (n + 1)
NTTN	R*8	MXZONS	—	number of tritons in each zone, used in computing the number of reactions on the next time step, used in CREATE
NDTN	R*8	MXZONS	—	same as NTTN except for deuterons
NHE3TN	R*8	MXZONS	—	same as NTTN except for He ³
DHE3RE	R*8	MXZONS	sh ⁻¹	number of D-He ³ reactions on a TN time step, used in CREATE, divided by the time step in TNBURN to give the D-He ³ rate of reaction
DTREAC	R*8	MXZONS	sh ⁻¹	same as DHE3RE except for D-T reactions
DDREAC	R*8	MXZONS	sh ⁻¹	same as DHE3RE except for D-D reaction
CABTN	R*8	—	—	coefficient used for computing particle slowing down Z^2/m
CABHE4	R*8	—	—	values of CAB for HE ⁴
CABHE3	R*8	—	—	values of CAB for HE ³
CABT	R*8	—	—	values of CAB for T
CABP	R*8	—	—	values of CAB for p
NDTO	R*8	MXZONS	—	initial number of deuterons and tritons in each zone, used to compute fractional burnup
CPEN	R*8	100	keV	energy boundaries defining the group structure used to accumulate the escaping charged particle spectrum
CPN	R*8	100	—	number of particles accumulated into each energy group on a TN time step, used in CPSPEC

COMMON/TNDDATA/

Variable	Type	Dimensions	Units	Description
INHE4, IRHE4, IUHE4, IVHE4, INHE3, IRHE3, IUHE3, IVHE3, INP, IRP, IUP, IVP, INT, IRT, IUT, IVT	I*4	—	—	indexes into TND to define the storage for N, R, μ , V for the transport calculation
ISPHE4, ISPHE3, ISPT, ISPP	I*4	—	—	indices into TND to define storage to accumulate spectra for He ⁴ , He ³ , T, and P
INHE4S, IRHE4S, IUHE4S IVHE4S, INPS, IRPS, IUPS, IVPS	I*4	—	—	indices into TND to define storage for D-He ³ reaction products
TND	R*8	16,000	—	storage vector to save information for time dependent particle tracking method, output spectra

COMMON/ZONING/

Variable	Type	Dimensions	Units	Description
REGMAS	R*8	MXREGN	g/cm ² ($\delta = 1$) g/cm ($\delta = 2$) g ($\delta = 3$)	region mass
REGMS1	R*8	MXREGN	same as above	mass of inner sub-region
REGMS2	R*8	MXREGN	same as above	mass of middle sub-region
REGMS3	R*8	MXREGN	same as above	mass of outer sub-region
ZONFAC	R*8	MXREGN	—	zone mass factor ($\Delta m_{j+1} = \Delta m_j * ZONFAC$)
ZONFAC1	R*8	MXREGN	—	zone mass factor for inner sub-region
ZONFAC2	R*8	MXREGN	—	zone mass factor for middle sub-region
ZONFAC3	R*8	MXREGN	—	zone mass factor for outer sub-region
SLABWD	R*8	—	cm	slab width
JZN1	I*4	MXREGN	—	number of zones in inner sub-region
JZN2	I*4	MXREGN	—	number of zones in middle sub-region
JZN3	I*4	MXREGN	—	number of zones in outer sub-region

COMMON/RADBC/

Variable	Type	Dimensions	Units	Description
TIMRBC	R*8	100	sec	table of times for radiation boundary condition
TRADBC	R*8	100	eV	radiation temperature applied at inner boundary
RBTABL	R*8	100,5	—	interpolation table
NTIMRB	I*4	—	—	number of times in table

COMMON/STRNGB/

LUNRH	I*4	20	—	logical unit numbers for input files
FILERH	C*60	20	—	input file names

COMMON/MFRAD3/

XMU	R*8	MXANGL	—	cosine angles for multiangle RT model
WTANGL	R*8	MXANGL	—	angle integration weight for multiangle RT model
NRTANG	I*4	—	—	number of angles for multiangle RT model

COMMON/MFRAD2/

Variable	Type	Dimensions	Units	Description
FR1A	R*8	MXZONS	J/cm ² /s	radiation flux from variable Eddington model
FRFD1A	R*8	MXGTAB	J/cm ² /s	frequency-dependent radiation flux from variable Eddington model
FRFD1C	R*8	MXZONS MXGTAB	J/cm ² /s	frequency-dependent radiation flux from variable Eddington model
RS2B	R*8	MXZONS	cm ^{δ-1}	$(r_j^{\delta-1})_{j-1/2}^{n+1}$
RAD	R*8	MXZONS	cm ^δ	$r_j^\delta - r_{j-1}^\delta$
RD	R*8	MXZONS	cm	$(r_j^{n+1} - r_{j-1}^{n+1})/2$
ED1	R*8	MXZONS	—	$(1 - f)/2f$
ED3	R*8	MXZONS	—	$(3f - 12)/2f$
A1	R*8	MXZONS	g/cm ²	$2\delta(\sigma_{j-1/2}^R + \sigma_{j+1/2}^R)/2$
E	R*8	—	—	used in the solution of the freq. dependent radiation energy densities
F	R*8	—	—	used in the solution of the freq. dependent radiation energy density

14. Input and Output Files

Table 14.1 lists the input, output and scratch files utilized by BUCKY-1. Also listed are their logical unit numbers (LUN), names (for UNIX systems), types, and a brief description of their contents. There are 7 types of input files. The main input file to be used for all radiation-hydrodynamics calculations is ‘bucky.inp’. This is the NAMELIST input file used to define the hydro problem (initial conditions, zoning, I/O, etc.). A detailed description of the variables used in this file is given in Section 15.

The EOS and opacity data tables for each material are read in and stored in COMMON at the beginning of the calculation. Unless an ideal gas EOS is used, the user must supply these tables. The file name is given by ‘eos.dat.II.KK’, where ‘II’ is either ‘uw’ if a University of Wisconsin EOS table (EOSOPA or IONMIX) or ‘sm’ if a SESAME table. The quantity ‘KK’ refers to the material ID — which is supplied by the user with the NAMELIST input variable IZEOS. Typically, this can be the Z of the plasma. For example, ‘eos.dat.uw.13’ could be used to define the EOSOPA table for aluminum. However, any integer could be used for any material. Using the material atomic number is simply a useful convention if dealing with non-mixtures. The SESAME tables are assumed to be in their “standard” ASCII format. A condensed listing of the SESAME EOS file for Al (No. 3717) is given in Figure 5.2.

For simulating plasmas irradiated by intense ion beams, the user can specify the beam parameters either in the namelist input file, or by supplying a file to be read in (‘bucky.beam.dat’). This file is read in by the subroutine INIT3. Currently, the format of this data file is specific to PBFA-II data generated from SOPHIA output [46]. However, the code can easily be modified to read in time-dependent ion beam parameters in a different format.

The file defined by the variable “flerh(1)” contains time-dependent radiation temperatures which are applied at the “inner” ($j = 1$) boundary. This has been used

Table 14.1. BUCKY-1 Input and Output Files

Unit Number	Name	Type	Description
2	nltert.inp	Input	NAMELIST input for non-LTE CRE modules
3	eos.dat.II.KK*	Input	EOSOPA (II=“uw”) or SESAME (II=“sm”) EOS/opacity data file
4	rt.atom.dat.NN**	Input	Atomic structure and rate data for CRE calculations
5	bucky.inp	Input	Hydro NAMELIST input file
6	bucky.out	Output	Main ASCII output file
8	bucky.bin	Output	Main binary output file (for plotting)
10	bucky.beam.data	Input	Incident ion beam parameters
11	xray.dat	Input	X-ray cross sections for cold material
12	cre.popul.dat	Output	Monitors status of CRE calculation
14	bucky.bd.dat	Output	Plottable boundary radiation flux data
15	bucky.enrgy.dat	Output	Plottable energy conservation data
16	bucky.regn.Ts.dat	Output	Average temperatures for each plasma region
17	filerh(1) [†]	Input	Incident radiation flux at boundary
18	pixsec.dat.NN**	Input	Photoionization cross sections for CRE calculation
41	rate 1	Output	Transition rate tables from CRE calculation
42	rate 2	Output	Rate coefficient tables from CRE calculation
49	bucky.ppCRE	Output	Plasma parameters which are used by CRE code for computing detailed spectra
54	aul.scratch	Scratch	Scratch file for CRE input
55	ioscratch	Scratch	Scratch file for hydro and CRE input
58	rt.inp.debug	Output	Writes namelist input file for standalone CRE code (NLTERT)
70+JJ [‡]	bucky.regn.JJ.Avgs [‡]	Output	Region-averaged quantities T , p , \bar{Z} , $dE/\partial x$, J_{beam} , E_{beam}

*KK = IZEOS (given in NAMELIST input; usually the atomic number)

**NN = atomic number

[†]filerh(1) is defined in hydro NAMELIST input

[‡]JJ = plasma region

to simulate the response of Al witness plates and Au foils to hohlraum radiation fields. The file is read in by the subroutine INIT4 if the NAMELIST variable IRADBC=1. The format simply assumes two-column data with 8 header records.

The file 'xraydat' contains x-ray cross sections for computing the deposition of x-rays in cold (nonionized) material. The data are from Adams and Biggs [44]. The file is read in if ISW(11)≠1. This data is generally used to determine the x-ray energy deposition in a buffer gas and solid or liquid surfaces exposed to the x-rays from a high-gain ICF target.

When a non-LTE CRE calculation is performed the collisional and radiative data is contained in 2 files: 'rt.atom.dat.NN' and 'pixsec.dat.NN', where NN is the atomic number of the gas species. These data are generated using the ATBASE [20] suite of atomic physics codes.

The primary output files are 'bucky.out' and 'bucky.bin'. 'bucky.out' contains the descriptive output, such as the temperature, density, pressure, etc. distributions at the selected simulation times for output. Binary data used for plotting is written to 'bucky.bin'. This data is currently read in and plotted using our BUCKY_PLOT post-processor, which now features a easy-to-use graphical user interface for plotting.

Other output files of note include: 'bucky.regn.Ts.dat', which contains (mass-weighted) average temperatures for each plasma region; 'bucky.ppCRE', which contains hydro results to be read in and post-processed with our CRE code for detailed spectral calculations; and 'bucky.regnJJ.Avgs' (JJ = region index), which contains several time-dependent region-averaged quantities relevant to ion beam-heated targets.

15. NAMELIST Input Variables

The user defines the parameters of a problem with the namelist input file. Through it, the user specifies the plasma constituents, initial conditions, zoning, time step controls, radiation transport model parameters, ion or laser beam characteristics, fusion burn parameters, and/or target chamber first wall properties. In addition, the user can specify the frequency of plottable output, and request the printing of various debug output. With the exception of parameters needed for a non-LTE line transport calculation, all of the namelist variables are contained in the file 'bucky.inp'. Non-LTE line transport variables are contained in 'nltert.inp'. Table 15.1 lists each of the namelist variable names, along with their type, dimensions, units, and default values. Table 15.2 contains a list of control switches (ISW) which are typically used to select various options. Table 15.3 defines elements of CON, an array of real constants used throughout the code. Table 15.4 lists the debugging array elements (IEDIT) and the subroutines in which they are utilized. Constants used in the fusion burn package (CONTN) are given in Table 15.5. Tables 15.6, 15.7, and 15.8 define the elements of ISWCRE, CONCRE, and IEDCRE, which are the non-LTE CRE counterparts of ISW, CON, and IEDIT.

In regards to zoning, the subroutine ZONER4 currently provides the greatest flexibility for setting up the spatial mesh. The grid is set up region by region. An example of this is shown in Fig. 15.1. For a multilayer target, a region would normally consist of a material layer. Note in Fig. 15.1 that there are 3 "materials" (Al, CH, and Au) and 4 "regions". The material index is used to calculate properties of a plasma species (e.g., EOS or opacity) while a region is used for setting up the zoning. In principle, each of the materials in this example could be subdivided into multiple regions.

In ZONER4, each region is divided into 3 subregions (see bottom of Fig. 15.1). The central portion consists of equal mass zones. The other subregion zone widths are based on

a constant mass progression factor (ZONFC1 and ZONFC3). Thus, in subregion 1:

$$\Delta m_{j+1} = \Delta m_j * (1 + \text{ZONFC1}),$$

while in subregion 3:

$$\Delta m_{j-1} = \Delta m_j * (1 + \text{ZONFC3}).$$

This allows for setting up the spatial grid with progressively smaller zone widths near boundaries. The total amount of mass in each region is defined with the input variable REGMAS. REGMS1 and REGMS3 define the masses in the inner and outer subregions, respectively. The mass in the central subregion is REGMAS-REGMS1-REGMS3. JMAX is the total number of zones. JMN and JMX are the minimum and maximum zone indices for each region. JZN1 and JZN3 are used to specify the number of zones in subregions 1 and 3, respectively. Several examples of input files are shown in Section 17.

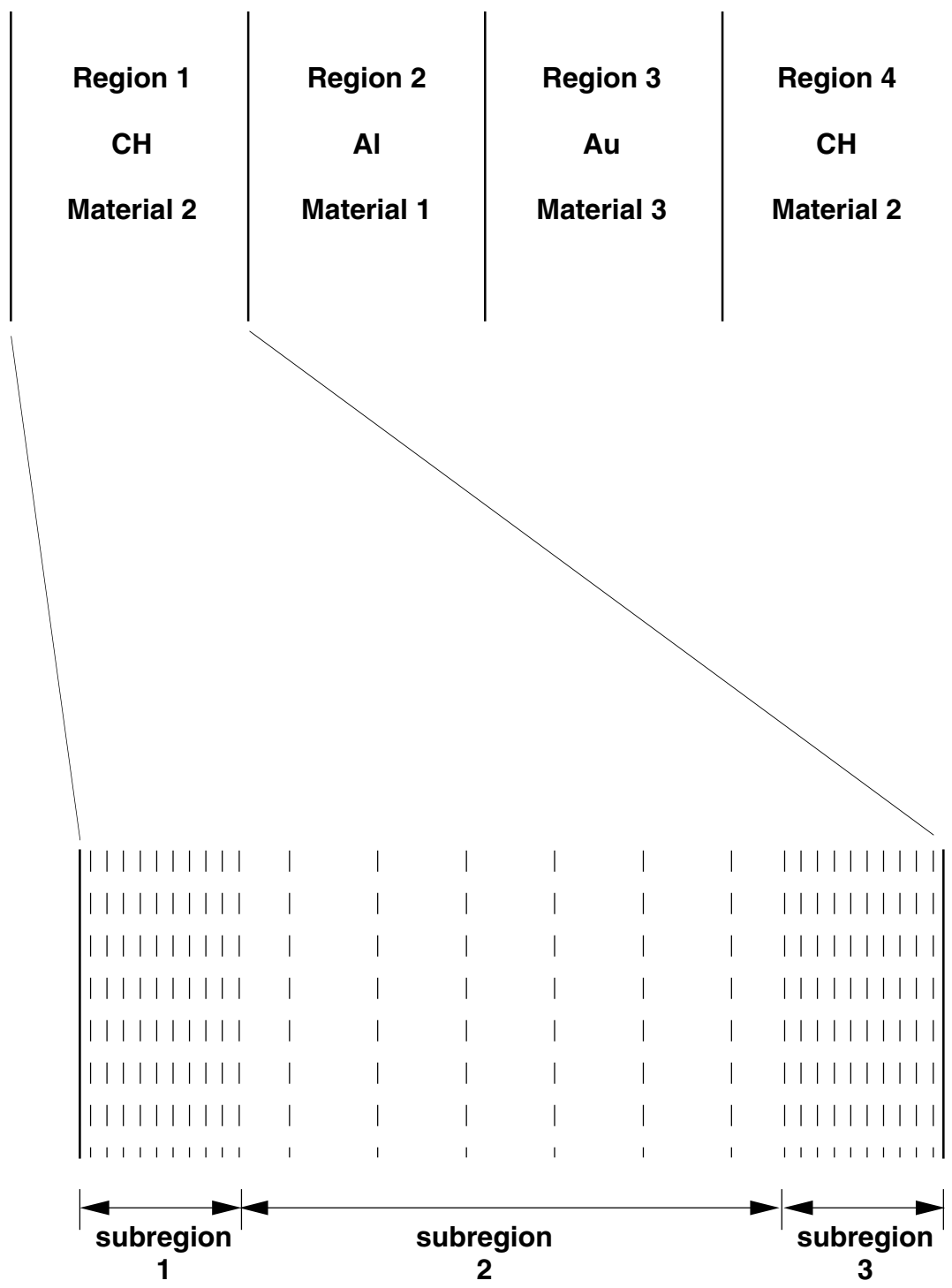


Figure 15.1. Schematic illustration of spatial grid setup using subroutine ZONER4.

PLASMA/TARGET VARIABLES

Variable Name	Type	Dimensions	Units	Default Value	Description
JMAT	I*4	—	—	1	material index for each zone
NMAT	I*4	—	—	1	number of materials
IZ	I*4	MXZONS	—	0	atomic number (used in target chamber x-ray deposition model)
ATN2B	R*8	MXZONS	—	0.	atomic number
ATW2B	R*8	MXZONS	amu	0.	atomic weight
IZEOS	I*4	MXMATR	—	0	identifier for EOS/opacity file
IDEOS	I*4	MXMATR	—	-1	format of EOS data $\left\{ \begin{array}{l} = 0 \text{ EOSOPA (old)} \\ = 1 \text{ IONMIX} \\ = 2 \text{ SESAME} \\ = 3 \text{ EOSOPA (new)} \end{array} \right.$
IDOPAC	I*4	MXMATR	—	-1	format of opacity data $\left\{ \begin{array}{l} = 0 \text{ EOSOPA (old)} \\ = 1 \text{ IONMIX} \\ = 3 \text{ EOSOPA (new)} \end{array} \right.$
RADCON	R*8	MXMATR,3	—	1.	multiplier for table opacities ($\sigma_R, \sigma_P^A, \sigma_P^E$)
DR2B	R*8	MXZONS	cm	0.	zone width (DR2B is input only if automatic zoning is not used)
DN2B	R*8	MXZONS	cm ⁻³	0.	ion density
TN2C	R*8	MXZONS	eV	0.	ion temperature
TE2C	R*8	MXZONS	eV	0.	electron temperature
TR2C	R*8	MXZONS	eV	0.	radiation temperature
Z2B	R*8	MXZONS	esu	0.	average charge
U1B	R*8	MXZONS	cm/s	0.	fluid velocity
TBC	R*8	—	eV	0.	temperature boundary condition
PRBC	R*8	—	J/cm ³	0.	pressure boundary condition

ZONING VARIABLES

Variable Name	Type	Dimensions	Units	Default Value	Description
IDELTA	I*4	—	—	0	if 1, planar geometry; if 2, cylindrical geometry; if 3, spherical geometry
JMAX	I*4	—	—	0	number of spatial zones
RADIUS	R*8	—	cm	0.	target chamber radius (at J = JMAX)
R1B	R*8	MXZONS	cm	0.	zone boundary positions
RINNER	R*8	—	cm	0.	inner radius of zone J = 1
NVREGN	I*4	—	—	0	number of vapor (plasma) regions
NCREGN	I*4	—	—	0	number of solid/liquid regions
JMN	I*4	MXREGN	—	0	minimum zone index of each region
JMX	I*4	MXREGN	—	0	maximum zone index of each region
REGMAS	R*8	MXREGN	g/x*	0.	region mass
ZONFAC	R*8	MXREGN	—	0.	mass progression factor: ($\Delta m_{j+1} = \Delta m_j * (1 + ZONFAC)$)
JZN1	I*4	MXREGN	—	0	number of zones in inner subregion
JZN3	I*4	MXREGN	—	0	number of zones in outer subregion
REGMS1	R*8	MXREGN	g/x*	0.	mass in inner subregion
REGMS3	R*8	MXREGN	g/x*	0.	mass in outer subregion
ZONFC1	R*8	MXREGN	—	0.	mass progression factor for inner subregion
ZONFC3	R*8	MXREGN	—	0.	mass progression factor for outer subregion

*x = cm² for planar, cm for cylindrical geometry.

INPUT/OUTPUT VARIABLES

Variable Name	Type	Dimensions	Units	Default Value	Description
IO	I*4	31	—	-1	output controller for text file: (1) hydrodynamic quantities (2) energy conservation (3) number densities (4) short edit (5) multifrequency radiation (6) fusion burn (9) CRE post-processing
IOBIN	I*4	—	—	-1	binary output frequency
NFDOUT	I*4	—	—	1	number of binary outputs per frequency-dependent binary output
IOCREG	I*4	—	—	0	region index for CRE post-processing output
FILERH	C*60	20	—	—	file names for input: (1) $T_R(t)$ at inner boundary
TPROUT	R*8	500	sec	10^{40}	output simulation times (if ISW(66) = 1)
DTPOUT	R*8	500	sec	-1.	if > 0 , TPROUT = TPRBEG + (i - 1) * DTPOUT
TPRBEG	R*8	500	sec	0.	if > 0 , TPROUT = TPRBEG + (i - 1) * DTPOUT
TPBOUT	R*8	500	sec	10^{40}	binary output simulation times (if ISW(66) = 1)
DTBOUT	R*8	500	sec	-1.	if > 0 , TPBOUT = TPBBEG + (i - 1) * DTBOUT
TPBBEG	R*8	500	sec	0.	if > 0 , TPBOUT = TPBBEG + (i - 1) * DTBOUT

TIME CONTROL VARIABLES

Variable Name	Type	Dimensions	Units	Default Value	Description
NMAX	I*4	—	—	0	maximum number of hydro time steps
TMAX	R*8	—	sec	0.	maximum simulation time
DTB	R*8	—	sec	1.e-12	initial time step
TA	R*8	—	sec	0.	initial simulation time
DTMIN	R*8	—	sec	$10^{-1} * DTB$	minimum time step
DTMAX	R*8	—	sec	$10^{-2} * TMAX$	maximum time step
TSCC	R*8	—	sec	0.05	time step control – Courant
TSCTN	R*8	—	sec	0.05	time step control – $\Delta T_i / T_i$
TSCTE	R*8	—	sec	0.05	time step control – $\Delta T_e / T_e$
TSCTR	R*8	—	sec	0.1	time step control – $\Delta E_R / E_R$
TSCV	R*8	—	sec	0.05	time step control – $\Delta V / V$
TGROW	R*8	—	sec	1.5	limits time step growth to TGROW * DTB
DTVAV	R*8	—	sec	0.	vaporization time step control
TSPEC	R*8	—	sec	-1.	special times for time step reset
DTSPEC	R*8	—	sec	0.	value of time step reset

RADIATION TRANSPORT VARIABLES

Variable Name	Type	Dimensions	Units	Default Value	Description
IRAD	I*4	—	—	2	radiation transport model: 0 ⇒ no radiation transport 1 ⇒ Eddington factor model 2 ⇒ diffusion model 3 ⇒ multiangle short characteristics model
NFG	I*4	—	—	0	number of frequency groups
IRADBC	I*4	—	—	0	flag or radiation at boundary: 0 ⇒ no incident radiation 1 ⇒ read data from 'filerh(1)'
IRADEF	I*4	—	—	1	boundary condition flag for Eddington factor model
NRTANG	I*4	—	—	2	number of angles used in multiangle RT model

ION DEPOSITION VARIABLES

Variable Name	Type	Dimensions	Units	Default Value	Description
IBEAM	I*4	—	—	0	ion beam flag: 0 ⇒ no ion beam 1 ⇒ outward moving beam 2 ⇒ inward moving beam
ANION	R*8	MXIDPX	—	0.	atomic number of ions
AWION	R*8	MXIDPX	amu	0.	atomic weight of ions
Q1MIN	R*8	MXIDPX	esu	0.	minimum charge state for ions
Q1INIT	R*8	MXIDPX	esu	1.	initial charge state for ions
TIONIN	R*8	MXIDPX	sec	0.	time grid for ion beam input
EIONIN	R*8	MXIDPT MXIDPE MXIDPX	keV	0.	kinetic energy per ion
XIONIN	R*8	MXIDPT MXIDPE MXIDPX	ions/s/x	0.	ion beam flux
NIT	I*4	—	—	200	number of ion time bins
NIE	I*4	—	—	1	number of ion energy bins
NIX	I*4	—	—	1	number of ion species
NQTDEP	I*4	—	—	5	number of charge states considered in time-dependent projectile charge model

*x = cm² for planar, cm for cylindrical geometry.

LASER DEPOSITION VARIABLES

Variable Name	Type	Dimensions	Units	Default Value	Description
ILASER	I*4	—	—	0	if > 0, compute laser energy deposition

FUSION BURN VARIABLES

ITN	I*4	—	—	0	If 0, no fusion burn calculation; if 1, only DT reactions; if 2, DT and DD reactions; if 3, DT, DD, and DHe ³ reactions if < 0 (-1, -2, or -3) fusion burn calculations starts after $T_{\text{ion}} > \text{CONTN}(1)$
NZBURN	I*4	—	—	0	number of zones where fusion reaction products are started
NABURN	I*4	—	—	3	number of angles for fusion reaction products
NAP	I*4	—	—	1	number of angles with $\mu > 0$ in which fusion reaction products are started
IBETA	I*4	—	—	2	number of time levels that charged particles starting in $\mu \leq 0$ are followed
DTTNMN	R*8	—	shakes	10^{-4}	minimum time step allowed for fusion burn cycle
JMAXTN	I*4	—	—	JMAX	maximum zone index containing fuel
DD2B	R*8	MXZONS	cm ⁻³	0.	deuterium number density
DT2B	R*8	MXZONS	cm ⁻³	0.	tritium number density
DO2B	R*8	MXZONS	cm ⁻³	0.	number density of non-DT species
ATWO	R*8	MXZONS	amu	0.	atomic weight of non-DT species
ZO2B	R*8	MXZONS	esu	0.	mean charge of non-DT species

FUSION BURN VARIABLES (Continued)

Variable Name	Type	Dimensions	Units	Default Value	Description
LHE4	I*4	—	—	2	switches to control transport method for 3.5 MeV alphas, 0.82 MeV He ³ , 3.02 MeV protons, 1.01 MeV tritons, 3.6 MeV alphas, and 14.7 MeV protons: 1 ⇒ local deposition 2 ⇒ time-dependent particle tracking
LHE3	I*4	—	—	1	
LP	I*4	—	—	1	
LT	I*4	—	—	1	
LHE4S	I*4	—	—	1	
LPS	I*4	—	—	1	
NG	I*4	—	—	0	
CPEN	R*8	100	keV	0.	lower energy boundary of groups used to accumulate charged particle spectrum (used when ISW(22) ≠ 0)
IRBORN	I*4	MXZONS	—	1	zone indices where charged particles are started (must be NZBURN of these)
INBORN	I*4	MXZONS	—	1	zone indices where charged particles containing fuel are started (must be JMAXTN of these)

WALL VAPORIZATION VARIABLES

Variable Name	Type	Dimensions	Units	Default Value	Description
NCZONS	I*4	—	—	0	number of Lagrangian cells in the condensed region
RHOCND	R*8	—	g/cm ³	0.	mass density of the condensed region
XKCOND	R*8	—	J/cm/s/eV	0.	thermal conductivity of the condensed region
QHEATV	R*8	—	J/g	0.	specific heat of vaporization of the condensed region
CPHEAT	R*8	—	J/g/eV	0.	specific heat of the condensed region
IZFILM	R*8	—	—	0.	atomic number of the condensed region
AWFILM	R*8	—	amu	0.	atomic weight of condensed region
TVAP0	R*8	—	eV	0.	vaporization temperature at 1 bar
TWALLB	R*8	—	eV	0.	temperature at the back of the condensed region
DELXC	R*8	MXZONS	cm	0.	zone widths for the condensed region
TCN2C	R*8	MXZONS	eV	0.	temperatures in the condensed region
DELXCT	R*8	—	cm	0.	total width of the condensed region

X-RAY DEPOSITION VARIABLES

Variable Name	Type	Dimensions	Units	Default Value	Description
FLUX	R*8	—	J	0.	the total energy of a blackbody x-ray spectrum
NXRG	I*4	—	—	25	the number of energy groups in the x-ray spectrum
KEV	R*8	—	keV	0.	the blackbody temperature of a blackbody x-ray spectrum
XEHIST	R*8	101	keV	0.	the bounds of energy groups in an arbitrary histogram
XAMP	R*8	100	J/keV	0.	the amplitude of the groups of an arbitrary histogram
CONFAC	R*8	2,2	—	1.	density multiplier in x-ray deposition calculation
NXRT	I*4	—	—	0	number of mesh times in time-dependent x-ray history
XRTIM	R*8	20	sec	0.	mesh times in time-dependent x-ray history
TDXAMP	R*8	100,20	J/keV-S	0.	time-dependent x-ray amplitudes; in this 2-dimensional matrix, the first index is the frequency group and the second is the time index

MISCELLANEOUS VARIABLES

Variable Name	Type	Dimensions	Units	Default Value	Description
ISW	I*4	100	—	Table 15.2	control switches
CON	R*8	100	—	Table 15.3	array of constants
IEDIT	I*4	100	—	-1	debugging switches (see Table 15.4)
IBENCH	I*4	20	—	0	switches for benchmark calculations
CONTN	R*8	20	—	Table 15.5	constants used in fusion burn model

INITIALIZATION FLAG FOR CRE CALCULATION

NLTEID	I*4	MXREGN	—	0	non-LTE radiative transfer (RT) flag (if > 0, use CRE RT model for line transport)
--------	-----	--------	---	---	---

CRE ATOMIC MODEL PARAMETERS

Variable Name	Type	Dimensions	Units	Default Value	Description
NGASES	I*4	MXREGN	—	1	number of gas species (maximum number = MXGASS)
ATOMNM	R*8	MXGASS	—	0.	atomic number
ATOMWT	R*8	MXGASS	amu	0.	atomic weight
FRACSP	R*8	MXZONS, MXGASS	—	1 for igas=1 0 for igas>1	fractional concentration of gases in each zone Example for homogeneous binary plasma with 20 zones: FRACSP(1,1) = 20*0.5 FRACSP(1,2) = 20*0.5 Example for layered plasma: FRACSP(1,1) = 10*1., 10*0. FRACSP(1,2) = 10*0., 10*1.
KGASRG	I*4	MXGASS, MXREGN	—	0	gas species index
SPREGN	R*8	MXGASS, MXREGN	—	0.	SPREGN[KGASRG(igas,iregn),iregn] = fractional gas abundance
WIZMIN	R*8	MXGASS,	—	0.	parameter for ionization window minimum
WIZMAX	R*8	MXGASS,	—	0.	parameter for ionization window maximum
ISELCT	I*4	MXLVLI, MXGASS	—	0	array to select atomic levels from atomic data files 1 ⇒ on (or select); 0 ⇒ off (default)

CRE RADIATIVE TRANSFER PARAMETERS

ILINEP	I*4	—	—	1	line profile type (1 ⇒ Doppler; 2 ⇒ Lorentz; 3 ⇒ Voigt)
ISWCRE (7)	I*4	100	—	0	compute photoexcitation if equal to 0
ISWCRE (8)	I*4	100	—	0	compute photoionization if equal to 0

OTHER CRE PARAMETERS

Variable Name	Type	Dimensions	Units	Default Value	Description
CONCRE	R*8	100	—	See Table 15.6	array of constants (see Table 15.6)
ISWCRE	I*4	100	—	0	array of integer switches (see Table 15.7)
IEDCRE	I*4	100	—	0	array of edit (debugging) flags (see Table 15.8)
IBENCH	I*4	20	—	0	array used for benchmark test calculations IBENCH(3) = 1: 2-level atom with $\kappa \propto r^{-2}$ 2: 2-level atom with $\kappa \propto r^{-2}$ and $B_\nu \propto r^{-2}$
IPLOT	I*4	30	—	0	array of plot switches (currently not used)

CRE CONVERGENCE PARAMETERS

ERRMXF	R*8	—	—	1.e-3	maximum error allowed in fractional populations during convergence procedure
IMAXSE	I*4	—	—	40	maximum number of iterations during convergence procedure
CRSWCH	R*8	20	—	1.0	collisional-radiative switching parameters (used in subroutine STATEQ; see [35]) (generally not needed for laboratory plasmas)
NGCYCL	I*4	—	—	4	apply Ng acceleration every NGCYCL'th cycle
NGORDR	I*4	—	—	2	order of Ng acceleration
NGBEGN	I*4	—	—	0	iteration cycle at which to begin Ng acceleration

Table 15.2. Integer Control Switches – ISW

Array Element	Value*	Description
2	= 10*	number of constant time steps used at the beginning of a calculation
3	= 1 = 2*	1- T ($T_{\text{ion}} = T_e$) plasma model 2- T ($T_{\text{ion}} \neq T_e$) plasma model
4	= 0*	user specifies zoning with DR2B > 0 automatic zoning 1 \Rightarrow automatic zoning using ZONERP 2–9 \Rightarrow automatic zoning using ZONER2 10–15 \Rightarrow automatic zoning using ZONERC 20–25 \Rightarrow automatic zoning using ZONER3 26–30 \Rightarrow automatic zoning using ZONER4
5	= 20*	frequency of tabulation of overpressure and heat flux at the outer boundary
6	= 0* = 1	hydrodynamic motion is computed no hydro motion
7	= 0* = 1 = 2 = 3	both boundaries fixed ($v_{\text{fluid}} = 0$) both boundaries free J = 1 fixed, JMAX free J = 1 free, JMAX fixed
8	= 0* = 1 = 2	no fast ion deposition use ion beam parameters from NAMELIST input file use ion beam parameters from ‘bucky.beam.dat’
9	= 0* = 1	reflective radiation boundary condition at J = 1 free radiation boundary condition at J = 1
11	= 0 = 1* = 2 = 3	initial x-ray deposition is computed calculation begins from input temperatures time-dependent x-rays only both time-dependent and initial x-ray deposition

Table 15.2. (Continued)

Array Element	Value*	Description
12	= 0* = 1	equation of state tables are used ideal gas equation of state is used; CON(5) must be input via NAMELIST
13	= 0* = 1	no quiet start use quiet start option; CON(19) defines temperature at which hydro starts
16	= 0* > 0	if negative temperature is found, print it and stop if negative temperature is found, fix it and print out every ISW(16)'th cycle.
20	= 0* = 2	no condensation or vaporization calculate vaporization of first surface
21	= 0* = 1	left-over particles in the TDPT algorithm are forced to stop by allowing them to transport until they stop or escape left-over particles are ignored (forgotten)
22	= 0* = 1	no escaping charged particle spectrum is computed an alpha particle spectrum is computed (CPEN specifies the energy groups, NG specifies the number of groups)
23	= 0* = 1	start charged particle reaction products in each zone group charged particle starting zones according to the indices in INBORN and IRBORN
24	= 0* = 1	use table look up to compute $\langle\sigma v\rangle$ (SIGMAV) for DT, DD, DHe ³ use analytic formulas to compute $\langle\sigma v\rangle$ (SIGMAV) for DT, DD, DHe ³
25	= 0* = 2	redistribute energy in wall vaporization model do not redistribute energy
27	= 0* = 1	get P and P -derivatives from EOS tables compute P and P -derivative from \bar{Z}
28	= 0* = 1	get C_v from specific energy table get C_v from table lookup

Table 15.2. (Continued)

Array Element	Value*	Description
29	= 0* < 0 > 0	get $(dE/dV)_T$ from specific energy table get $(dE/dV)_T$ from ENNTAB table get $(dP/dT)_V$ from PNTTAB table
30	= 0* = 1	use input values for properties of film calculate properties of film
31	= 0* = 1	use Q1INIT (= constant) for ion charge in ion deposition calculations compute time-dependence of debris ion charge states
32	= 0* = 1	no debris ion mass added to vapor cells add debris ion mass to vapor cells as ions stop
34	= 0* = 1	no electron thermal flux limit is used classical flux limit is used
38	= 0* = 1	calculate variable Eddington factor use CON(38) for Eddington factor
48	= 0* = 1	calculate ion stopping (dE/dx) use CON(48) for ion stopping (dE/dx)
50	= 0* = 1	no non-LTE CRE line radiation transport use non-LTE CRE model for line radiation transport (automatically set by NLTEID)
66	= 0* = 1	output results based on number of hydro cycles output results based on simulation time
71	= 0* = 1	use 1st order method for short characteristics radiation transport use 2nd order method for short characteristics radiation transport
77	= 0* = 1	get Z2B from table lookup compute Z2B from ZO2B in NUMDEN

*An asterisk indicates default value.

Table 15.3. Real Constants–CON

Array Element	Default Value*	Description
1	1.55e3	coefficient for electron thermal conductivity
2	7.71e1	coefficient for ion thermal conductivity
3	3.445e-8	coefficient for electron thermal flux limit
4	1.e-10	small term to avoid divide by zero in flux-limited radiation diffusion term
5	0.	if non-zero, it is used as a constant value for $\log \Lambda$; normally, $\log \Lambda$ is computed
6	1.371e-5	$4 \sigma/c$ ($\text{J cm}^{-3} \text{ eV}^{-4}$)
8	0.64	$\overline{\Delta E}_{DT}/(\rho R)_o$ for neutron deposition rate calculation ($\text{MeV cm}^2/\text{g}$)
9	1.602e-19	J/eV
14	2.403e-19	$3/2$ J/eV
16	1.371e-5	coefficient for radiation energy density ($\text{J/cm}^3/\text{eV}^4$)
18	1.0	ion shock heating term
19	0.15	temperature for quiet start option (eV)
21	1.414	coefficient for Von Neumann artificial viscosity
22	3.e10	multigroup radiation absorption term
23	6.33e4	multigroup radiation emission term
24	1.e10	multigroup radiation diffusion conduction term
25	3.e10	radiation diffusion flux limit
26	1.e-20	minimum allowable multigroup radiation energy density
27	3.e10	variable Eddington radiation flux term
28	6.059e10	coefficient for electron-ion coupling term
29	0.5	minimum Z-value used in electron-ion coupling and ion conductivity
31	1.0	wall vaporization rate multiplier
32	1.0	wall condensation rate multiplier

Table 15.3. (Continued)

Array Element	Default Value*	Description
33	0.	vaporization/condensation flux correction
34	31.2	coefficient for reducing condensation rate due to presence of a non-condensable gas
35	1.	charge exchange cross section multiplier for fast ion energy deposition
36	0.	mass progression factor for automatic zoning in ZONER2 and ZONERC.
37	0.	mass progression multiplier for condensed region
38	0.333	if ISW(38) = 1 or planar geometry, use for variable Eddington factor
42	1.	multiplier for (dE/dx) in ion stopping model
43	1.	multiplier for intensities in cold x-ray deposition model
44	1.	multiplier for ion beam current (flux) densities in ion stopping
45	2.0	ion thermal velocity term
47	1.	relative debris ion velocity term
48	0.	if ISW(48) = 1, use constant (dE/dx) (eV cm ² /ion)
75	1.	multiplier for radiation temperature boundary condition
77	1.	multiplier for fusion charged particle deposition rate
80	35.e-9	collapse time for implosion benchmark calculation (sec)
81	7.5e9	laser intensity for implosion benchmark calculation (J/s)
82	0.96	time constant for implosion benchmark calculation

Table 15.4. Debugging Switches

Array Element	Subroutine Writing Debug Output		Array Element	Subroutine Writing Debug Output		Array Element	Subroutine Writing Debug Output
32	ABCPL1		14	HYDROD		17	RADTR1
1	ABCPL2		50	IONDEP		17	RADTR1
62	ABCRD1		85	IZIAIT		17	RADTR2
21	ABCRD2		37	JZONE		17	RADTR3
46	CPSPEC		47	LOCAL		26	RCOND
54	DEDX		36	NEGTCCK		83	RMUV
39,40	DELTAV		19	NUMDEN		65,67	SHORTC
18	DEPLET		9	OMEGAC		45	SIGMAV
51,91	ECHECK		64	OPACMG		86	SLOW
52	EDEPOS		90	OUT3		13	TABLE2
63	EDFACT		31	PCOND1		13	TABLE4
20	EMISSN		31	PCOND2		13	TABLEO
42	ENEMA		27	PLSCF1		16	TEMPBC
35	ENERGY		27	PLSCF2		81	TNBURN
24	EOS		12	POINT		44	TNREAC
41	EOS1		12	POINTO		43	TNSLOW
38	FDS		17,22	RADCOF		33,34	TRANSP
7	GASDEP		66	RADDEN		55	WALLVP

Table 15.5. Description of Constants in Vector – CONTN

CONTN	Value	Description
1	4.E0	lower limit on T_i for computing thermonuclear reactions. Also if $ITN < 1$ then after T_i becomes greater than this, the thermonuclear calculation is started
2	6.9325E-13	coefficient for thermal velocity used in SLOW
3	8.35E-46	coefficient for charged particle slowing down on electrons SLOWE
4	6.67E-69	coefficient for charged particle slowing down on ions SLOWI
5	1.E22	lower limit on D and T density for computing thermonuclear reactions – to avoid computations where very few reactions will occur
6	2.E0	value of DTTNMN used to force particles to slow down in TRANSP (see ISW(21))
7	.666E0	correction for average chord length in 1st zone when only 3 directions are used; this is used in zone 1 when only 3 directions are used to avoid having all particles traverse the zone along its full diameter
8	.5E0	when fast charged particles thermalize in a zone, this fraction of the lost energy is given to the electrons and the rest is given to the ions
9	.98E0	when the cosine of the direction angle is $> \text{CONTN}(9)$ it is set to 1 so that square root calculations are avoided in RMUV
10	.7939E0	fraction of radius of first zone where particles are started. One half of the first zone mass is inside this radius and the other half is outside this radius
11	1.E0	fraction of charged particles deposited in local deposition option
12	1.E0	fraction of T that burn in flight due to beam-plasma nonthermal reactions
13	1.E0	fraction of He^3 that burn in flight due to beam-plasma nonthermal reactions

Table 15.6. Control Switches - ISWCRE

Array Element	Value*	Description
6	0*	Start with populations from previous hydro time step
	1	Start with LTE populations
	2	Start with coronal populations
	3	Return LTE populations
	4	Return coronal populations
7	0*	Include photoexcitation effects in calculation of atomic level populations
8	0*	Include photoionization effects in calculation of atomic level populations
20	0*	Non-LTE equation of state: $E = E_{\text{ion}} + E_e + E_{\text{iz}}$
	1	$E = E_{\text{ion}} + E_e + E_{\text{iz}} + E_{\text{degen}}$
	2	$E = E_{\text{ion}} + E_e + E_{\text{iz}} + E_{\text{DH}}$
	3	$E = E_{\text{ion}} + E_e + E_{\text{iz}} + E_{\text{degen}} + E_{\text{DH}}$
23	0*	Compute Voigt parameter
	1	Set Voigt parameter = CONCRE (23)
	2	Estimate T and a_{voigt} from rate coefficients
30	0	Compute \bar{g} in Stark width calculation
	1*	Set $\bar{g} = 0.2$ in Stark width calculation
34	0*	Use LAPACK matrix scaling
	1	Use LAPACK + NLERT matrix scaling
38	0*	No equation of state calculation
	1	Compute internal energy and pressure (Not currently an option)
39	0*	No multigroup opacity calculation
	1	Compute multigroup opacities (Not currently an option)
99	0*	Dump output and stop when ill-conditioned matrix is encountered

An asterisk () indicates default value.

Table 15.7. Real Constants - CONCRE

Array Element	Default Value	Description
6	1.e-30	Minimum value of fractional level population
12	0.1	Scaling parameter for statistical equilibrium matrix elements
19	1.e-5	Minimum fractional population used to test convergence
20	1.0	Multiplier for natural line width
21	1.0	Multiplier for Doppler line width
22	1.0	Multiplier for Stark line width
23	1.0	Multiplier for Voigt profile broadening parameter (see also ISWCRE (23))
24	1.0	Multiplier for ion dynamic broadening
		(hydrogenic Lyman series)
26	1.0	Multiplier for bound-bound opacity
27	1.0	Multiplier for bound-free opacity
28	1.0	Multiplier for free-free opacity
42	1.0	Multiplier for collisional deexcitation rate
43	1.0	Multiplier for spontaneous emission rate
45	1.0	Multiplier for collisional recombination rate
46	1.0	Multiplier for radiative recombination rate
47	1.0	Multiplier for dielectronic recombination rate
57	0.3	Minimum value of $\Delta E/T$ for ionization windowing
58	30.	Maximum value of $\Delta E/T$ for ionization windowing

Table 15.8. Debugging Switches - IEDCRE

Array Element	Subroutine Writing Debug Output
7	ABSEMS
18	CCSLAB
18	CLSLAB
12,55	GETCF1
12,55	GETCF2
16	GETPOP
78	GPOPAC
48	IIXSEC
44	INITC2
28,29	INNLTE
32	IZWDO
61	LINEPR
66,80	LINWID
62	LODCB1
62	LODCB2
11,27	LOPACS
1,14,54	MATRX0
77	MESHMG
78	MGOPAC
34	NGACCL
63	NLPOPS
41	RATCOF
47,81	READA2
6,15	STATEQ
92	VOIGT
81	WSTARK

16. Compiling and Running

In this section, we briefly describe how to set up BUCKY-1 for running a calculation. Figure 16.1 shows an example MAKEFILE for this procedure. We start with the source (“.src”) files for each subroutine and the file containing the common blocks. At the top of the comdecks file are 2 “*define” statements: “*define hp” and “*define double”. The first is used to specify the platform for running. Options are “hp” for HP workstations, “sun” for SUN workstations, “rs6” for IBM RS6000 workstations, and “cray” for CRAY supercomputers. This tells the preprocessor to look for machine-dependent strings in the source code, and load them into the FORTRAN deck (“.f” files). An example of this is the time and date of the calculations, which are printed out at the top of the output. The second string, “double”, refers to double precision for variables beginning with A-H and O-Z. This is highly recommended for 32-bit workstations. For 64-bit machines such as a CRAY supercomputer, single precision (“*define single”) should be adequate.

Near the top of the MAKEFILE are two directories for the source code files, and one for the destination directory (“destdir”) where the user will run the calculation. The first source directory (“dold”) is the location of files for the latest “base”, or version, of BUCKY-1 (base 7 in the example). The second contains files which have been modified from the base version. The sequence of commands at the end of the MAKEFILE — subroutine by subroutine — run the preprocessor (using a simple “update” algorithm) to create a “.f” file, which is then compiled. Any compilation errors are written to a file named “Errs”.

The user can specify compilation flags on the ‘make’ command line. This is most easily done using an ‘alias’ command. For example, one can define aliases such as (for ksh shell);

```
alias mkb='rm -f Errs; make "FFLAGS=+E1 +T -g -C" -f Bucky.make bucky.exe; more Errs'
```

```
alias mkbf='rm -f Errs; make "FFLAGS=+E1 +T +O1" -f Bucky.make bucky.exe.opt; more Errs'
```


Then, by simply typing “mkb” or “mkbf” from the source decks directory, one gets either an executable which can be used with a debugger “a.out”, or an optimized executable “a.out.opt”. These files are placed in the directory specified by “destdir” at the top of the MAKEFILE.

17. Sample Calculations

In this section, we show example input decks for 5 calculations. Also shown are some selected results which the user can compare with to check if the code is installed and running properly. The examples are: (1) the isentropic compression of a DT shell; (2) a shock breakout simulation for a radiatively-driven Al witness plate; (3) a LIBRA implosion simulation; (4) the fusion burn and breakup of a LIBRA target; and (5) a simulation of the response of a non-LTE target chamber buffer gas to a high-gain ICF microexplosion.

17.1. Example 1: Isentropic Compression of a DT Shell

This is a calculation performed to benchmark the code against the previously published results of Kidder [47]. The input file is shown in Figure 17.1. `IBENCH(1) = -2` indicates this is a “benchmark” calculation in which a specific time-dependent pressure boundary condition is applied. It also specifies that the initial temperature and density distributions be set up as in the Kidder [47] calculation. The inner radius (`RINNER`) of the shell is 0.12 cm in this spherically symmetric (`IDELTA = 3`) calculation. An ideal gas EOS is used (`ISW(12) > 0`) for DT (`ATW2B = 2.5`). `Z2B = 1` specifies that the DT is fully ionized. No radiation transport is considered (`IRAD = 0`). `CON(80)`, `CON(82)` and `PRBC` are used to specify the time-dependent pressure at the outer boundary. The calculation is run out to a simulation time (`DTMAX`) of 18.15 ns.

The zoning option used (`ISW(4) = 26` \Rightarrow subroutine `ZONER4` is used) divides the plasma into 1 region (`NVREGN = 1`) and 3 sub-regions (see Sec. 15 for a discussion of this zoning option). The mass of the DT is 75 μg , which is usually specified directly with `REGMAS`. However, because the densities are readjusted after the zoning takes place (at present, this occurs only for this series of implosion benchmark calculations), the number specified by `REGMAS` *in this case* is not the true region mass, but was adjusted to give 75 μg with the density profile given by Kidder.

```

$input
c ...      ibench(1) = -2          ibench(1)=1 => laser-driven implosion calc.
           rinner = .1200
c ...      bench 2
           prbc = 1.535e4
c ...      con(80) = 17.77e-9     con(80) = collapse time (sec)
           con(82) = 0.9600       con(82) = scaled transition time
c ...      bench 2
           con(80) = 17.77e-9
           con(82) = 0.9600
c ...      laser beam input (or pres. b.c.)
           ilaser = 1
           con(81) = 7.5e9        con(81) = laser power (psi0) (J/sec)
c ...      irad=0 => no radiation
           irad=2 => MG Diff. model
           irad=3 => MG, MA RT model
c ...      irad = 0
           Max. run time
           nmax = 100000
           tmax = 18.15e-9
           dtb = 1.e-15
c ...      if isw7=1, allow free expansion of both boundaries
           if isw7=2, allow free expansion of outer boundary
           isw(7) = 1
c ...      EOS PARAMETERS
           if isw12=1, use ideal gas (Z_bar=0)
           if isw12=2, use ideal gas (Z_bar=1)
           set con5 = 1 (=log lambda) for ideal gas case
           isw(12) = 2
           con(5) = 1.
c ...      EOS file type
           (ideos: 0=>UW/WP ; 1=>UW/IONMIX ; 2=> SESAME)
           (ideos: < 0 => ideal gas)
c ...      Opacity file type
           (idopac: 0=>UW/WP ; 1=>UW/IONMIX)
           (idopac: < 0 => ideal gas)
           idopac(1) = -1
           ideos(1) = -1
           izeos(1) = 0
c ...      TIME STEP PARAMETERS
           tsctr = 0.05
           tsctn = 0.02
           tscte = 0.02
           tsc = 0.1
           tscv = 0.02
           dtmin = 1.e-17
           dtmax = 1.e-10
c ...      ZONING PARAMETERS
           nvreg = 1
           idelta = 3
           isw(4) = 26
           isw4=20-25 for spherical region zoning
           isw4=26-30 for spherical sub-region zoning
c ...      ZONING and TARGET PARAMETERS
           jmax = 40
           jzn1(1) = 10
           jzn3(1) = 10
           zonfc1(1) = 0.1
           zonfc3(1) = 0.3
           regmas(1) = 188.e-6
           regm1(1) = 40.e-6
           regm3(1) = 40.e-6
           regmas: mass in grams
c ...      plasma parameters
           jmat(1) = 100*1
           atw2b(1) = 100*2.5
           atwo(1) = 100*0.
           zo2b(1) = 100*0.
           dn2b(1) = 100*4.8e22
           dd2b(1) = 100*2.4e22
           dt2b(1) = 100*2.4e22
           do2b(1) = 100*0.
           tn2c(1) = 100*1.
           te2c(1) = 100*1.
           tr2c(1) = 100*0.025
           tbc = 0.025
c ...      OUTPUT CONTROL PARAMETERS
           isw(66) = 1
           io(1) = 3*100
           dtpout = 5.e-9
           dtbout = 0.010e-9
           tpbeg = 17.0e-9
           iobin = 500
           isw(5) = 100
           nfdout = 10000
Send

```

Figure 17.1. Example input file for implosion benchmark calculation.

Figure 17.2 shows Lagrangian zone positions as a function of time from the BUCKY-1 simulation (3 plot on the left). On the right are the results of Kidder. Note that the trajectories of the DT zones are very similar in the 2 calculations, including the time of void closure.

17.2. Example 2: Al Witness Plate Shock Breakout

This is a simulation of a shock breakout experiment involving an Al witness plate attached to the side of a high-Z hohlraum. The namelist input file is shown in Figure 17.3. The hohlraum radiation field is represented by a time-dependent radiation boundary condition ($IRADBC = 1$), which is currently a 1-T Planckian spectrum, $T_R(t)$. The input file for $T_R(t)$ is ‘SNL.Al.burn.dat’. Note that the file input values are multiplied by 1.06 ($CON(75)$).

Radiation is transported using the multiangle short characteristics model ($IRAD = 3$). Two angles are used ($NRTANG$). The EOS/opacity data utilized is generated by EOSOPA [5], ($IDEOS$ and $IDOPAC = 0$), and is contained in the file ‘eos.dat.uw.13’ ($IZEOS = 13$). The mass of the Al foil is 0.0486 g/cm^2 , which corresponds to a thickness of $180 \text{ }\mu\text{m}$. The initial conditions are $T = 0.1 \text{ eV}$ ($TN2C$) and solid density ($DN2B = 6.0e22$).

Results from this calculation are shown in Figure 17.4. Also shown are shock breakout data from NOVA experiments performed by R. Olson [48].

17.3. Example 3: LIBRA Implosion Simulation

Figure 17.5 shows an example input file which could be used to run an implosion calculation for a high-gain light ion-driven target. (This is not meant to be a “working” target, but only to illustrate how to set up the input file.) The target is a spherical ($IDELTA = 3$) multi-material target composed of an inner DT layer of 5 mg ($REGMAS(1) = 5.e-3$), a CH ablator of 9.08 mg, a C foam layer of 17.4 mg (which is zoned up as 2 regions: a 6.9 mg

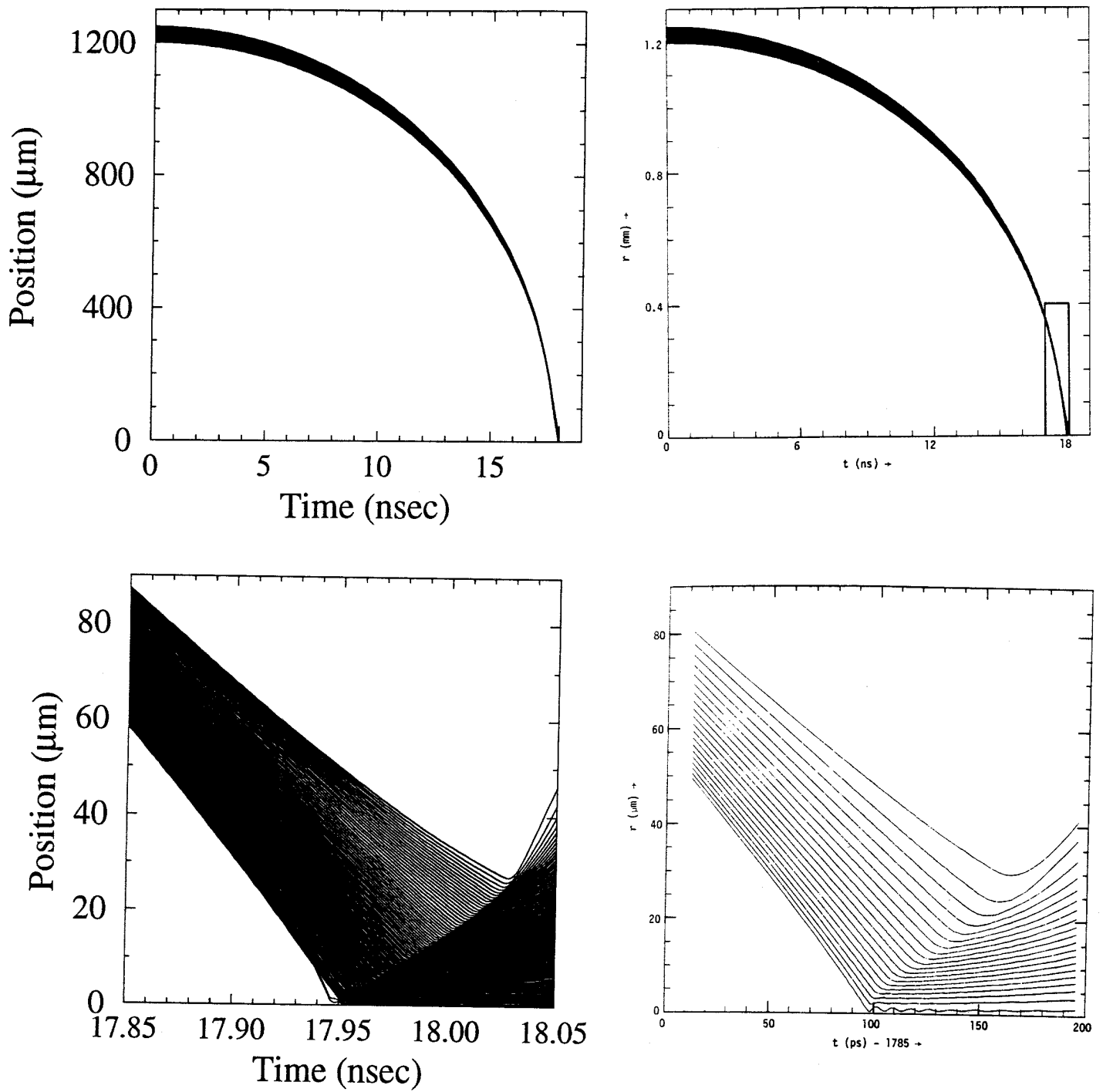


Figure 17.2. Lagrangian zone positions vs. time for implosion benchmark calculation. Left: BUCKY-1 results; Right: Kidder [47] results.

```

$input
c ...
c      irad=2 => MG Diff. model
c      irad=3 => MG, MA RT model
c      irad = 3
c      nrtang = 2
c ...
c      nfg = 25
c ...
c      iradbc = 1
c ...
c      filerh(1) = 'SNL.Al.burn.dat'
c ...
c      con(75) = 1.06
c ...
c      isw(6) = 0
c ...
c      isw(13) = 1
c      con(19) = 0.15
c ...
c      isw(3) = 1
c ...
c      nmax = 100000
c      tmax = 2.5e-9
c      dtb = 1.e-15
c ...
c      isw(7) = 1
c ...
c      isw(9) = 1
c ...
c      izeos(1) = 13
c      ideos(1) = 0
c      idopac(1) = 0
c ...
c      tsctr = 0.10
c      tsctn = 0.05
c      tscte = 0.05
c      tscc = 0.05
c      tscv = 0.05
c      dtmin = 1.e-17
c      dtmax = 1.e-10
c ...
c      nvregn = 1
c      idelta = 1
c      isw(4) = 26
c ...
c      jmax = 100
c      jzn1(1) = 20
c      jzn3(1) = 20
c ...
c      zonfc1(1) = 0.1
c      zonfc3(1) = 0.1
c ...
c      regmas(1) = 4.86e-2
c      regms1(1) = 0.49e-2
c      regms3(1) = 0.49e-2
c ...
c      jmat(1) = 100*1
c      iz(1) = 100*13
c      atn2b(1) = 100*13.
c      atw2b(1) = 100*27.
c      dn2b(1) = 100*6.0e22
c ...
c      tn2c(1) = 100*0.1
c      te2c(1) = 100*0.1
c      tr2c(1) = 100*0.025
c      tbc = 0.025
c ...
c      isw(66) = 1
c      io(1) = 2*500
c      dtpout = 0.2e-9
c      dtbout = 0.05e-9
c      nfdout = 4
c ...
c      $end

```

```

radiation transport parameters
iradbc => radiation boundary condition
File for Radiation Boundary Condition
con75 = multiplier for T-rad at boundary
turn hydro off if isw6=1
quiet start option (if isw13=1)
1-T (isw3=1) or 2-T (isw3=2) option
if isw3=3 => simult. soln. of TR and pl.E (1-T)
Max. run time
if isw7=1, allow free expansion of both boundaries
if isw9<>1, use reflective rad. bc at j=1
EOS PARAMETERS
EOS file type
(ideos: 0=>UW/WP ; 1=>UW/IONMIX ; 2=> SESAME)
Opacity file type
(idopac: 0=>UW/WP ; 1=>UW/IONMIX)
TIME STEP PARAMETERS
ZONING PARAMETERS
TARGET PARAMETERS
(0.0486 g/cm2 => 180-micron-thick Al)
OUTPUT CONTROL PARAMETERS

```

Figure 17.3. Example input file for Al shock breakout calculation.

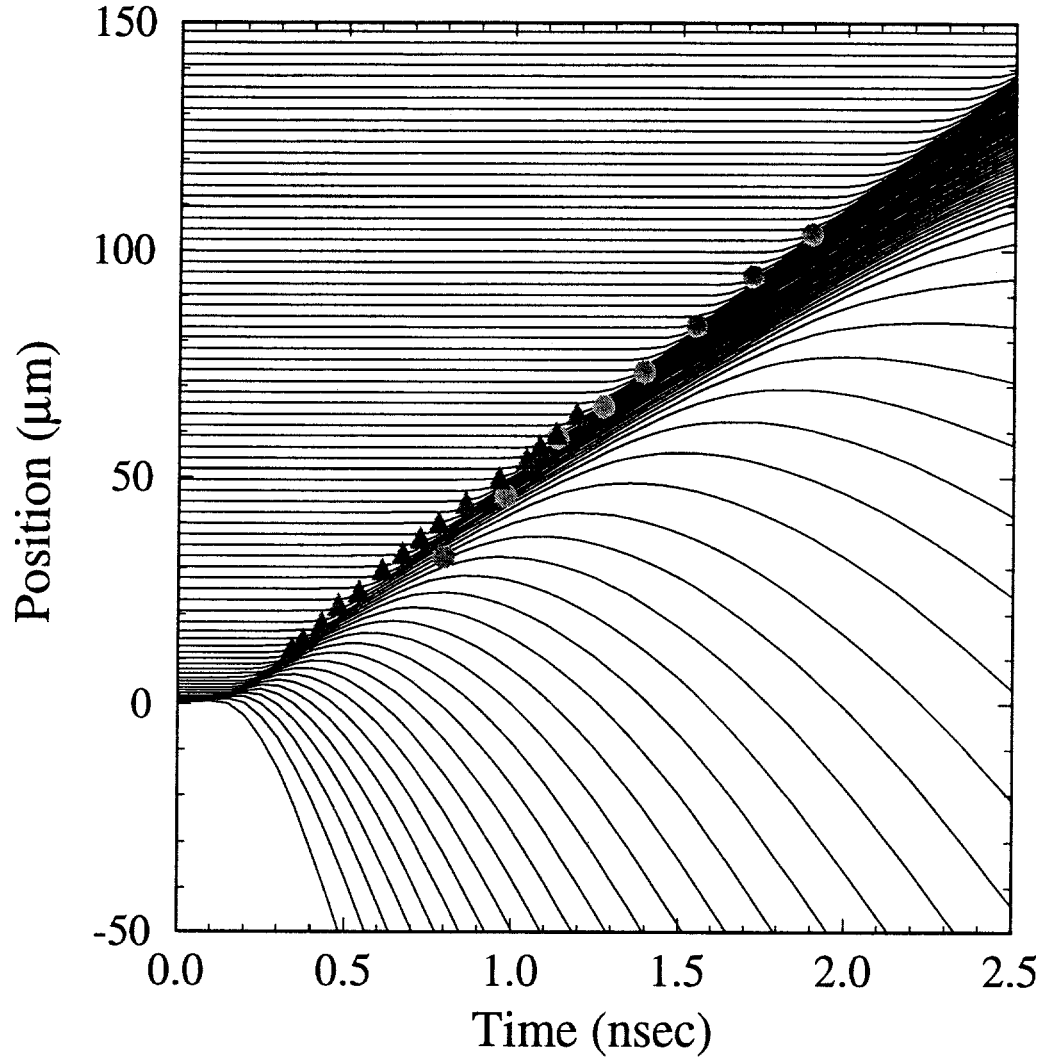


Figure 17.4. Lagrangian zone positions vs. time for Al shock breakout calculation.

```

$input
c ...      1-T (isw3=1) or 2-T (isw3=2) option
c ...      isw(3) = 2
c ...      nmax = 50000      Max. run time
c ...      tmax = 60.e-9
c ...      dtb = 1.e-14
c ...      TIME STEP PARAMETERS
c ...      tsctr = 0.1
c ...      tsctn = 0.05
c ...      tscte = 0.05
c ...      tscc = 0.08
c ...      tscv = 0.05
c ...      dtmin = 1.e-17
c ...      if isw7=1,allow free expansion of both boundaries
c ...      if isw7=2,allow free expansion of outer boundary
c ...      isw(7) = 1
c ...      if isw9<>1,use reflective rad. bc at j=1
c ...      isw(9) = 0
c ...      EOS PARAMETERS
c ...      EOS file type
c ...      (ideos: 0=>UW/WP ; 1=>UW/IONMIX ; 2=> SESAME)
c ...      (ideos: < 0 => ideal gas)
c ...      Opacity file type
c ...      (idopac: 0=>UW/WP ; 1=>UW/IONMIX)
c ...      (idopac: < 0 => ideal gas)
c ...      idopac(1) = 0, 0, 0, 0
c ...      ideos(1) = 0, 0, 0, 0
c ...      izeos(1) = 1, 5, 6, 79
c ...      ZONING PARAMETERS
c ...      idelta = 3
c ...      isw4=20-25 for spherical region zoning
c ...      isw4=26-30 for spherical sub-region zoning
c ...      isw(4) = 20
c ...      ZONING and TARGET PARAMETERS
c ...      nvregm = 5
c ...      jmax = 100
c ...      jmat(1) = 25*1, 25*2, 25*3, 25*4
c ...      jmn(1) = 1, 26, 51, 61, 76
c ...      jmx(1) = 25, 50, 60, 75, 100
c ...      inner radius of innermost zone (cm)
c ...      rinner = .086
c ...      regmas(1) = 5.0e-3, 9.08e-3, 6.9e-3, 10.5e-3, 180.e-3
c ...      zonfac(1) = 0.02, 0.05, 0., 0., 0.18
c ...      atw2b(1) = 25*2.5, 25*6.5, 25*12., 25*197.
c ...      atn2b(1) = 25*1., 25*3.5, 25*6., 25*79.
c ...      atwo(1) = 25*0., 25*6.5, 25*12., 25*197.
c ...      zo2b(1) = 25*0., 25*3.5, 25*6., 25*50.
c ...      dn2b(1) = 25*5.22e22, 25*9.27e22, 10*1.01e21, 15*0.51e21, 25*5.90e22
c ...      do2b(1) = 25*0., 25*9.27e22, 10*1.01e21, 15*0.51e21, 25*5.90e22
c ...      dd2b(1) = 25*2.61e22, 25*0., 25*0., 25*0.
c ...      dt2b(1) = 25*2.61e22, 25*0., 25*0., 25*0.
c ...      tn2c(1) = 100*0.1
c ...      te2c(1) = 100*0.1
c ...      tr2c(1) = 100*0.025
c ...      tbc = 0.
c ...      RADIATION TRANSPORT PARAMETERS
c ...      irad=2 => MG Diff. model
c ...      irad = 2
c ...      # frequency groups
c ...      nfg = 20
c ...      ION ENERGY DEPOSITION
c ...      isw(8) = 1
c ...      ibeam =2 => start ions at outermost zone (prop. inward)
c ...      ibeam = 2
c ...      isw(31) = 0
c ...      con(44) = 1.
c ...      qlimit = 3.
c ...      qlmin = 0.
c ...      anion = 3.
c ...      awion = 7.
c ...      square pulses for foot and main pulse
c ...      tionin(1) = 0., 1.e-15, 40.00e-9, 40.01e-9, 60.00e-9, 60.01e-9
c ...      xionin(1,1,1) = 0., 6.242e24, 6.242e24, 62.42e24, 62.42e24, 0.
c ...      eionin(1,1,1) = 22.e3, 25.e3, 28.e3, 28.e3, 37.e3, 30.e3
c ...      nix = 1
c ...      nie = 1
c ...      nit = 200
c ...      FUSION BURN ENERGY DEPOSITION
c ...      itn = 0
c ...      quiet start option (if isw13=1)
c ...      isw(13) = 1
c ...      con(19) = 0.5
c ...      I/O PARAMETERS
c ...      isw(66) = 1
c ...      io(1) = 3*100
c ...      dtpout = 5.e-9
c ...      dtbout = 2.e-9
c ...      tpbeg = 0.e-9
c ...      iobin = 500
c ...      isw(5) = 100
c ...      nfdout = 10000
$end

```

Figure 17.5. Example input file for LIBRA implosion calculation.

inner and 10.5 mg outer component), and an Au case of 240 mg. There are 40 spatial zones (JMAX) and the array JMAT is used to specify the material index for each zone (1 \Rightarrow DT, 2 \Rightarrow CH, 3 \Rightarrow C, 4 \Rightarrow Au). The EOS/opacity file of each material is identified by its atomic number (see IZEOS), except for CH, where the data has been put in ‘eos.dat.uw.05’.

The initial temperature throughout the target is 0.1 eV (TN2C and TE2C). The density distributions are specified by DN2B. Note that DN2B should equal the sum of DD2B (deuterium), DT2B (tritium), and DO2B (“other”; i.e., non-DT).

Radiation is transported using a 20-group (NFG) radiation diffusion (IRAD = 2) model.

This has an inward-propagating (IBEAM) ion beam composed of fully charged Li ions (ANION, AWION, Q1INIT). The variables TIONIN, EIONIN, and XIONIN specify a 40 ns, 30 TW foot and a 20 ns, 300 TW main pulse of 30 MeV Li ions.

Figure 17.6 shows the beam energy deposition in the target at simulation times of 20, 40, 50, and 60 ns. The range shortening due to hot stopping can be easily seen.

17.4. LIBRA Fusion Burn and Target Breakup

Figure 17.7 shows the input file for a LIBRA target breakup [7] simulation. The composition of the target is similar to that in the above example. The main difference from above is that the initial conditions are meant to be approximately representative of those at the start of ignition. The DT shell is divided into 3 regions, with a central high-temperature core (TN2C = 8000 eV, DN2C = $1.2e25$ cm⁻³), surrounded by 2 lower temperature, but higher density DT regions. The DT is surrounded by layers of CH, C, and Pb. In this calculation there is no ion beam as the target starts at conditions capable of sustaining DT burn.

The fusion burn package is turned on (ITN = 1). There are 10 burn zones (NZBURN) and the number of angles used in the charged particle tracking algorithm (NABURN) is 3.

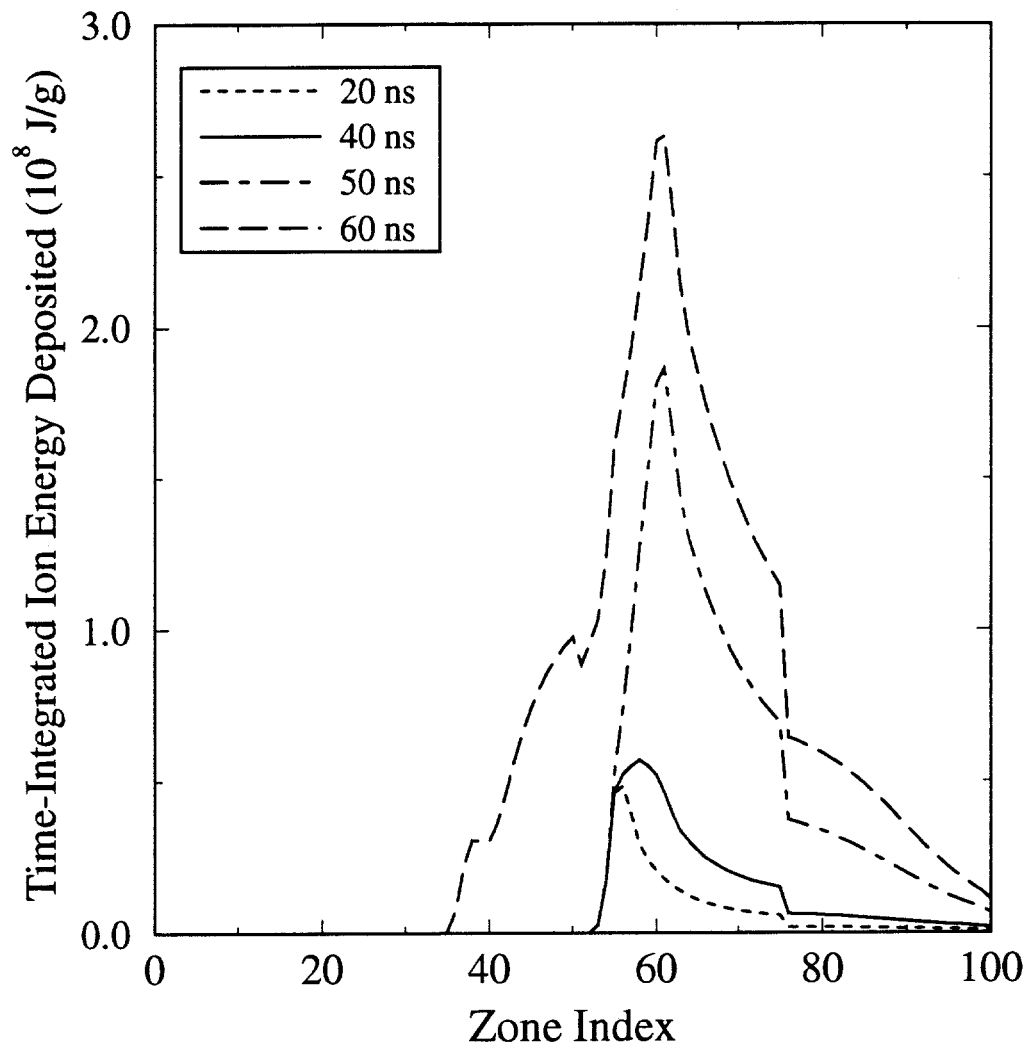


Figure 17.6. Time-integrated ion energy deposition profiles for LIBRA implosion simulation.

Sample results for the frequency-dependent x-ray output and the overall energy partitioning are shown in Figure 17.8.

17.5. Example 5: Target Chamber Non-LTE Buffer Gas Simulation

Figure 17.9 shows the input file for a target chamber calculation involving a non-LTE buffer gas. The target chamber has a radius (RADIUS) of 6.5 meters, and is filled with a Ne buffer gas (ATN2B = 10, ATW2B = 20) of density $3.54 \times 10^{16} \text{ cm}^3$ (≈ 1 torr at room temperature). The solid first wall (NCZONS = 40) is composed of graphite (RHOCND = 2.26 g/cm³; IZFILM = 6). Vaporization of the first wall material is modelled by setting ISW(20) = 2. The x-ray flux from the target located at the center of the chamber is specified by XEHIST and XAMP using a model with 48 frequency groups (NXRG). The values in the x-ray flux array XAMP are multiplied by CON(43). The target debris ions expand radially outward (IBEAM = 1) in a 5 ns square pulse. EIONIN and IONIN specify the ion kinetic energies and particle fluxes. Four different ion species (NIX) are considered (protons, “DT”, He, and C) for this direct-drive target.

Radiation for the continuum is transported using a 20-group (NFG) diffusion model (IRAD=2). For this calculation, the opacity tables were generated without any contributions from bound-bound transitions. Line radiation is treated separately using a non-LTE CRE model (NLTEID = 1). When this option is used, a second namelist file, ‘nltert.inp’, is read in containing the atomic modeling and radiation transport parameters (see Figure 17.10). A total of 108 atomic energy levels was selected for this calculation (sum of non-zero ISELECT elements). Detailed results from calculations of this type are described elsewhere [13].

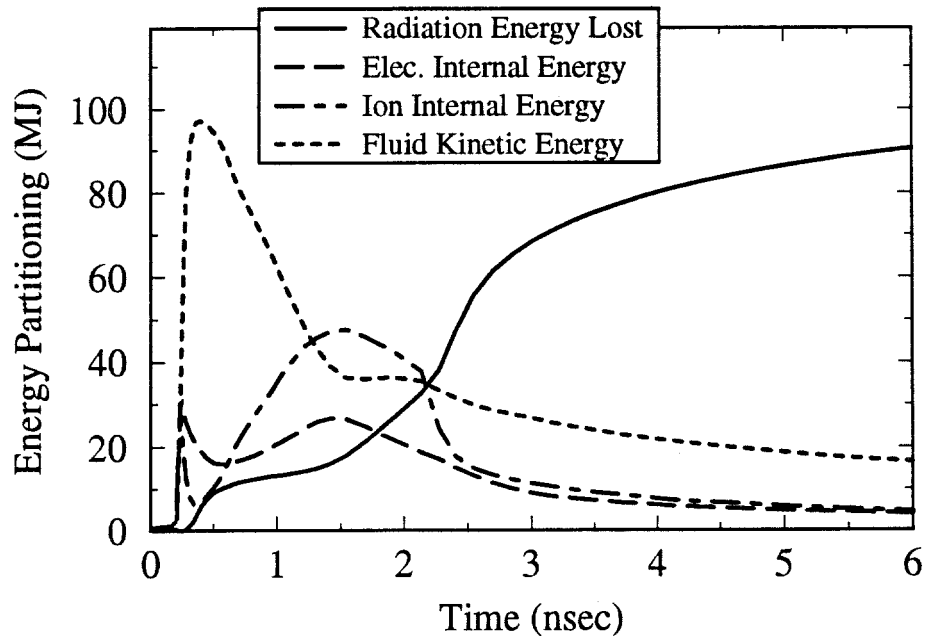
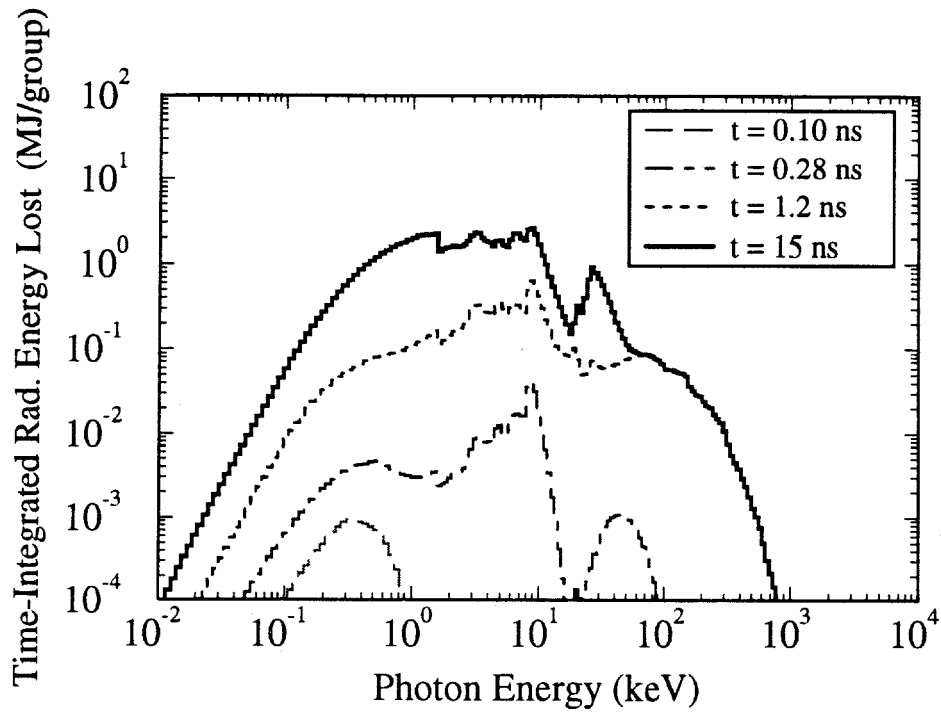


Figure 17.8. Time-integrated x-ray output and energy partitioning from LIBRA target breakup simulation.

```

Singput
c ...
c ... nltcid(1) = 1                                CRE variables (do CRE if nltcid=1)
c ...                                         irad=0 => no radiation
c ...                                         irad=2 => MG Diff. model
c ...                                         irad=3 => MG, MA RT model

c ... irad = 2
c ... nfg = 20
c ... isw(3) = 1                                1-T (isw3=1) or 2-T (isw3=2) option
c ...                                         Max. run time

c ... rmax = 100000
c ... tmax = 120.e-6
c ... dtb = 1.0e-12
c ... dtcmax = 2.e-6

c ... EOS file type
c ... (ideos: 0=>UW/WP ; 1=>UW/IONMIX ; 2=> SESAME)
c ... (ideos: < 0 => ideal gas)
c ... Opacity file type
c ... (idopac: 0=>UW/WP ; 1=>UW/IONMIX)
c ... (idopac: < 0 => ideal gas)

c ... ideos(1) = 1, 1
c ... idopac(1) = 1, 1
c ... izeos(1) = 10, 6

c ... isw(27) = 1                                When using IONMIX, must set isw27=1
c ... ZONING PARAMETERS

c ... nvregn = 1
c ... idelta = 3
c ... isw(4) = 3
c ... con(36) = 0.1
c ... con(37) = 0.4
c ... radius = 650.

c ... jmax = 50
c ... jmat(1) = 50*1, 40*2,
c ... iz(1) = 50*10

c ... TARGET CHAMBER BACKGROUND GAS PROPERTIES

c ... atn2b(1) = 50*10.
c ... atw2b(1) = 50*20.
c ... tn2c(1) = 50*0.5
c ... te2c(1) = 50*0.5
c ... tr2c(1) = 50*0.1
c ... dn2b(1) = 50*3.54e16
c ... tbc = 5.e-2

c ... TARGET X-RAY SPECTRUM

c ... isw(11) = 0
c ... con(43) = 4.490
c ... nxrg = 48
c ... xehist = 0.e+0,
c ... 0.05e+0, .1e+0, .15e+0, .2e+0, .25e+0, .3e+0,
c ... .35e+0, .4e+0, .45e+0, .5e+0, .55e+0, .6e+0,
c ... .65e+0, .7e+0, .75e+0, .8e+0, .9e+0, 1.e+0,
c ... 1.2e+0, 1.4e+0, 1.65e+0, 2.e+0, 2.3e+0, 2.7e+0,
c ... 3.1e+0, 3.5e+0, 4.e+0, 4.5e+0, 5.e+0, 5.5e+0,
c ... 6.e+0, 6.6e+0, 7.2e+0, 8.e+0, 8.8e+0, 9.3e+0,
c ... 10.e+0, 12.5e+0, 15.65e+0, 19.56e+0, 24.45e+0, 30.56e+0,
c ... 38.2e+0, 47.75e+0, 59.69e+0, 74.61e+0, 93.26e+0, 100.15e+0
c ... xamp = 0.0000e+0,
c ... 1654628., 3322684., 3351032., 3162294., 2642332., 2613984.,
c ... 2651284., 2566240., 2557288., 2051500., 2037326., 2023152.,
c ... 2023152., 2003756., 1588234., 1578536., 1578536., 1233884.,
c ... 1054098., 888486., 694824.4, 524661.8, 416864.8, 274602.6,
c ... 219324., 172997.4, 127118.4, 94070.6, 79896.6, 69482.44,
c ... 60500.6, 53413.6, 48213.98, 44334.78, 42962.14, 44096.06,
c ... 47736.54, 36964.3, 26609.82, 22924.58, 17583.22, 13614.5,
c ... 10160.52, 7231.724, 4868.396, 3114.55, 2193.24

c ... VAPORIZATION MODEL PARAMETERS

c ... isw(20) = 2
c ... isw(30) = 0
c ... nczons = 40
c ... delxct = 1.
c ... rhocond = 2.26
c ... cpheat = 8240.
c ... qheatv = 59730.
c ... xkcond = 15500.
c ... tvap0 = 0.338
c ... twallb = 0.0259
c ... awfilm = 12.
c ... izfilm = 6
c ... tcn2c(51) = 45*0.151

c ... TARGET DEBRIS ION PARAMETERS

c ... ibeam = 1
c ... isw(8) = 1
c ... isw(31) = 1
c ... con(44) = 4.0
c ... qlimit = 1., 1., 2., 6.
c ... qimin = 0., 0., 0., 0.
c ... anion = 1., 1., 2., 6.
c ... awion = 1., 2.5, 4., 12.

c ... nix = 4
c ... nie = 1
c ... nit = 10
c ... tionin(1) = 0., 1.00e-12, 5.e-9, 5.001e-9
c ... xionin(1.1.1) = 0., 2.0896e28, 2.0896e28, 0.
c ... xionin(1.1.2) = 0., 3.88e28, 3.88e28, 0.
c ... xionin(1.1.3) = 0., 7.46e27, 7.46e27, 0.
c ... xionin(1.1.4) = 0., 1.045e28, 1.045e28, 0.
c ... eionin(1.1.1) = 137.8, 137.8, 137.8, 137.8
c ... eionin(1.1.2) = 117.35, 117.35, 117.35, 117.35
c ... eionin(1.1.3) = 187.7, 187.7, 187.7, 187.7
c ... eionin(1.1.4) = 1650., 1650., 1650., 1650.

c ... OUTPUT CONTROL PARAMETERS

c ... isw(66) = 0
c ... io(1) = 500, 500, -1, 500, -1
c ... iobin = 250
c ... isw(5) = 20

Send

```

Figure 17.9. Example input file ('bucky.inp') for non-LTE buffer gas simulation.

```

$input1
c ... iswcre(9) = 1          if iswcre(9)<>0, continue with old pop's if not converged
c ... concre(55) = 0.03    Min. Optical Depth considered for Line transport calc.
c ... wizmin(1) = 0.5      ionization windowing boundaries (for each gas species)
c ... wizmax(1) = 8.
c ... ##### Initial Populations #####
c          iswcre6= 0      start with pop's from previous hydro cycle
c          = 1          start with LTE populations
c          = 2          start with coronal populations
c          = 3          start with AND RETURN LTE populations
c          = 4          start with AND RETURN coronal populations
c          iswcre(6) = 0
c ... Bound-bound (iswcre7) and Bound-Free (iswcre8) coupling:
c          < 0          local (diagonal) couple only
c          = 0          zone-to-zone coupling (includes off-diag)
c          > 0          no photoexcitation/photoionization
c          iswcre(7) = -1, 1
c ... Debugging aids
c ... convergence parameters (populations)
c          imaxse = 40
c          errmxfl = 1.e-2
c ... atomic data parameters
c          atomnm(1) = 10.
c          atomwt(1) = 20.
c          ilinep = 3
c ... ngases = # of gases by region
c          kgasrg(1,1) = 1      kgasrg(iigas,iregn) = gas index
c          spregm(1,1) = 1.    spregm(kgasrg(iigas,iregn),iregn)=fraction gas abundance
c ... select Neon levels
c          iselct( 1,1) = 15*1
c          iselct( 19,1) = 15*1
c          iselct( 38,1) = 15*1
c          iselct( 58,1) = 10*1
c          iselct( 78,1) = 10*1
c          iselct( 98,1) = 10*1
c          iselct(118,1) = 10*1
c          iselct(138,1) = 10*1
c          iselct(157,1) = 8*1
c          iselct(177,1) = 4*1
c          iselct(197,1) = 1
$end

```

Figure 17.10. Non-LTE atomic data input file ('nltert.inp') for non-LTE buffer gas simulation.

References

- [1] Moses, G.A., “PHD-IV — A Plasma Hydrodynamics, Thermonuclear Burn, Radiative Transfer Computer Code,” University of Wisconsin Fusion Technology Institute Report UWFD-194 (Revised August 1985).
- [2] Moses, G.A., Peterson, R.R., and McCarville, T.J., “MFFIRE - A Multifrequency Radiative Heat Transfer Hydrodynamics Code,” *Computer Physics Communications* **36**, 249 (1985).
- [3] Peterson, R.R., MacFarlane, J.J., and Moses, G.A., “CONRAD — A Combined Hydrodynamics–Condensation/Vaporization Computer Code,” University of Wisconsin Fusion Technology Institute Report UWFD-670 (Revised July 1988).
- [4] MacFarlane, J.J., “NLTE — A Code for Computing the Radiative Properties of Non-LTE Plasmas,” University of Wisconsin Fusion Technology Institute Report UWFD-931 (December 1993).
- [5] Wang, P., “EOSOPA — A Code for Computing the Equations of State and Opacities of High Temperature Plasmas with Detailed Atomic Models,” University of Wisconsin Fusion Technology Institute Report UWFD-933 (December 1993).
- [6] Badger, B., et al., “HIBALL — A Conceptual Heavy Ion Beam Fusion Reactor Study,” University of Wisconsin Fusion Technology Institute Report UWFD-625 (December 1984).
- [7] MacFarlane, J.J., Moses, G.A., Wang, P., Sawan, M.E., and Peterson, R.R., “Numerical Simulation of Target Microexplosion Dynamics for the LIBRA-SP Inertial Confinement Fusion Reactor,” University of Wisconsin Fusion Technology Institute Report UWFD-973 (December 1994).
- [8] Peterson, R.R., Moses, G.A., MacFarlane, J.J., and Wang, P., *Fusion Technology* **26**, 780 (1994).
- [9] Wang, P., MacFarlane, J.J., Moses, G.A., and Mehlhorn, T.A., “Atomic Physics Calculations in Support of Numerical Simulations of High Energy Density Plasmas,” presented at the 36th Annual Meeting of the APS Division of Plasma Physics, Minneapolis, MN (November 1994).
- [10] Peterson, R.R., Simmons, K., MacFarlane, J.J., Wang, P., and Moses, G.A., “Computer Simulations of the Debris and Radiation Emission from an Ignited NIF Target,” presented at the 36th Annual Meeting of the APS Division of Plasma Physics, Minneapolis, MN (November 1994).
- [11] MacFarlane, J.J., Wang, P., Peterson, R.R., and Moses, G.A., presentations at Lawrence Livermore National Laboratory and Los Alamos National Laboratory (1995).
- [12] J.J. MacFarlane and P. Wang, *Phys. Fluids* **B3**, 3494 (1991).

- [13] MacFarlane, J.J., Peterson, R.R., Wang, P., and Moses, G.A., *Fusion Technology* **26**, 886 (1994).
- [14] MacFarlane, J.J., Moses, G.A., and Peterson, R.R., *Phys. Fluids* **B1**, 635 (1989).
- [15] Peterson, R.R., in “Laser Interaction and Related Plasma Phenomena, Vol. 7,” edited by H. Hora and G. Miley, Plenum Publ. Corp., p. 591 (1986).
- [16] Peterson, R.R., *Fusion Technology* **13**, 279 (1988).
- [17] Bailey, J.E., et al., in preparation (1995).
- [18] MacFarlane, J.J., Wang, P., Chung, H.K., and Moses, G.A., “Spectral Diagnostics, Ion Stopping Power, and Radiation-Hydrodynamics Modeling in Support of Sandia Light Ion Beam Fusion Experiments,” University of Wisconsin Fusion Technology Institute Report UWFD-979 (April 1995).
- [19] MacFarlane, J.J. and Cassinelli, J.P., *Astrophys. J.* **347**, 1090 (1989).
- [20] Wang, P., “ATBASE Users’ Guide,” University of Wisconsin Fusion Technology Institute Report UWFD-942 (December 1993).
- [21] Melhorn, T.A. “A Finite Material Temperature Model for Ion Energy Deposition in Ion-Driven ICF Targets,” SAND80-0038, Sandia National Laboratories, Albuquerque, NM, May 1980; also *J. Appl. Phys.* **52**, 6522 (1981).
- [22] Richtmyer, R.D. and Morton, K.W., *Difference Methods for Initial Value Problems*, Interscience Publishers, New York (1967).
- [23] Spitzer, L., *Physics of Fully Ionized Gases*, Second Edition, Interscience Publishers, New York (1962).
- [24] Anderson, E., et al., LAPACK Users’ Guide (SIAM, Philadelphia, 1992).
- [25] MacFarlane, J.J., *Astron. Astrophys.* **264**, 153 (1992).
- [26] Ng, K.C., *J. Chem. Phys.* **61**, 2680 (1974).
- [27] Auer, L., in Numerical Radiative Transfer, edited by W. Kalkoten, Cambridge University Press, Cambridge, U.K. (1987), p. 101.
- [28] Apruzese, J.P., Davis, J., Duston, D., and Whitney, K.G., *J.Q.S.R.T.* **23**, 479 (1980).
- [29] Apruzese, J.P., *J.Q.S.R.T.* **25**, 419 (1981).
- [30] Apruzese, J.P., *J.Q.S.R.T.* **34**, 447 (1985).
- [31] Mihalas, D., Stellar Atmospheres, Second Edition, Freeman and Company, New York (1978).
- [32] Burgess, A. and Chidichimo, M.C., *Mon. Not. R. Astron. Soc.* **203**, 1269 (1983).

- [33] Seaton, M.J., in Atomic and Molecular Processes, edited by D.R. Bates, Academic, New York (1962) p. 374.
- [34] Sobelman, I.I., Vainshtein, L.A., and Yukov, E.A., Excitation of Atoms and Broadening of Spectral Lines, Springer-Verlag, New York (1981).
- [35] Post, D.E., Jensen, R.V., Tarter, C.B., Grasberger, W.H., and Lokke, W.A., *At. Data Nucl. Data Tables* **20**, 397 (1977).
- [36] MacFarlane, J.J. , “IONMIX - A Code for Computing the Equation of State and Radiative Properties of LTE and Non-LTE Plasmas,” *Comput. Phys. Commun.* **56**, 259 (1989).
- [37] “SESAME: The Los Alamos National Laboratory Equation of State Database,” LANL Report LA-UR-92-3407, edited by S.P. Lyon and J.D. Johnson (1992).
- [38] Lindhard, J. and Scharff, M., “Energy Dissipation by Ions in the keV Range,” *Phys. Rev.* **124**, 128 (1961).
- [39] Knudson, H., Haugen, H.K., and Hvelplund, P., “Single-Electron-Capture Cross Sections for Medium and High Velocity, Highly Charged Ions Colliding with Atoms,” *Phys. Rev.* **A23** , 597 (1981).
- [40] Hyman, E., Mulbrandon, M., and Giuliani, J.L., “Charge Exchange Cross Section Update,” ETHANL Proceedings No. 7, SRI International, Menlo Park, CA, July 1987.
- [41] Duderstadt, J.J., and Moses, G.A., Inertial Confinement Fusion (Wiley, New York, 1982), p. 145.
- [42] Goel, B., and Henderson, D.L., “A Simple Method to Calculate Neutron Energy Deposition in ICF Targets,” Kernforschungszentrum Karlsruhe Report No. KfK-4142 (1986).
- [43] McCarville, T.J., Moses, G.A., and Kulcinski, G.L., “A Model for Depositing Inertial Confinement Fusion X-Rays and Pellet Debris Into a Cavity Gas,” University of Wisconsin Fusion Technology Institute Report UWFD-406 (April 1981).
- [44] Adams, K.G. and Biggs, F., “Efficient Computer Access to Sandia Photon Cross Sections II,” SC-RR-71-0507, Sandia Laboratory, Albuquerque, NM, December 1971.
- [45] Labuntov, D.A., and Kryukov, A.P., *Int. J. Heat Mass Transfer* **22**, 989 (1979).
- [46] Hail, T.A., private communication (1995).
- [47] Kidder, R.E., *Nucl. Fusion* **16**, 3 (1976).
- [48] Olson, R.E., private communication (1994).